UQAC
Université du Québec
à Chicoutimi

RELATIONSHIP BETWEEN THERMAL CONDUCTIVITY AND ELECTRICAL CONDUCTIVITY IN B_4C PARTICLE REINFORCED ALUMINUM MATRIX COMPOSITES

PAR

CONG LI

MÉMOIRE PRÉSENTÉE À L'UNIVERSITÉ DU QUÉBEC À CHICOUTIMI EN VUE DE L'OBTENTION DU GRADE DE MAÎTRISEES EN INGÉNIERIE

Jury :

X.Grant Chen	Director of research	UQAC	President of Jury
Kun Liu	Co-director of research	UQAC	
Laszlo Kiss	Co-director of research	UQAC	
Zhan Zhang	Research Professor	UQAC	
Emad Elgallad	Research Professor	UQAC	

QUÉBEC, CANADA

© CONG LI, 2022

RÉSUMÉ

Le présent travail vise à explorer les facteurs influençant la conductivité thermique et la conductivité électrique et à établir la relation entre la conductivité thermique et la conductivité électrique dans les composites Al-B_4C. Dans cette étude, on a utilisé des composites Al-B_4C avec différentes matrices d'aluminium et diverses fractions volumiques de B_4C. Leur microstructure, y compris les particules de renfort et les produits de réaction, a été caractérisée. De plus, l'évolution de la conductivité thermique et électrique a été étudiée, et leur relation a été établie.

Dans cette étude, la microscopie optique et la microscopie électronique à balayage ont été utilisées pour observer l'évolution de la microstructure avec différentes particules (type, taille et fraction volumique) et différentes matrices (1xxx, 3xxx et 6xxx). Le conductimètre thermique à flash laser et le conductimètre électrique SIGMASCOPE ont été utilisés pour surveiller la conductivité thermique et électrique. Les effets de la taille des particules, de la fraction volumique, de la résistance interfaciale thermique/électrique sur la conductivité thermique et électrique ont été étudiés en conjonction avec des modèles de prédiction de la conductivité thermique et électrique. Une équation empirique entre la conductivité thermique et la conductivité électrique a été établie. Les résultats de ce travail sont divisés en deux parties.

Dans la première partie, on a étudié les effets de la fraction volumique et de la taille des particules, ainsi que l'effet du traitement thermique, de la température d'essai et de l'épaisseur de laminage sur l'évolution de la conductivité thermique et électrique des composites 1100-B4C, tout en combinant divers modèles de prédiction de conductivité thermique et de conductivité électrique. Les résultats montrent que le produit de réaction augmente à mesure que la fraction volumique des particules augmente et que la conductivité thermique et la conductivité électrique diminuent de manière linéaire avec la fraction volumique croissante des particules B_4C. Cependant, la température de test dans la plage de 20 à 250 ℃ n'a aucun effet sur la conductivité thermique et l'épaisseur de laminage n'a aucun effet sur la conductivité thermique et la conductivité électrique.Alors que la conductivité thermique et la conductivité électrique ont augmenté sous l'effet du traitement thermique allant jusqu'à 430℃ /4h suivi d'un plateau sous l'effet des températures encore plus élevées. Parmi les différents modèles de prédiction, Bruggeman-ET et Bruggeman sont les plus appropriés pour prédire la conductivité thermique et la conductivité électrique des composites 1100-B_4C, respectivement. Enfin, une relation linéaire est établie pour présenter la relation entre la conductivité thermique et la conductivité électrique dans les composites 1100-B_4C étudiés.

Dans la deuxième partie, on a étudié la relation entre la conductivité thermique et la conductivité électrique dans d'autres composites à matrice métallique d'aluminium (6xxx/3xxx-B_4C et 6061-Al_2O_3), tout en combinant les modèles de prédiction de la conductivité thermique et de la conductivité électrique. Les résultats montrent que bien qu'avec des matrices et des particules de renforcement différentes, la relation entre la conductivité thermique et la conductivité électrique dans les composites étudiés 6xxx/3xxx-

B_4C et 6061-Al_2O_3 est toujours linéaire et correspond à l'équation empirique obtenue à partir de 1xxx-B_4C.

ABSTRACT

The present work focuses to explore the influencing factors of thermal conductivity and electrical conductivity and to establish the relationship between thermal conductivity and electrical conductivity in Al-B_4C composites. Al-B_4C composites with different aluminum matrices and various volume fractions of B_4C were used in the study. Their microstructure, including the reinforcement particles and reactions products, was characterized while the evolution of thermal conductivity and electrical conductivity was studied, and their relationship was established.

In this study, optical microscopy and scanning electron microscopy were used to observe the evolution of microstructure with different particles (type, size and volume fraction) and different matrices (1xxx, 3xxx and 6xxx). Laser Flash Thermal Conductivity Meter and SIGMASCOPE Electrical Conductivity Meter were used to monitor thermal and electrical conductivity. The effects of particle size, volume fraction, interfacial thermal resistance/electrical resistance on thermal and electrical conductivity were studied in conjunction with thermal and electrical conductivity prediction models. An empirical equation between thermal conductivity and electrical conductivity was established. The results of this paper are divided into two parts.

In the first part, the effects of particle volume fraction, particle size, heat treatment as well as the testing temperature and rolling thickness on the evolution of thermal and electrical conductivity of 1100-B_4C composites were investigated by combining various thermal conductivity and electrical conductivity prediction models. The results show that the reaction product increases as the particle volume fraction increases and both thermal conductivity and electrical conductivity is linearly decreasing with the increasing volume fraction of B_4C particles. However, the testing temperature in the range of 20-250℃ is no effect on thermal conductivity, and rolling thickness is found no effect on thermal conductivity and electrical conductivity. While, both thermal conductivity and electrical conductivity increased after heat treatment until 430℃/4h followed by a plateau with further increasing temperatures. Among the various prediction models, Bruggeman-ET and Bruggeman are the most suitable ones for predicting the thermal conductivity and electrical conductivity of 1100-B_4C composites, respectively. Finally, a linear relationship is established to present the relationship between thermal conductivity and electrical conductivity in studied 1100-B_4C composites.

In the second part, the relationship between thermal conductivity and electrical conductivity in other aluminum metal matrix composites (6xxx/3xxx-B_4C and 6061-Al_2O_3) was investigated combining thermal conductivity and electrical conductivity prediction model. The results show that though with different matrix and reinforcement particles, the relationship between thermal conductivity and electrical conductivity in studied 6xxx/3xxx-B_4C and 6061-Al_2O_3 also composites are still linear and fits the empirical equation obtained from 1xxx-B_4C composites.

TABLE OF CONTENTS

LIST OF TABLES

LIST OF FIGURES

LIST OF SYMBOLS

α	A constant of the unity order/thermal diffusivity (m^2/s)/A dimensionless parameter/Denotes an excitation
ΔT	Associated temperature drops across an interface (K)
∇T	Temperature gradient (K/m)
Δx	Specimen thickness (m)
δ	Standard depth of penetration (m)
Θ_D	Debye temperature (K)
λ	Electrical conductivity of aluminum (S/m)
μ	Magnetic permeability (H/m)
μ_0	Absolute permeability (H/m)
μ_{rel}	Relative permeability (dimensionless)
μ_e	Mobility of electrons ($m^2/(V \cdot s)$)
μ_h	Mobility of holes ($m^2/(V \cdot s)$)
ρ	Electrical resistivity of the material from which the resistance is Made ($\Omega \cdot m$)/Electrical resistivity ($\Omega \cdot m$)/Material density (kg/m^3)
ρ_m	Density of matrix (kg/m^3)
ρ_r	Density of particle (kg/m^3)
σ	Electrical conductivity (S/m)
σ_{eff}	Effective electrical conductivity of the composite material (S/m)
σ_m	Electrical conductivity of matrix (S/m)
σ_p	Electrical conductivity of particle (S/m)
τ_e	Collision time of electrons (seconed)
τ_h	Collision time of holes (seconed)
ϕ	Volume fraction of particle (vol%)
ϕ_m	Maximum packing volume fraction of particles (vol%)
ω	Phonon frequency (Hz)
A	Metered area (m^2)
a_k	Kapitza radius (m)

C	Total specific heat (J/(kg·K))
c	A constant (dimensionless)
C_m	Specific heat capacity of matrix (J/(kg·K))
C_p	Specific heat (J/(kg·K))
e	Electrical charge of electrons (coulomb)
1/e	Eddy current density (dimensionless)
f	Measurement frequency (Hz)
h	Penetration depth (m)/Planck's constant (J/Hz)
h_c	Interface thermal conductance ([W/(m^2·k)])
I	Test current (A)
$I_{\sim}$	Excitation current (A)
K	Thermal conductivity ([W/(m·k)])/Total thermal conductivity of aluminum/Thermal conductivity of metal solids ([W/(m·k)])
K_e	Thermal conductivity of electron gas ([W/(m·k)])
K_l	Thermal conductivity of phonon gas ([W/(m·k)])
k	Thermal conductivity of non-metallic or atomic fraction ([W/(m·k)])
k_B	Boltzmann constant (J/K)
k_{eff}	Effective thermal conductivity of the composite material ([W/(m·k)])/Effective thermal conductivity of hot plate test ([W/(m·k)])
k_m	Thermal conductivity of the matrix ([W/(m·k)])
k_p	Thermal conductivity of the particle ([W/(m·k)])
L	Lorenz Constant (2.45×10^{-8} Volt^2/K^2)/Length of wire wound to make a resistance (m)/Sample thickness (m)/ Thickness of the sample (m)
l	Mean free path of phonons (m)/mean free path of the photons responsible for radiant heat transfer (m)/Mean free path (m)
m_e	Electron mass (kg)
m_h	Hole mass (kg)
N_e	Charge density (C/m^3)
n	Electron concentration (C/m^3)
$\bar{n}$	average number of photons (dimensionless)
p	Holes density (holes/m^2)
Q	Heat flow rate(/J/s)/Heat flow (W/m^2)/Heat power (dimensionless)/heat flow through unit interface area per unit time (W/s)

q	Heat flux (W/m^2)
R	Conductor resistance (Ω)/Test resistance (Ω)
R^2	R-squared (dimensionless)
R_{Bd}	Interface thermal resistance ([$(m^2 \cdot k)/W$])
R_{lead}	Total lead resistance (Ω)
S	Cross sectional area (m^2)
T	Absolute temperature (K)
$T_{hot} - T_{cold}$	Temperature differential across the specimen (K)
T_0	Initial temperature (K)
$t_{1/2}$	The time ($t_{1/2}$) of the thermogram takes to reach half of the maximal temperature increase (second)
V_M	Voltage measured by meter (V)
V_R	Voltage across resistor (V)
v	Velocity (m/s)
v_m	Phonon velocity of matrix (m/s)
v_r	Phonon velocity of reinforcement (m/s)
W	A constant with respect to temperature (dimensionless)

LIST OF ABBREVIATIONS

Al	Aluminum
Al-B_4C MMCs	Boron carbide reinforced aluminum matrix composites
Al-MMCs	Aluminm metal matrix composites
Al-micro SiC	Micro size silicon carbide reinforced aluminum matrix composites
AlN	Aluminium nitride
Al-nano SiC	Nano size silicon carbide reinforced aluminum matrix composites
Al-SiC MMCs	Silicon carbide reinforced aluminum matrix composites
AMM	acoustic mismatch model
Bruggeman-ET model	Every and Tzou verified Bruggeman model
CTE	Coefficients of thermal expansion
Cu	Copper
DMM	Diffusion mismatch model
EC	Electrical conductivity
EBSD	Electron Backscatter Diffraction
EDS	Energy dispersive X-ray spectroscopy
EMT	Effective medium theory
Fe	Iron
GHP	Guarded hot plate
HT	Heat treatment
ITC	Interface thermal conductivity
MMCs	Metal matrix composites
Mg	Magnesium
OM	Optical microscopy
SiCp/Al MMCs	High content of SiC particles reinforced aluminum matrix composites
SEM	Scanning electron microscopy
TC	Thermal conductivity

Ti	Titanium
TPS	The transient planar heat source method
TTR	Transient thermal reflectance
1100-B_4C MMCs	Boron carbide reinforced 1100 aluminm alloy matrix composites
3004-B_4C MMCs	Boron carbide reinforced 3004 aluminm alloy matrix composites
6061-Al_2O_3 MMCs	Alumina reinforced 6061 aluminm alloy matrix composites
6063-B_4C MMCs	Boron carbide reinforced 6063 aluminm alloy matrix composites
6351-B_4C MMCs	Boron carbide reinforced 6351 aluminm alloy matrix composites
1xxx-B_4C MMCs	Boron carbide reinforced 1xxx aluminm alloy matrix composites
3xxx-B_4C MMCs	Boron carbide reinforced 3xxx aluminm alloy matrix composites
6xxx-B_4C MMCs	Boron carbide reinforced 6xxx aluminm alloy matrix composites

ACKNOWLEDGEMENTS

First of all, I would like to warmly thank my supervisor, Professor X.-Grant Chen, for giving me the opportunity and financial support to pursue a master's degree at the University of Québec à Chicoutimi. Special thanks to him for his patience in teaching me to maintain a logical and scientific way of thinking and writing, as well as the influence on the way I approach and think about problems, which I will use for a lifetime.

Thanks to my co-supervisor Prof. Kun Liu for his guidance and all his help and guidance throughout the master's study. Thanks to my co-supervisor Prof. Laszlo Kiss for his kind help and encourage throughout the master's study. Thanks to Professor Zhan Zhang for teaching me important SEM techniques.

I would like to thank Mr. Samuel Dessureault and Mr. Félix Tremblay for their help with laboratory training and sample processing. Thanks to Mr. Guillaume Bonneau for his kind help with thermal conductivity test and encourage throughout the master's study.

Specially thanks to my friends LiYing Cui and Chaima Hajji for their meticulous care and help in my life and study. Finally, I would like to express my heartfelt thanks to my parents and all my other friends for their selfless support and encouragement. Without your help I would not be able to complete my dissertation independently

The project was carried out with financial support from the Natural Sciences and Engineering Research Council of Canada (NSERC) and Rio Tinto Alcan as part of the NSERC Industrial Research Chair in Aluminum Processing Metallurgy at the University of Quebec, Chicoutimi (UQAC). I would like to thank both organizations for their support during my studies.

CHAPTER 1 INTRODUCTION

1.1 Background

Metal matrix composites (MMCs) are widely used in modern engineering applications because of their specific properties, such as: high strength, weight ratio and ductility, low coefficients of thermal expansion (CTE) and high thermal stability, and superior wear resistance, high specific stiffness and satisfactory corrosion resistance [1]. Among the MMCs, the particle-reinforced aluminum matrix composites are one of most applicable composites. For example, boron carbide reinforced aluminum matrix composites (Al-B_4C MMCs) are widely used as the break plates in autos and neutron absorbers in nuclear industries [2]. During these applications, the service temperature can be high, such as 300-350℃, leading to the much stricter requirements on the composites, especially the thermal conductivity. Therefore, how to improve the thermal conductivity of MMCs is always one of industrial concerns for their development and applications.

Since the traditional measurement of thermal conductivity is complex and time-consuming, therefore, electrical conductivity has been developed to be one indicator for the thermal conductivity and the relationship between electrical conductivity and thermal conductivity has been well established in aluminum alloys [3]. Generally, the relationship follows the Wiedemann-Franz's law that $K=L\times T\times\sigma$, where K is the thermal conductivity (in W/m·K), T is the absolute temperature (in K), L is the Lorenz Constant (2.45×10^{-8} $Volt^2/K^2$), and σ is the electrical conductivity (S/m) and the Wiedemann-Franz law applies rigorously only to the metals where both electric and thermal conductivities are dominated by the kinetics of the electron gas [3]. However, due to the lower thermal/electrical conductivity of particles in MMCs, the complex reactions between particles and matrix as well as the various reaction layers and reaction products [4-6], limited work has been performed on the relationship

between electrical conductivity and thermal conductivity in particle-reinforced Al matrix composites. Therefore, it is urgent to discover this relationship in MMCs for their wider applications.

On the other hand, researchers have been working on improving the thermal conductivity of MMCs, most of which focus on the particle itself [4-6]. It is reported that volume fraction, particle size as well as the particle morphology are greatly related to the thermal conductivity [7, 8]. Generally, it is widely accepted that lower volume fraction, bigger size and near-spherical shape of particle is helpful to increase the thermal conductivity of MMCs [7, 8]. However, there is no clear conclusion about the interaction layer and reaction products on the evolution of thermal conductivity. Meanwhile, limited open literature can be reviewed on the approaches to affect the electrical/thermal conductivity on MMCs, such as the influence of heat treatment and hot deformation on the evolution of electrical/thermal conductivity. Therefore, the project adopted a program for these aspects to explore ways to improve thermal conductivity and try to establish the relationship between electrical conductivity and thermal conductivity in particle-reinforced aluminum matrix composites.

1.2 Objective

The objective of present research is to systematically investigate the thermal conductivity behavior of aluminum matrix composites as a function of particle types (B_4C and Al_2O_3), volume fraction as well as various aluminum matrices, including 1xxx, 3xxx and 6xxx aluminum alloys. The effect of the interface between the particles and the aluminum matrix of the composites in this study on thermal conductivity will be investigated by various thermal conductivity prediction models. Then the empirical equations between electrical conductivity (EC) and thermal conductivity (TC) will be tried to establish using the experiment data to

provide a predictive tool for industrial applications. In addition, the influence of heat treatment and hot deformation on the evolution of EC and TC of composites will also be studied aiming to find the approaches to improve their EC and TC. This research can be divided into 3 parts as follows:

Part I: Fully characterize the microstructure of MMCs, including particles, reaction products and reaction layers (types and volumes) with different aluminum matrices and reinforce particles. In this section, optical microscopy (OM), scanning electron microscopy (SEM) and energy dispersive X-ray spectroscopy (EDS) have been used to characterize the distribution of particles in the matrix. The microstructure of the material and the analysis of the reaction products were also examined.

Part Ⅱ: Investigate the evolution of TC and EC in designed MMCs with different matrices and reinforcing particles (type, size and volume fraction) under various conditions (as rolled and annealed). EC and TC will be measured by a conductivity meter and laser flash thermal conductivity meter.

Part Ⅲ: Introduce the EC and TC prediction models to study the influence of the factors, such as particle type and volume and interface thermal resistance on the evolution of EC and TC. Meanwhile, the relationship between EC and TC will be established.

References

[1] K. Ma, E. J. Lavernia, and J. M. Schoenung, "Particulate reinforced aluminum alloy matrix composites-a review on the effect of microconstituents," *Rev. Adv. Mater. Sci*, vol. 48, no. 2, pp. 91-104, 2017. [Online]. Available: https://www.ipme.ru/e-journals/RAMS/no_24817/01_24817_lavernia.pdf.

[2] X. G. Chen, "Application of AL-B4C metal matrix composites in the nuclear industry for neutron absorber materials," *TMS Annual Meeting*, vol. 2006, pp. 343-350, 01/01 2006. [Online]. Available: https://www.researchgate.net/publication/279766054_Application_of_AL-B4C_metal_matrix_composites_in_the_nuclear_industry_for_neutron_absorber_materials.

[3] L. Kempf, C. Smith, and C. Taylor, "Thermal and Electrical Conductivities of Aluminum Alloys," *Trans. Amer. Inst. Min. Metall. Engrs*, vol. 124, pp. 287-298, 1937. [Online]. Available: https://aimehq.org/resources/digital-library.

[4] L. Jiang, P. Wang, Z. Xiu, G. Chen, X. Lin, C. Dai, and G. Wu, "Interfacial characteristics of diamond/aluminum composites with high thermal conductivity fabricated by squeeze-casting method," *Materials Characterization*, vol. 106, pp. 346-351, 2015, doi: https://doi.org/10.1016/j.matchar.2015.06.023.

[5] J. Molina, J. Narciso, L. Weber, A. Mortensen, and E. Louis, "Thermal conductivity of Al–SiC composites with monomodal and bimodal particle size distribution," *Materials Science and Engineering: A*, vol. 480, no. 1-2, pp. 483-488, 2008, doi: https://doi.org/10.1016/j.msea.2007.07.026.

[6] M. Wu, L. Hua, J. Zhou, and Y. Yin, "Advances in thermal conductive aluminum alloys and aluminum matrix composites," *Cailiao Daobao/Materials Review*, vol. 32, no. 5 Part A, pp. 1486-1495, 2018, doi: https://doi.org/10.11896/j.issn.1005-023X.2018.09.013.

[7] T. Wang, R. Wu, J. Zhang, and B. Liu, "Development of aluminum conductive materials," *Cailiao Kexue yu Gongyi/Material Science and Technology*, vol. 22, no. 6, pp. 53-61, 2014. [Online]. Available: http://hit.alljournals.cn/mst_cn/ch/first_menu.aspx?parent_id=download.

[8] Y. Wang, "Research on thermal conductivity of particle reinforced aluminum matrix composites " Master Dissertation, Material Science and Engineering Nanchang Hangkong University, Nanchang, China 2010. [Online]. Available: https://cdmd.cnki.com.cn/Article/CDMD-10406-1010120394.htm. [王寅, "颗粒增强铝基复合材料导热性能分析," 南昌航空大学, 南昌, 中国 2010.]

CHAPTER 2 LITERATURE REVIEW

2.1 Particle-reinforced aluminum matrix composites and their applications

Just as the name implies, the particle-reinforced metal matrix composites are composed with reinforcement and metal matrix. The primary purpose of the reinforcements in composite materials is bearing most of the applied load while the matrix bonds the reinforcement together and transfers and distributes the external load to a single reinforcement [1]. For example: metal materials, such as aluminum (Al), are prone to plastic deformation because the metal bond has no directionality [2]. Ceramic materials usually have many advantages such as high hardness, strength, modulus, high-temperature durability and low thermal expansion [1]. Therefore, by adding a ceramic reinforcing phase, various properties of metal matrix can be optimized, thereby obtaining a composite material with both excellent properties. Therefore, for the selection of reinforced particles, the performance parameters of the particles need to be considered. B_4C and SiC are currently commonly used ceramics in particle-reinforced aluminum matrix composites [3]. Its advantages and disadvantages when used as an enhanced phase are shown in Table 2-1 [4-9].

Table 2-1 Advantages and disadvantages of two ceramic reinforcements [4-9].

Particle Type	Advantage	Disadvantage
B_4C	1. Good neutron absorption. 2. High hardness, second only to diamond and cubic boron nitride. 3. Impact resistance, wear resistance, high stiffness. 4. Low density. 5. Excellent thermal stability, low thermal. expansion coefficient. 6. Remarkable chemical inertness.	1. Low fracture toughness. 2. High cost. 3. Low thermal conductivity. 4. Low electrical conductivity.

SiC	1.High strength, high hardness, high modulus and high wear resistance. 2.Excellent thermal properties, and low coefficient of thermal expansion and good thermal conductivity. 3. Low density. 4. High corrosion resistance. 5. Low cost.	1. Low fracture toughness. 2. Low electrical conductivity.

Note: The contents are cited from references 4-9.

By comparing the performance of the particle reinforcement phase, it can be found that B_4C has lower density, higher hardness, and better overall performance than Al_2O_3 particles and SiC particles [4, 5].

Taking Al-B_4C MMCs as an example, as a commonly used ceramic, B_4C has excellent properties, such as low density, high strength and hardness, and good chemical inertness [8]. The research of B_4C reference metal matrix composites have a history of several decades. The composites of aluminum (Al), titanium (Ti), iron (Fe), copper (Cu), magnesium (Mg) and other metals and B_4C have become the main research objects [10-13]. Among them, Al and its alloys have the advantages of being a light material, good toughness, low cost, and density similar to boron carbide. Therefore, using Al or Al alloy as the matrix of metal composite of Al-B_4C MMCs formed by adding B_4C has attracted much attention [14, 15].

The fabrication methods will influence the properties of aluminum matrix composites. So, it is important to know the good fabrication methods for aluminum matrix composites. Fabrication methods used for aluminum matrix composites can be broadly divided into two typical methods as powder metallurgy processing and liquid processing. Meanwhile, there are still some other methods like compo-casting, squeeze casting, spray casting, friction stir

processing, etc., but these other manufacturing processes used up to a lesser extent [16]. The details of some methods are described as follow:

Powder metallurgy: The powder metallurgy processing (route shown as Figure 2-1) is a method in which metal powder and ceramic powder are uniformly mixed and then subjected to different heat treatments after cold pressing to obtain a metal-ceramic composite material. This method allows the composite materials to have excellent dimensional capability, acceptable price, and excellent surface quality [17].

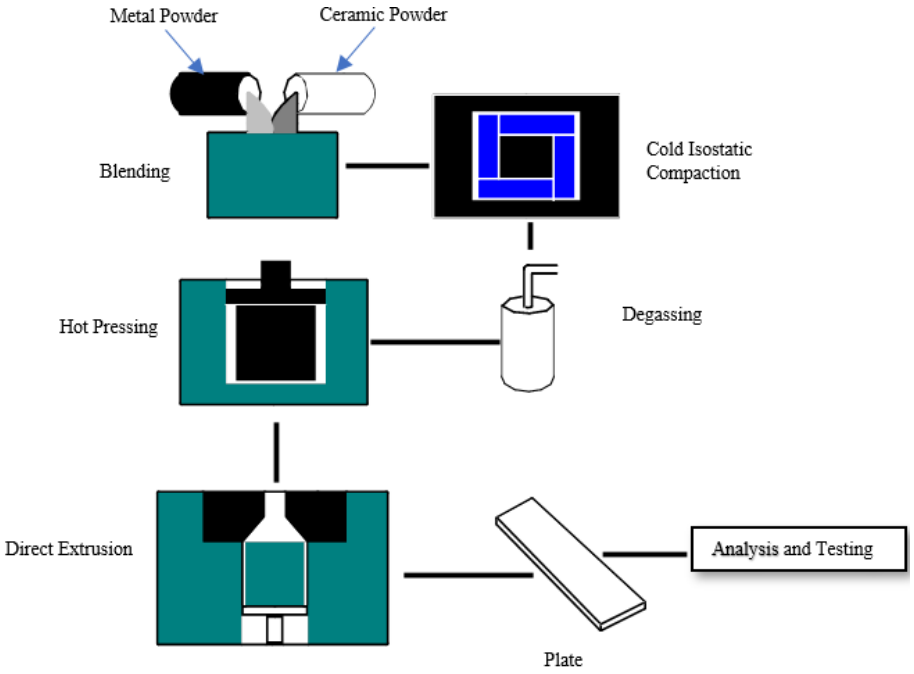

Figure 2-1 Powder metallurgy manufacturing route. Rebuilt from ref. [18].

Liquid metallurgy: By mixing B_4C powder into liquid aluminum and stirring, the advantage of this method is that it can be used in a high-efficiency and low-cost process for large-scale production. B_4C powder can be easily incorporated into liquid aluminum to ensure uniform distribution. The size and concentration of B_4C powder can be varied in a wide range (up to 30% B_4C). The process route for manufacturing Al-B_4C MMCs final product is shown

in Figure 2-2. One of the main challenges in the liquid mixing process is to control the interface reaction between the liquid aluminum and the ceramic powder. By adding Ti to the liquid aluminum, a protective layer can be formed around the surface of the B_4C, which can prevent the interface reaction and improve the wettability of the B_4C and the liquid aluminum [17, 19].

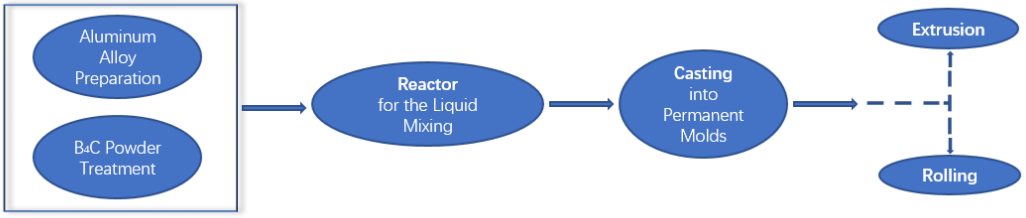

Figure 2-2 The process route for producing Al-B_4C MMCs final products. Rebuilt from ref. [19].

The stabilizing effect of Ti almost eliminates the secondary reaction phase and large particle clusters, thus ensuring the uniform distribution of B_4C particles in the liquid phase process. In addition, the density of B_4C (2.5 g/cm^3) is very close to that of liquid aluminum (2.36 g/cm^3 at 700℃). Once the B_4C particles were incorporated into the liquid aluminum and well protected in situ by Ti, neither sedimentation, segregation nor agglomeration was observed during the DC casting process. As a result, a casting structure with uniform B_4C distribution from the beginning to the end of the casting is obtained [17].

Spray casting/deposition methods: Atomized crick of molten material droplets with a very high velocity are impacted on a preheated substrate, the reinforcing particles are also co-impacted with the melt spray allowing reinforcement particles engulfment in the molten or partially molten metal droplets to form a composite [20].

Friction stir processing: Composites are manufactured when the matrix is in solid state condition. It is effective and efficient technique which can be used to refine microstructure and to fabricate MMCs [20].

The Al-B_4C MMCs has been widely used in nuclear power technology. As a component of composite materials, it is used in neutron radiation protection devices and the adjustment of high-heat fast-neutron nuclear reactor protection device. Specifically, the intrinsic property of B_4C made the Al-B_4C MMCs an attractive neutron shielding material for transport baskets, storage baskets for spent fuel, and storage barrels or neutron absorption plates. It has been widely used in armor and nuclear industry materials [21, 22]. In addition, it has certain applications in military, electronics and sports. such as bulletproof panel materials, armored vehicle materials and computer hard disk materials, bicycle frames etc. are their main application directions [23, 24].

2.2 Electrical conductivity of aluminum matrix composites

2.2.1 Measurement of Electrical conductivity

According to law of resistance, the formula related to electrical resistivity and the nature of the material is as follows:

$$R = \rho \frac{L}{S} \tag{2-1}$$

Where R is conductor resistance, ρ is the electrical resistivity of the material from which the resistance is made, L is Length of wire wound to make a resistance, S is cross-sectional area of wire wound to form a resistance. Units of R is (Ω), ρ is (Ω·m) is commonly

used in engineering technology. The conversion relationship between them is 1 μΩ·cm = 10^{-8} Ω·m = 10^{-6} Ω·cm = 10^{-2} Ω·mm^2, *L* is (m) and *S* is m^2 [25, 26].

The relationship between electrical resistivity and electrical conductivity is shown in the following formula (electrical conductivity definition formula):

$$\sigma = \frac{1}{\rho} \tag{2-2}$$

Where σ is electrical conductivity (S/m), ρ is the electrical resistivity (Ω·m). Relative electrical conductivity (% IACS) is also commonly used in engineering, which represents the electrical conductivity of materials. Internationally put standard soft copper at room temperature, the electrical resistivity ρ = 0.01724 Ω·mm^2/m is regarded as 100%, and the percentage of the electrical conductivity of other materials compared with it is the relative electrical conductivity of the material. Traditionally, we usually calculate the electrical conductivity by measuring the electrical resistivity. The method of measuring the electrical resistance of a material varies depending on the electrical resistance of the material [27, 28]. The main measurement methods include Two-Wire resistance measurements and four-wire (Kelvin) resistance measurements [29, 30] and eddy current method [31-33].

Two-Wire Resistance Measurements: As shown in Figure 2-3, the gray box is the multimeter which contains both the voltage measurement and current source. The V_M (Voltage measured at the meter) is not measured directly on the resistance under test (*R*), it is calculated by connecting the high and low pins of the multimeter. This method uses the current source and voltage measurement circuitry inside the multimeter. The measured resistance is obtained by the current supplied by multimeter (*I*) and the voltage measured at the meter (V_M). However,

the resistance of the leads from the multimeter to the resistor under test (R_{lead}) can interfere with the resistance measurement. Therefore, the equation for this measurement is as follows:

$$Measured\ \ Resistance = \frac{V_m}{I} = R + 2 \times R_{Lead} \tag{2-3}$$

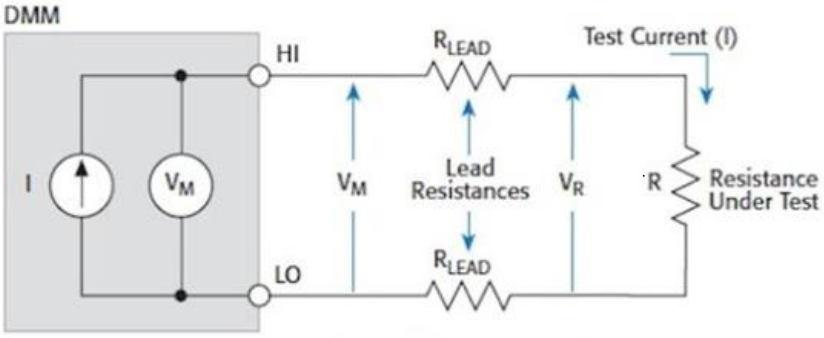

Figure 2-3 Schematic diagram of two wire resistance measurement [30].

The error of this test method mainly comes from R_{LEAD}. Since the test current (I) causes a small voltage drop across the lead resistance, the voltage (V_M) measured by the meter will not be exactly the same as the voltage (V_R) directly across the test resistance (R) and can cause considerable errors. Typical lead resistance ranges from 10mΩ to 1Ω, so it can be difficult to obtain accurate two-wire resistance measurements when the resistance under test is less than 100Ω.

Four-Wire (Kelvin) Resistance Measurements: For the four-wire method current source and voltage source are two independent machines, and the voltage sensing line is separated from the current supply line. As shown in Figure 2-4, the test current (I) is forced through the test resistance (R) via one set of test leads, while the voltage (V_M) across the device under test is measured through a second set of leads (sense leads). Although some small current

(usually less than 100pA) may flow through the sense leads, it is usually negligible and generally negligible for all practical purposes. Therefore, the voltage (V_M) measured by the meter is essentially the same as the voltage (V_R) across the resistor (R). Therefore, the determination of the resistance value is much more accurate than the two-wire method. At the same time, when the voltage sensing lead is connected close to the resistor under test, it is possible to avoid including part of the resistance of the test lead in the measurement. The equation for this measurement is as follows :

$$V_M = V_R \tag{2-4}$$

$$\frac{V_M}{I} = \frac{V_R}{I} \tag{2-5}$$

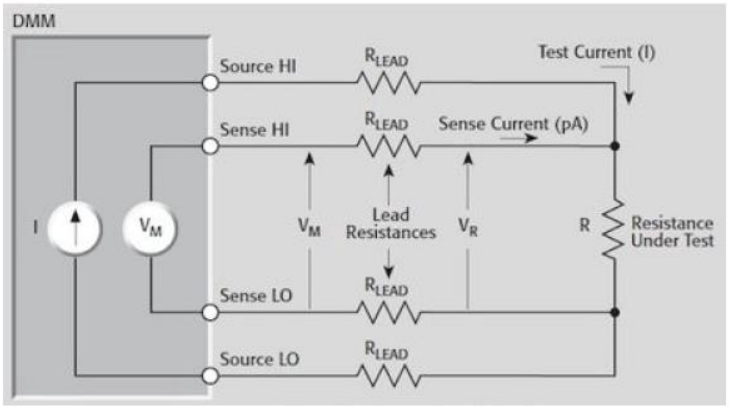

Figure 2-4 Schematic diagram of four wire resistance measurement [30].

Eddy current method: The concept of eddy current method is based on the principles of electromagnetic induction. When a coil (also called a probe) carrying an alternating current approaches the surface of the conductive material, eddy currents are induced on the surface and near the surface of the conductive material due to the alternating magnetic field generated by

the coil. The eddy current in the material generates an alternating magnetic field, which reacts to the coil. The magnitude of this reaction is affected by the conductivity of the material surface and near the surface, so that the conductivity of the non-ferromagnetic conductive material can be detected. The schematic diagram of eddy current method, as shown in the Figure 2-5 [31].

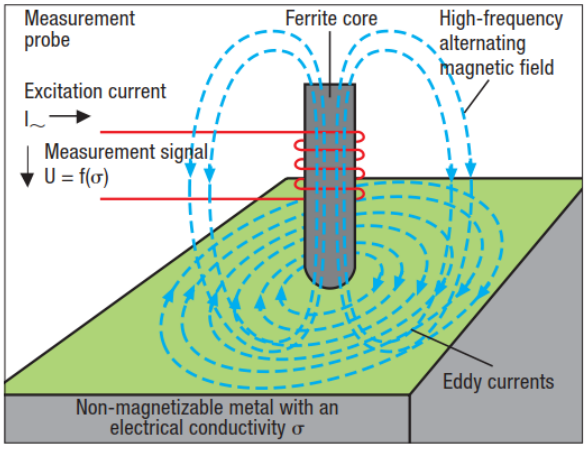

Figure 2-5 Schematic diagram of eddy current method [32].

The advantages of the eddy current method are included instantaneous results, little part preparation, no hazardous materials required, sensitive to small flaws, little to no operator danger. But there still have some limitations like the inspection is limited to electrically conductive materials, flaws that run parallel to the surface are difficult to detect, ferromagnetic materials have permeability effects that conflict with conductivity, capability is related to the skill of the operator. And the test accuracy will be affected by temperature, variations in theseparation between the probe coil and the surface of the sample, edge effect (tests should not be performed within two coil diameters of any discontinuity, such as an edge, hole, or notch unless coil manufacturer's instructions allow), uniformity of sample, surface treatments and roughness, instrument stability and sample thickness. Take the sample thickness as an example, the penetration depth δ of the eddy currents is established by the measurement frequency f, which determines the minimum permissible thickness of the specimen, as shown in the Figure

2-6. Eddy-current density decreases exponentially with depth (that is, distance from the metal surface). The depth at which the density is approximately 37 % (1/e) of its value at the surface is called the standard depth of penetration δ. Calculate the standard depth of penetration for nonmagnetic materials using one of the following formulas [31-33]:

$$\delta = \frac{1}{\sqrt{\pi \mu \sigma f}} \tag{2-6}$$

These formulas are for nonmagnetic materials when the relative permeability, $\mu_{rel}=1$. If the thickness of the sample the reference standards is at least 2.6δ, the effect of thickness is negligible. Smaller depths of penetration (higher frequencies) may be desirable for measuring surface effects. The eddy-current density decrease with depth is also affected by the coil diameter. The change due to coil diameter variation is not considered in the above equation [33].

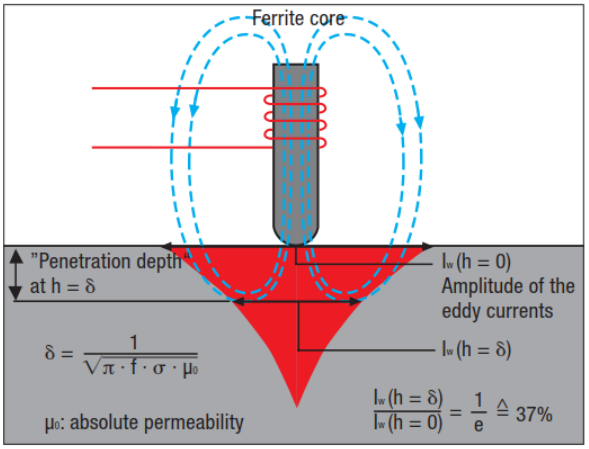

Figure 2-6 Schematic diagram of eddy current method standard depth of penetration [32].

In general, the eddy current method is the important way we use to test electrical conductivity in the experimental and industry work at present. And many electrical conductivity meters with high measurement accuracy have been developed using this principle. Take the SIGMASCOPE® SMP10 electrical conductivity meter as an example, it can measurement of the electrical conductivity of all non-magnetic metals, even stainless steel, euro coins, etc. Measurement range is 0.3-63 MS/m, or 0.5 - 108 %IAC. Measurement accuracy at +20°C: ≥ 0.5 % (1-100 % IACS) depending on the measurement frequency. Up to 16 measurements per sec, lift-off-compensation up to 0.5 mm and smallest diameter of the measurement area is 13 mm and the phase-sensitive measurement signal evaluation enables a contact-free determination of the electrical conductivity, for example, under paint or synthetic coatings of up to 500 µm in thickness. This also minimizes the influence of surface roughness [32].

2.2.2 Factors affecting the electrical conductivity of aluminum matrix composites

Adding reinforcing phases, such as B_4C and Al_2O_3, to aluminum matrix will improve the hardness and yield strength. But its electrical conductivity will be reduced to a certain extent. This is because the electrical conductivity mechanism of B_4C and Al_2O_3 is different from that of aluminum alloys [34, 35], as shown in Tables 2-2 and 2-3 [36-38]. In essence, the electrical conductivity (σ) has two influencing factors: electrons charge density ($N_e e$) and mobility (μ_e). Where N_e is the density of electron and e is the electron charge. The charge density is essentially the number of mobile electrons in the material, and the mobility is related to the mean free path. In metals, the mobility of electrons is relatively low, but the high concentration of electrons gives it a very high charge density [28].

Table 2-2 Electrical resistivity of some typical treated aluminum alloys at room temperature [37].

Alloy	Treatment	Electrical resistivity (Ω·m)
1100	H18	3.02×10^{-8}
3004	-	4.1×10^{-8}
6061	T6	4.0×10^{-8}
6351	T6	3.8×10^{-8}

Note: The data are cited from reference 37.

Table 2-3 Electrical resistivity of particles at room temperature [36, 38].

Particle Type	Electrical resistivity (Ω·m)
B_4C	7.14×10^{-4}
Al_2O_3	1×10^{12}

Note: The data are cited from reference 36 and 38.

Fickett et al. [39] found that the electrical conductivity of of "pure" aluminum is affected by phonons, electrons, internal and external interfaces, vacancies and gaps, chemical impurities in the forms of metal elements, Kondo-type differences, dislocations and stacking faults, superconductivity and magnetic fields, and the impact of interactions between mechanisms.

However, B_4C is a semiconductor and Al_2O_3 is insulator [40, 41]. Different structures determine different scattering mechanisms and electronic conductive mechanisms. Taking semiconductors as an example, the electrical conductance reaction is the transport characteristics of charge carriers in an external field, as well as the number and type of carriers (electrons or holes). Specifically, the electrical conductivity of electrons is as follows [28, 42, 43]:

$$\sigma = ne\mu_e + pe\mu_h \tag{2-7}$$

Where σ is electrical conductivity, n is the electron concentration, e is the electric charge of electrons, μ_e is the mobility of electrons, p is the holes density, μ_h is the mobility of holes.

$$\mu_e = e\tau_e / m_e \ ; \ \mu_h = e\tau_h / m_h \tag{2-8}$$

Where τ_e is the collision time, m_e is the electron mass; τ_h is the collision time, m_h is the hole mass. Semiconductor conductors usually have both electrons and holes, so for semiconductors, their electrical conductivity is the sum of the two [42]. Since the electrical conductivity of the resulting composite material is determined by the matrix alloy and the embedded particles, there are many factors that affect the electrical conductivity.

The electrical properties of aluminum matrix composites are related to the properties and morphology of their components. Among them, the electrical conductivity of the constituent phases, the volume fraction and distribution of the constituent phases, the size, shape, orientation and spacing of the constituent phases, and the interaction between the constituent phases will affect the electrical conductivity of aluminum matrix composites [44].

First of all, the type of reinforcement particles is very important, especially the electrical conductivity of the particles. To improve the mechanical properties, the aluminum matrix is usually combined with non-conductive or semiconducting particles. However, the addition of non-conductive particles (see the example in Figure 2-7 [45]) will significantly reduce the electrical conductivity of the metal [34, 35].

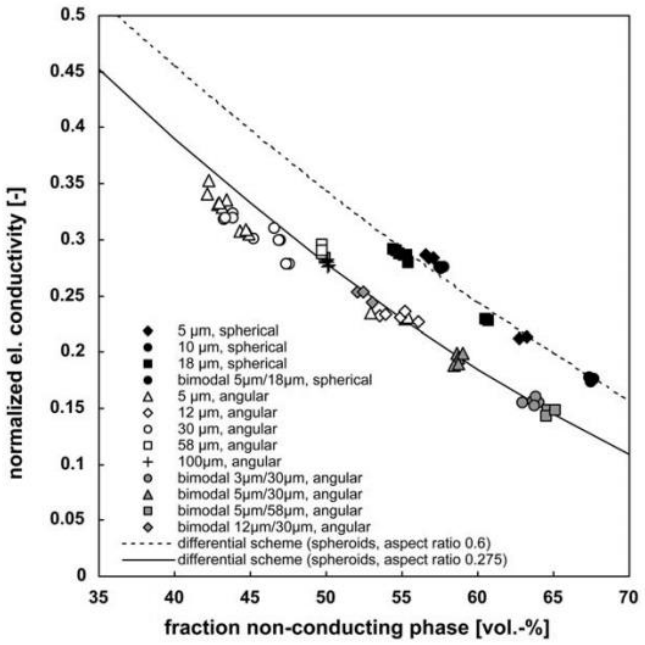

Figure 2-7 The electrical conductivity of various average particle sizes and two different shapes of aluminum/alumina particle composites varies with the volume fraction of the non-conductive phase. Authorization obtained from 2003 Elsevier [45].

For the semiconducting particles, taking Al-B_4C MMCs as an example, the volume ratio or content of B_4C in aluminum matrix composites is very important. As the B_4C content increases, the electrical conductivity of Al-B_4C MMCs will decrease, as shown in Figure 2-8. Since B_4C particles are semiconductors, when Al is replaced by semiconductor compounds such as B_4C, it will reduce the electrical conductivity of Al-B_4C MMCs nanocomposites. On the other hand, B_4C particles are the source of electron dispersion in Al-B_4C MMCs nanocomposites, which further limits the electrical conductivity of Al-B_4C MMCs nanocomposites [34]. This rule also applies to other aluminum matrix composites with non-conductive or semiconducting particles.

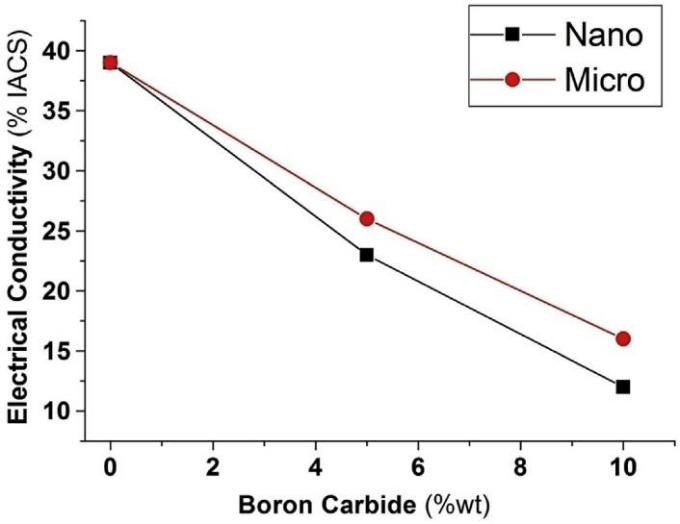

Figure 2-8 Electrical conductivity of Al-B_4C vs. the content of B_4C (wt%) with nano- and micro-size. Authorization obtained from 2019 Elsevier B.V. [34].

In addition, the size of B_4C particles will also affect the electrical conductivity of Al-B_4C MMCs. Because nanoparticles have a smaller size and higher specific surface area, which results in closer distance between particles than micro-particles, then the electrical conductivity of aluminum matrix composites reinforced with B_4C nanoparticles is lower than that of B_4C micro-particles. This is confirmed in Figure 2-8. The same phenomenon was found in Yao et al. [46] study on Al-SiC MMCs, where the conductivity of Al-nano SiC (15 nm) is about 1/5 that of Al-micro SiC (2 μm).

Meanwhile, the uniformity of particle distribution also has a certain effect on electrical conductivity. If the particles are not well distributed in the aluminum matrix, they will behave like two separate phases, so they will not interact with each other. There are many channels inside the material, and electrons can easily move in these channels without being affected by the semiconductor B_4C particles, resulting in higher electrical conductivity than the uniform distribution [35].

2.2.3 Predictive model of the electrical conductivity

It can be seen from the above that there are many and complex factors that affect the conductivity of aluminum matrix composites. Therefore, while studying the preparation methods of particle-reinforced composite materials, researchers have also done a lot of work on the electrical conduction behavior and theoretical models of composite materials [47].

From a practical point of view, it is important to predict the change in electrical conductivity with the increase in the volume fraction of reinforcing particles. Initially, researchers used the simplest mixing rule to predict the electrical conductivity. When the electrical conductivities of both phases are comparable, the parallel model (equation 2-9) is usually satisfied [44].

$$\sigma_{eff} = \sigma_p \phi + \sigma_m (1-\phi) \tag{2-9}$$

Where σ_{eff} is the effective electrical conductivity, σ_p is the electrical conductivity of particle, σ_m is the electrical conductivity of matrix, ϕ is the volume fraction of particle.

In the nineteenth century, Maxwell also conducted certain research on this aspect [48]. Maxwell's equation was originally applied to infinitely diluted spherical filler particles. It assumes that, in the case of dilution, the intensity field in the composite material is proportional to the average intensity field in the matrix, but when calculating the matrix field, the weighted average of the intensity field and the volume fraction of inclusions in the matrix is equal to the remote application an intensity field.

According to the Maxwell equation, the exact expression for the effective electrical conductivity is given by [48]:

$$\frac{\sigma_{eff}}{\sigma_m} = 1+3\frac{(\sigma_p - \sigma_m)}{(\sigma_p + 2\sigma_m)}\phi \tag{2-10}$$

Wagner extended the Maxwell model to higher concentrations of dispersed phase and proposed the Maxwell-Wagner equation (also known as Wiener's rule) [49]:

$$\frac{(\sigma_{eff} - \sigma_m)}{(\sigma_{eff} + 2\sigma_m)} = \frac{(\sigma_p - \sigma_m)}{(\sigma_p + 2\sigma_m)}\phi \tag{2-11}$$

The effective medium (EM) theory, which is also called Model of Bruggeman, was first proposed by Bruggeman in 1935 and can be showed as [50]:

$$\frac{(\sigma_p - \sigma_{eff})}{(\sigma_p - \sigma_m)}\left(\frac{\sigma_m}{\sigma_{eff}}\right)^{\frac{1}{3}} = (1-\phi) \tag{2-12}$$

However, the EM theory is not suitable for the percolating systems where the particles may encounter each other, making the area of validity of this model limited to the dilute cases. Hence, the classical percolation theory has been applied to describe the conducting performance of percolating systems. But the percolation theory has two shortcomings. One is that it is only applicable in the situation with a huge property difference of components. The other is the phenomenological nature of the percolation equation with fitting parameters that bear no clear correlation to the actual features of microstructure [51].

Researchers developed some new models or equations to predict effective electrical conductivity of concentrated particulate composites. For instance, using a differential scheme combined with the solution of an infinitely dilute dispersion of particles in a continuous matrix, two new equations were proposed in 2007 [52]. The second of the new equations can be written as:

$$\frac{(\sigma_p - \sigma_m)}{(\sigma_p - \sigma_{eff})}\left(\frac{\sigma_{eff}}{\sigma_m}\right)^{\frac{1}{3}} = \left(1 - \frac{\phi}{\phi_m}\right)^{-\alpha\phi_m} \quad (2\text{-}13)$$

Where ϕ_m is the maximum packing volume fraction of particles where the particles contact each other, and α is a constant of the unity order. In the special circumstance of $\alpha = 1$ and ϕ_m =1, this model reduces to the classical Bruggeman equation.

2.3 Thermal conductivity of aluminum matrix composites

2.3.1 Measurement of thermal conductivity

Thermal conductivity is defined as:

$$K = -\frac{Q}{\nabla T} \quad (2\text{-}14)$$

Where Q is the heat flow rate vector across a unit cross section perpendicular to Q , T is the absolute temperature and ∇T is the gradient of the temperature [43].

In scientific experiments and engineering design, the thermal conductivity of the materials used need to be accurately measured by experimental methods. So, choosing the appropriate test method is the most important thing.

At present, the measurement methods of thermal conductivity are divided into two categories: steady-state method and transient method, which have their own different test principles [53, 54]. There are four typical measurement methods introduced in detail as follow:

A. **Steady-state method**

The guarded hot plate (GHP): the guarded hot plate is the most used and most effective method for measuring the thermal conductivity of insulation materials. The disadvantage is time-consuming and other potential disadvantages are that the temperature gradient must be relatively large, the specimen width must be large, but size is usually not a serious issue, the contact resistance between the thermocouple and the specimen surface poses a major source of error. In addition, the accuracy of this method is not good. Despite these disadvantages, the standardized GHP method is the ideal apparatus for researchers and scientists in the field of insulation testing and it is considered an absolute measurement method. The practical applicability requires careful consideration of the array content: (a) attaining steady-state conditions; (b) the unidirectional heat flow in the area under analysis, the temperatures of the hot and cold surfaces, and the specimens' thickness; and (c) other factors influencing the unidirectional heat [54].

The guarded hot-plate setup is comprised of cold plates, a hot plate, a system of guard heaters, and thermal insulation. Hot plate is electrically heated, and the cold plates are Peltier coolers or liquid-cooled heat sinks. The configuration is arranged symmetrically, with guarded hot plates located on the sides while the heater unit is sandwiched between two specimens or a single specimen and an auxiliary layer. The guarded hot-plate measurements are analyzed on the fundamental of the heat transfer in the infinite slab geometry. Since specimen dimensions are finite, unidirectional heat flow is achieved through the use of guard heaters. The

temperature of a thermal guard is maintained at the same temperature as its adjacent surface (which is considered as an auxiliary heater/heat sink), to prevent heat loss from the specimen and heat source/heat sink, and as a result, unidirectional heat flow is attained. After a steady state is reached, the heating and cooling plates have stable temperatures. Then the thermal conductivity can be determined based on the heat input, the temperature difference through the specimen, the thickness of the specimen, and the size of the metered area of heat transfer. Steady-state conditions may change with respect to specimen type, specimen size, and mean temperature [54].

Take the two-specimen apparatus (Figure 2-9) as an example, the specimens of the homogeneous material with the same thickness are interposed between the hot guard heaters and the cold plates. For two specimen apparatuses, the auxiliary heaters may be placed above and below the specimens. A well-defined, user-selectable temperature difference is established between the hot and the cold plates. The power rate input in the hot plate with metered area A is measured when thermal equilibrium is reached at steady-state conditions. When the control system is used, the plate temperatures reach stability. It is assumed that the measured heat power rate is transferred across the specimen due to guarded heaters. After thermal equilibrium has developed and the heating and cooling plates are kept in stable temperatures, the thermal conductivity can be calculated from the input values. The input values are the heat power Q, the temperature differential across the specimen ($T_{hot} - T_{cold}$), the specimen thickness (Δx), and the heat transfer area (center metered area, A). From the measured input values, the effective thermal conductivity can be calculated using the following unidirectional steady-state heat transfer equation [54]:

$$k_{eff} = \frac{Q}{2} \frac{\Delta x}{A \cdot \Delta T} \tag{2-15}$$

Where the heat flow Q is obtained by measuring a power (or half power for two specimen) generated in an electrical heater.

As a requirement the apparatus must test two specimens simultaneously in the form of a slab with a standard size (such as 300 mm × 300 mm or different sizes). A fixed heat rate must be applied by an electric heater. This arrangement produces a heat flow across the two specimens, flowing outward toward two plates chilled by a Peltier or a liquid cooling system. The main advantage is that heat loss from the hot plate can be controlled more effectively due to the symmetrical arrangement of the specimen on each side of the heater. Unlike the single-specimen method, the symmetrical setup can be used for investigating solid materials. For measuring the thermal conductivity of nonsolid materials, it is necessary to heat the specimen from the top to avoid convection [54].

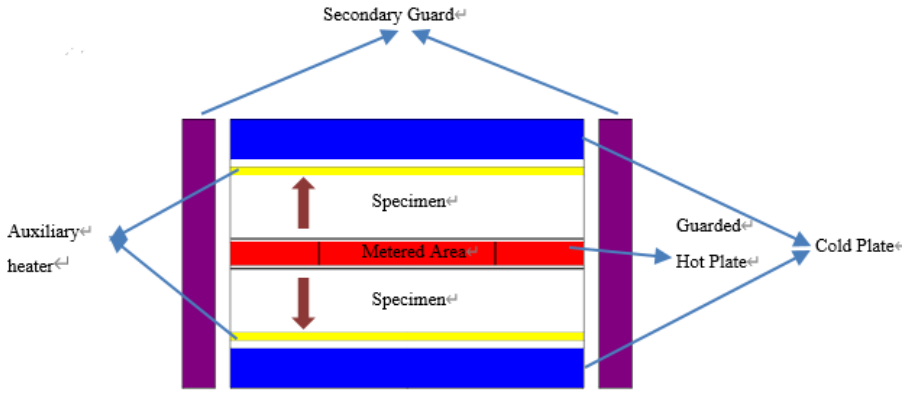

Figure 2-9 The apparatus of guarded hot-plate method for thermal conductivity measurement. Rebuilt from ref. [53].

The GHP is most suitable for dry homogeneous specimens, but it is unsuitable for materials in which there is a potentiality for moisture migration. It can be used to test the thermal properties of nonmetals such as thermal insulation materials, polymers glasses, and ceramics, as well as liquids and gases in the temperature range between about 80 and 800 K. Additionally, determining the temperature difference is a major challenge with the GHP method when measuring materials with high thermal conductivity, such as metals. Therefore, in these types of tests, the contact resistance between the specimen and the heater or cold plate must be considered [54].

The heat-flow meter: heat-flow meters are accurate and fast apparatuses and is easy for measuring the thermal conductivity of low-conductivity materials. The maximum temperature limits are approximately 200°C for the heat-flow meter method and about 100°C in practical applications. The heat-flow meter design resembles to setup of the single-specimen guarded hot-plate apparatus. The basic idea of the heat-flow meter is deducing the heat flux based on the measurement of a drop in temperature throughout a thermal resistor.

The specimen is placed between two plates held in different temperatures, with one being heated and the other plate being cooled, as shown in Figure 2-10. Heat flux transducers are used to measure the heat flow through the specimen. The heat flux is determined in a current with the measurement of a voltage drop through an electrical resistor. Sensors provide an electrical output signal. The measured signal and the change in thermovoltage are proportional to the drop in temperature drop occurring throughout the plate Heat flux sensors are most often composed of a series of connections of thermocouples spanning a thermal resistor, e.g., a thin ceramic or plastic plate. A second heat flux is occasionally applied at the cold plate is in order to measure radial heat loss and also to reduce the time needed for the measurement. This reduction intime poses an advantage for this method when measuring of insulation materials.

The temperature of the plates is measured and adjusted to the desired set point when reaching a constant value. Steady-state conditions occur when the amount of heat flux is equal at each point of the layered system. After thermal equilibrium is established, the test is determined under the conditions. In order to calculate thermal conductivity, the steady-state temperatures, the specimen's thickness, the specimen's metered area, and the heat flux input to the hot plate are used. The heat flux output is usually calibrated with various reference standards [54].

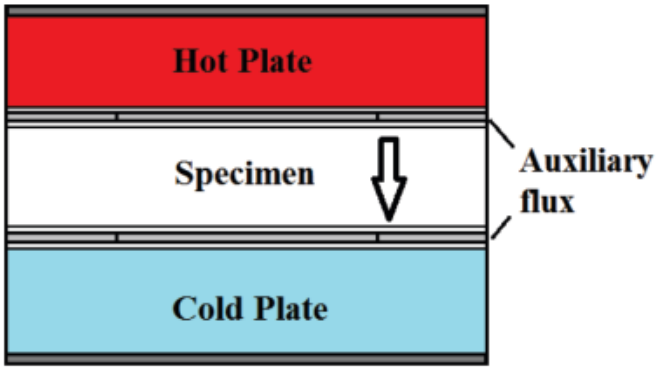

Figure 2-10 Schematic design of heat-flow meter basically [54].

Insulation materials and polymers ($k < 0.3$ W/ (m K)) are usually tested via the heat-flow meter method, and sometimes it is used for glasses and ceramics and for other materials with thermal conductivities lower than about 5 W/(m K). For insulation materials at about room temperature, the measurement uncertainties are approximately 3%, and at high temperatures the uncertainties are between 10 and 20%. Steady-state stability can be reached in short times, resulting in productivity gains. The stable case, however, is valuable for providing repeatability, the long-term consistency of a specimen [54].

B. **Transient method:**

The transient planar heat source method (TPS): TPS uses an instantaneous thermal plane probe (Hot Disk probe), which is also called the Hot Disk method. The Hot Disk probe is made of thermal resistance material nickel, covered with insulating material (polyimide, mica, etc.), and the probe has a self-heating function.

As shown in Figure 2-11, the principle of this method is that a temperature probe with self-heating function is placed in the sample, and a constant heating power is applied to the probe during testing to increase the temperature. The thermal resistance coefficient of nickel-the relationship between temperature and resistance is linear, and the heat loss can be known by understanding the change of resistance, which reflects the thermal conductivity of the sample. Then, the relationship between the temperature change with time on the probe itself and the spherical surface separated from the probe by a certain distance is measured, and the thermal conductivity and thermal diffusivity of the sample are obtained through mathematical model fitting.

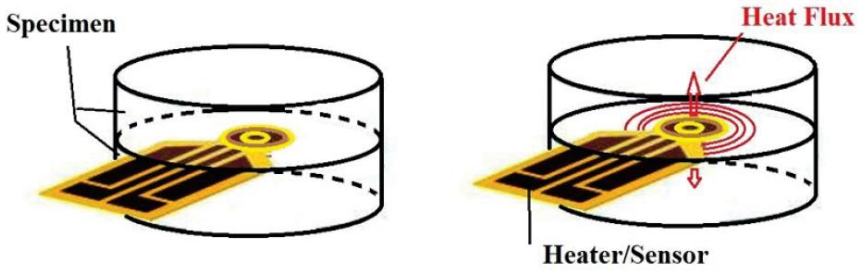

Figure 2-11 The schematic and principle of the hot disk [54].

This method is able to measure thermal conductivity, thermal diffusivity and heat capacity per unit volume at the same time. The property can be measured in a temperature range between 0.005-500W/(m·K), and high accuracy (±3%), good repeatability (±1%), short

measurement time (single measurement 3-5min) and easy operation. In addition, the main advantages of the hot-disk measurement are that it produces results quickly (usually in under 10 min), and that different sensor sizes can be used to accommodate different specimen types. And the hot disk requires using specimen sizes that are usually much smaller than those used in other techniques. Meanwhile, it can teste samples like metals, alloys, ceramics including high conducting ceramics like aluminum nitride (AlN), high critical temperature materials, minerals, polymers, composites, glass, fabrics, paper, glass wool, foam, powder, biomaterial, and liquids, as well as materials with anisotropic thermal properties, etc. It is not affected by contact thermal resistance, and has and high accuracy [54].

Laser flash method: It is one of the most often used methods for ascertaining the thermal properties of solids. The method can investigate to properties of glasses, metals, and ceramics without significant limitations due to uncertainties of the achievable measurement [53]. The property can be measured in a temperature range between 100 and about 3000℃.

This method original proposed by Parker [55]. It assumes an isotropic and adiabatic sample (no heat loss). The thermal diffusivity (α) is determined from the thickness (L) of the sample and the time ($t_{1/2}$) the thermogram takes to reach half of the maximal temperature increase. It can be used, with additional measures, to also measure other thermophysical properties (specific heat (C_p), thermal conductivity (K), etc.). If given the density of a material the thermal conductivity can be calculated by using the following equation [55-57]:

$$\alpha=0.1388\left(\frac{L^2}{t_{1/2}}\right)\rightarrow \alpha=K/\rho C_p \tag{2-16}$$

The principle of laser flash test method like follow [55-57]:

For the thermal diffusivity measurement, it is fast while providing values with excellent accuracy and reproducibility. This method is conducted through heating a specimen with a short laser pulse on the front side, and the temperature increase on the rear face is recorded as a function of time. The thermal diffusivity is then determined from this thermogram. Figure 2-12 shows the schematic and principle of the laser flash method.

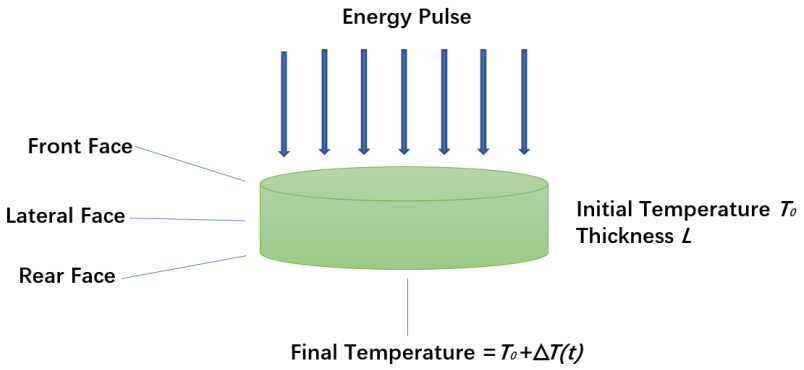

Figure 2-12 The schematic and principle of the laser flash method. Rebuilt by ref. [56].

The characteristic shape of the temperature increase curve is depicted in Figure 2-13. If no heat loss is involved, the temperature of the rear face will rise to a maximum and remain at that level indefinitely.

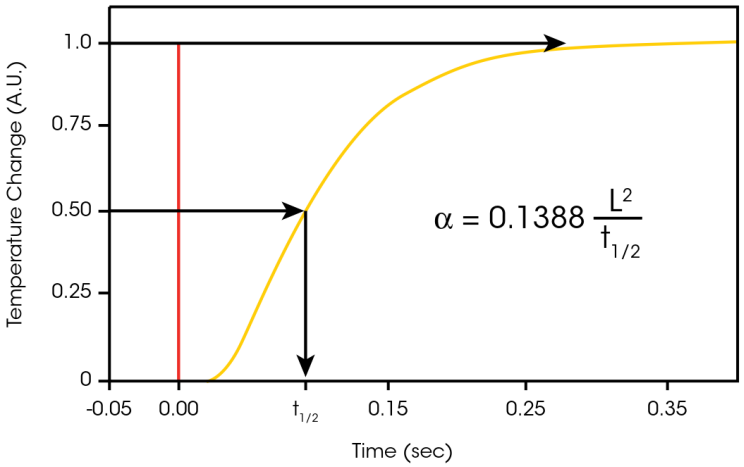

Figure 2-13 The schematic for temperature increases [56].

For the specific heat capacity measurement theory by laser flash method the process is more complex than thermal diffusivity. It includes temperature rise, quantitative definition of the heat pulse, intervening media: for other than ambient testing, it is usually necessary to isolate the sample from the ordinary environment. The window (s) that are placed between the laser and the sample have a certain amount of absorption and reflection associated with them. Even coated windows, (designed to minimize the latter), have serious problems at elevated temperatures. It is not unusual to lose 10 to 15% of the energy per surface in addition to the attenuation caused by the body itself. Mirrors and optics, if used further complicate putting an exact figure on these losses. These properties are also temperature and time sensitive. In addition, the problems associated with the sample also have influence, equally important to defining the exact overall magnitude of the pulse is the fraction which is actually absorbed by the sample. There are a number of conditions impacting upon this, such as the configuration and thermal limitations [55].

Major advantages are that the test requires very small, usually 12 mm diameter and few millimeters thick samples and it is very fast; the actual measurement takes few seconds, and the same instrument can test a very broad range of thermal diffusivities. It can be used to test samples up to much higher temperatures than steady state methods, even to melting in some cases. Major disadvantages of the flash method: the equipment is usually expensive due to the heat pulse generation, the optical detection and the high-speed data acquisition; porous and non-homogeneous materials require special care to properly process the thermogram [55-57].

2.3.2 Factors affecting the thermal conductivity of aluminum matrix composites

There are many factors that affect the TC of aluminum matrix composites. In essence, the propagation mechanism of heat in aluminum matrix composites is the fundamental reason that affects the thermal conductivity of aluminum matrix composites. However, it is manifested in the physical structure and properties of the matrix and particles, as well as the influence of the interface reaction on the thermal conductivity [43, 58].

Heat energy can be transmitted through solids via electrical carriers (electrons or holes), lattice waves (phonons), electromagnetic waves, spin waves, or other excitations. In metals electrical carriers carry most of the heat, while in insulators lattice waves are the dominant heat transporter. Normally, the total thermal conductivity K can be written as a sum of all the components representing various excitations:

$$K = \sum_{\alpha} K_{\alpha} \tag{2-17}$$

Where α denotes an excitation.

The heat conduction in metal solids is realized through lattice vibrations and electron movement, so it can be described together with "phonon gas" and "electron gas" The equation is as follows:

$$K = K_l + K_e \tag{2-18}$$

Where K is the thermal conductivity in metal solids, K_l is the thermal conductivity of phonon gas, K_e is the heat conduction of electron gas.

Equation (2-18) can then be generalized to

$$K = \frac{1}{3}\sum_{\alpha} C_\alpha v_\alpha l_\alpha \tag{2-19}$$

Where C is the total specific heat, v is the velocity , l is the mean free path and the summation is over all excitations, denoted by α [43].

During the movement of phonons and electrons, they collide with impurities, defects, grain boundaries, phase boundaries, etc. in the crystal, causing scattering of electrons and phonons, and also causing some anharmonic effects. At the same time, the addition of trace elements and heat treatments will also have an impact on thermal conductivity. At present, the effects of element solid solution, second phase precipitation, extrusion temperature and deformation degree on alloys has been studied. These factors will all affect the thermal conductivity of Al [43, 59-61]. For example, after extrusion, most of the crystal grains become equiaxed crystals, the size of the crystal grains is not uniform after extrusion, and the particles aggregate in the as-cast state. The impurities are broken, and the pores are compressed [62].

These factors will affect the thermal conductivity of Al alloy. In addition, temperature also has a certain effect on the thermal conductivity. High temperature reduces the mobility of the electrons, thereby reducing the thermal conductivity. But this allows heat to be conducted through the movement of the lattice, so the thermal conductivity of the metal shows a different law of change: as the temperature rises, it keeps, slightly increases, or slightly decreases [43].

The thermal conductivity difference comes from the different relaxation times of phonons. For semiconductors: B_4C (17-42 W/(m·K)) and SiC (490 W/(m·K)), the heat conduction process is mainly through the crystal lattice [63, 64]. For a perfectly ideal crystal the thermal conductivity is determined by the inverse process of phonon collision, the model is given as follow [65]:

$$\begin{cases} l \propto \frac{1}{n} \approx \frac{k_B T}{hw}, T >> \theta_D \\ l \propto e^{\theta_D / 2T}, T << \theta_D \end{cases} \quad (2\text{-}20)$$

However, the thermal conductivity (phonon propagation) of a material is not only dependent on temperature. Defects in the actual material materials also decrease the mean free path of phonons (i.e., decrease in phonon relaxation time). In fact, there are four main mechanisms of phonon scattering that affect the properties of heat conduction: The process of phonon collision. The thermal resistance caused by phonon collision and scattering is the main source of thermal resistance in the crystal, and it is more significant when the temperature is higher than the Debye temperature; Phonon scattering caused by point defects. The change in thermal resistance caused by point defects has nothing to do with temperature; Grain boundary scattering; Phonon scattering caused by dislocations. Therefore, the material composition, impurities and their state, grain size and number of grain boundaries, defects, etc., will all affect

the thermal conductivity of B_4C [43, 63, 64].

It can be seen from above that the transmission of thermal energy in MMCs is achieved through the transmission of lattice waves (phonons) and free electrons. The ability of phonons and free electrons to transmit thermal energy will be weakened by the scattering of geometric interfaces. Thereby reducing the thermal conductivity of the composites. The particle content and particle size determine the size of the scattering area. The more particles in the composites and the finer the particle size, the larger the scattering area provided and the greater the reduction in the thermal conductivity of the composites. When the particles of the same content are distributed differently in the matrix, the geometric interface formed by the particles and the matrix has different scattering effects on the phonons and free electrons in the direction of heat conduction. If the scattering effect produced by uniformly distributed spheres is used as a comparison standard, then the more uneven the particle distribution, the worse the symmetry of the particle shape, the more the scattering effect will deviate from this standard, and this deviation can be positive or negative. This will increase or decrease the thermal conductivity of composites [43, 66].

Specifically, the factors that affect the thermal conductivity of aluminum matrix composites can basically be classified according to the reinforcement phase and processing technology, and temperature will have some influence on it. The thermal conductivity, volume fraction, distribution, size, etc. of the reinforcing phases, porosity, and the interface between the reinforcing phase and the aluminum matrix will all affect the overall thermal conductivity of the material [66-68].

A. The effect of reinforcement particle volume fraction on thermal conductivity of particle reinforced aluminum matrix composite

The volume fraction of the reinforcement particles in the particle-reinforced aluminum matrix composite material has the greater impact on the thermal conductivity. It is generally believed that the larger the volume fraction of the reinforcing particles, the smaller the thermal conductivity. For example, Chen et al. [19] through research on Al-B_4C MMCs at room temperature (25℃), it is found that the thermal conductivity decreases with the increase of the B_4C content in the matrix. The following data is obtained by this studying that the thermal conductivity is 195 W/(m·K), when the B_4C volume fraction is 6%, while it changes to 173W/(m·K), with increasing volume fraction of B_4C to 15%, and further decreases to 120W/(m·K) when the volume fraction of B_4C increases to 30 %. Meanwhile, Lee et al. [69] obtained through the studying the thermal conductivity of SiC_p/Al MMCs found that after adding high content of SiC particles, with the SiC particles volume fraction increase the thermal conductivity decreases. Yang et al. [70] through research on diamond/Ag composite materials found that the thermal conductivity decreases with the increase volume fraction of diamond particles.

Researchers studied thermal conductivity prediction models to better explore the relationship between thermal conductivity and particle volume fraction. They found that the thermal conductivity of composites is not only related to the volume fraction of the reinforcement but also to the thermal conductivity of each component phase. Theoretically, when the thermal conductivity of the particle phase is greater than the thermal conductivity of the matrix phase, then the thermal conductivity of the composite material should be greater than the thermal conductivity of the matrix material, and with the increase of the volume fraction, the thermal conductivity of the composites should be gradually increased [70-72]. However, the actual results are contrary to this. This is because the thermal conductivity of

particle-reinforced metal matrix composites is also closely related to particle distribution and interfacial thermal resistance. In general, the particle phase of composites prepared under mature process can be uniformly distributed, so the influence of particle distribution on its thermal conductivity can be negligible. The interfacial thermal resistance has a strong influence on the thermal conductivity due to the different compatibility of the sonic velocity (phonon frequency and Debye temperature) of the reinforcing particles with the metal [70, 73, 74]. Therefore, exploring the thermal conductivity and interfacial thermal resistance of composites is a key issue.

B. The effect of the interface between reinforcement and aluminum alloy matrix on the thermal conductivity of composites

Ma et al. [75] have shown that the poor interfacial wettability of particle-reinforced aluminum matrix composites results in a large number of pores remaining after infiltration. Since thermal conductivity decreases with increasing porosity, the thermal conductivity of composites is affected and decreases. Meanwhile, Sun et al. [76] found that this phenomenon also exists in diamond/Al composites with B_4C coatings. In addition, if the reinforcing phase reacts with the matrix, the thermal conductivity of the material can also be affected. For example, Kawai et al. [77] believed that the Al_4C_3 or $MgAl_2O_4$ reaction layer easily existed in the Al-SiC MMCs, which would reduce the thermal conductivity of the material, and this adverse effect increases with the degree of interfacial reaction. But Chu et al. [78] found that a small amount of Al_4C_3 produced in infiltrating SiC_p/Al MMCs can increase the thermal conductivity. They believe that appropriate interfacial reactions can enhance interfacial bonding and reduce interfacial thermal resistance. However, Al_4C_3 is easily decomposed in contact with water, which leads to debonding of the interface and greatly reduces the stability of the composites [79-81]. Therefore, the research on the influence of Al_4C_3 on the thermal conductivity of aluminum matrix composites needs to be further explored. At present, the

optimization methods of diamond/Al interface can be divided into three types: metal-based alloying, diamond surface coating and advanced forming technology. Through interface optimization, a layer of carbide can be formed between the diamond and the metal matrix to improve the bonding strength of the interface, reduce interface defects, and thus improve the thermal conductivity of the interface. Metal matrix alloying or application of diamond surface coatings are effective methods to prevent Al_4C_3 formation by introducing an interfacial layer between Al and diamond. Many researchers have combined theoretical models and experiments to study the effect of diamond/Al composite interface structure on thermal conductivity and interfacial thermal resistance, which greatly improves the thermophysical properties of composites [81-85].

C. The effect of reinforcement particle size on thermal conductivity of composites

The particle size of the reinforcing particles also has a great influence on the thermal conductivity. It is generally believed that when the volume fraction is constant, the larger the particle size, the greater the thermal conductivity, as shown in Figure 2-14. For example, Hasselman et al. [86] found that with the increase of particle size in SiC_p/A1 composites, the interfacial area per unit volume of the composites decreases, and the influence of the interfacial thermal resistance decreases, resulting in an increase in the thermal conductivity of the composites. Researchers [70, 86, 87] have found that when the particle size is less than 10 μm, the thermal conductivity of the composite is lower than that of the matrix alloy due to the large amount of interfacial thermal resistances. Only when the average particle size is greater than 10 μm can the thermal conductivity of the composite be higher than that of the base alloy. This is consistent with the study of particle critical radii in EMT (Effective Medium Theory). When the particle size of the reinforcement is smaller than the critical radius, the thermal conductivity of the composite material is smaller than that of the matrix. Only when the particle size of the reinforcement is larger than the critical radius, the reinforcement particles can become an

effective medium and contribute to the thermal conductivity of the composites.

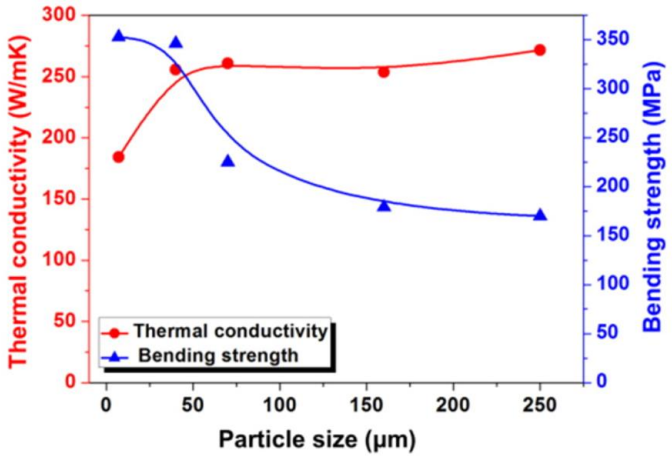

Figure 2-14 The effect of SiC particle size on the thermal conductivity and flexural strength of aluminum-silicon carbide composites. Authorization obtained from 2015 Elsevier [68].

D. The effect of particle morphology on the thermal conductivity of composites

In general, particle geometry has a significant effect on thermal conductivity. Wang et al. [66] conducted a simulation study on high volume fraction SiC particle reinforced aluminum matrix composites (SiC_p/Al) composites and found that the thermal conductivity of spherical particles is greater than that of irregular particles under the same volume fraction. The thermal conductivity of the composites is because the spherical particles have the smallest surface area, so the more irregular the particle surface, the larger the total surface area under the same volume fraction, the greater the interfacial thermal resistance, and the lower the thermal conductivity should be. However, Tekce et al. [88] found that in copper-reinforced polymer composites, the thermal conductivity of the composites of plates is greater than that of spherical particles at the same volume fraction. As shown in Figure 2-15, at a volume fraction of 30 vol%, the thermal conductivity of the composites of plates is 3.7 W/(m·K) and that of spherical particles is 1.1 W/(m·K).

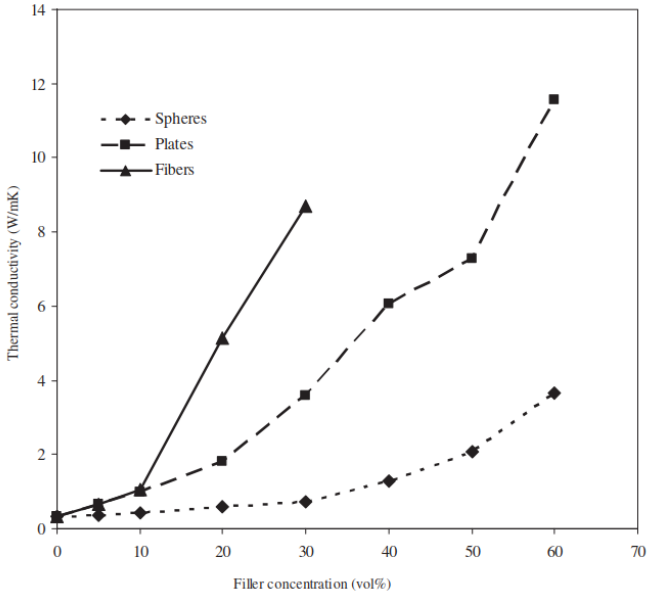

Figure 2-15 The effect of copper particle shape on the thermal conductivity of copper reinforced polymer composites. Authorization obtained from 2007, SAGE Publications [88].

E. The effect of temperature on the thermal conductivity of aluminum matrix composites

Chen et al. [19] found that 1100-B_4C MMCs generally have good thermal conductivity, and the thermal conductivity at high temperature 100-300℃ is almost independent of temperature. Meanwhile, S. V. et al. [89] found that the thermal conductivity curve of the Al-B_4C MMCs exhibits a smooth decreasing slope with increasing temperature throughout the measurement interval. The thermal conductivity remained basically unchanged in the range of 100-300℃ while the Al-B_4C MMCs decreased from 120 to 115 W/(m·K) at 300-600℃.

2.3.3 Predictive model of the thermal conductivity of aluminum matrix composites

It can be seen from the above that there are many and complex factors that affect the thermal conductivity of aluminum matrix composites. Therefore, while studying the preparation methods of particle-reinforced composites, researchers have also done a lot of

research on the thermal conduction behavior and theoretical models of composites.

From a practical point of view, it is important to predict the change in thermal conductivity with increasing volume fraction of reinforcing particles. Parallel model (equation 21) is suitable when the second phase appears as isolated spherical particles, and both matrix and second phase aligned parallel to the direction of heat flow. [90]. The effective thermal conductivity is given by:

$$k_{eff} = k_p\phi + k_m(1-\phi) \tag{2-21}$$

Where k_m is thermal conductivity of the matrix, k_p is thermal conductivity of particles, the dependence of the effective electrical conductivity on the volume fraction is linear, and the k_{eff} is effective thermal conductivity of the composite material.

In the last century, Maxwell also conducted certain research in this area. Maxwell's equation was originally applied to infinitely diluted spherical filler particles. It assumes that in the case of dilution, the intensity field in the composite material is proportional to the average intensity field in the matrix, but when calculating the matrix field, the weighted average matrix of the intensity field and the volume fraction of inclusions is equal to the remote application intensity field [48].

According to Maxwell's equation, the expression of effective thermal conductivity is:

$$\frac{k_{eff}}{k_m} = 1+3\frac{(k_p - k_m)}{(k_p + 2k_m)}\phi \tag{2-22}$$

Among them, k_{eff}, k_m and k_p are the thermal conductivity of the composites, the matrix and the reinforcing particles (filler or dispersed phase), respectively, and ϕ is the volume fraction of the reinforcing particles. Maxwell's formula was found to be valid only in the case of low ϕ (under about 25%).

Eucken [91] extended it to allow calculation for multiple different phases of filler particles in one continuous matrix phase.

$$\frac{(k_{eff}-k_m)}{(k_{eff}+2k_m)}=\frac{(k_p-k_m)}{(k_p+2k_m)}\phi \tag{2-23}$$

The effective medium theory, also known as the Bruggeman model, was first proposed by Bruggeman in 1935 and can be expressed as [50]:

$$\frac{(k_p-k_{eff})}{(k_p-k_m)}\left(\frac{k_m}{k_{eff}}\right)^{\frac{1}{3}}=(1-\phi) \tag{2-24}$$

In the classic EMT, the Bruggeman scheme is considered the most accurate for high filler volume fractions. Using Bruggeman's method, Every and Tzou [87] modified the results of Benveniste to obtain an expression for the effective thermal conductivity of particle composites. Their formula is:

$$\left(\frac{k_{eff}-k_p(1-\alpha)}{k_m-k_p(1-\alpha)}\right)^{3/(1-\alpha)}\left(\frac{k_m}{k_{eff}}\right)^{(1+2\alpha)/(1-\alpha)}=(1-\phi)^3 \tag{2-25}$$

Where α is a dimensionless parameter depending on interface thermal resistance between filler and matrix. It is defined as $\alpha = a_k/a$, where a is the particle radius, and a_k is the Kapitza radius ($a_k = R_{Bd} \times k_m$).

It can be seen from the above that the interface between the matrix and the particles will affect the thermal conductivity. Therefore, in the composite material, the interface between the metal and the ceramic phase is also a key issue. The interface thermal resistance R_{Bd} (the reciprocal of the interface thermal conductivity, h_c) prevents the heat transfer between the two phases. This resistance caused the thermal conductivity of the composite material to depend on the size of the ceramic particles, Hasselman and the workers dealt with this issue in particular [92].

The interface thermal conductance (ITC), h_c, is generally defined as the ratio of the heat flux density q and the associated temperature drop ΔT across an interface:

$$R_{Bd} = \frac{\Delta T}{Q} \tag{2-26}$$

Where ΔT is associated temperature drop ΔT across an interface, Q is the heat flow through unit interface area per unit time.

The interface thermal conductance (ITC), h_c is defined as the ratio of the heat flux density q and the associated temperature drop ΔT across an interface:

$$h_c = \frac{q}{\Delta T} \tag{2-27}$$

At ceramic/metal interfaces, h_c is due to the differences in phonon density of states of both phases, resulting in partial rejection of the incoming phonons at the interface. There exist different models to calculate the rejected fraction of phonons. At present, the more commonly used interface thermal resistance calculation models are the acoustic mismatch model (AMM) and the diffusion mismatch model (DMM) for comparison. In addition, the interface thermal conductivity can be directly measured by transient thermal reflectance (TTR) technology [92].

2.4 Relationship between EC and TC in Al alloys and aluminum matrix composites

It can be seen from the above that thermal conductivity plays an important role in life and industrial production, and there are many factors that affect thermal conductivity. But measuring thermal conductivity is complicated, time-consuming and expensive, so it would save a lot of time and money if it could be characterized by exploring the relationship between thermal conductivity and electrical conductivity and using electrical conductivity to characterize it.

As mentioned earlier, the thermal conductivity of a metal is closely related to its electrical conductivity according to the Wiedemann-Franz law. This is also due to the inherent high density of conducting electrons present in metallic bonds. Similar to thermal conductivity, there are many factors that affect the electrical conductivity of solid metals. Lattice defects,

secondary phases, and grain boundaries can all cause electron scattering, which reduces conductivity. The thermal conductivity and electrical conductivity of pure metals are both affected by temperature. In pure metals, heat conduction is achieved by the migration of free electrons and the vibration of the lattice and mainly depends on the former. The electrical conductivity of pure metals is mainly affected by the charge density and mobility. Therefore, as the temperature increases, lattice vibrations increase and the probability of subsequent electron collisions with atoms in the crystal structure increases, so both thermal and electrical conductivity decrease [43].

The mathematical relationship between the electrical and thermal conductivity of metals is called the Wiedemann-Franz law:

$$K / \sigma = \mathrm{W} \tag{2-28}$$

Where W is a constant with respect to temperature. Then, Lorenz extended the formula to:

$$\frac{K}{\sigma T} = L \tag{2-29}$$

Where L is the Lorenz constant (2.45×10^{8}), this relationship can be expressed by Boltzmann equation and this relationship is only applicable to a single metal alloy [93]. On this basis, L. W. KEMP et al. [94] discussed the relationship between electrical conductivity and thermal conductivity in Al alloys as shown in Figure 2-16. These ideas are expressed mathematically as follows:

$$K = c\lambda T + k \tag{2-30}$$

Where K is the total thermal conductivity, k is the thermal conductivity of non-metallic or atomic fraction (0.03), λ is the electrical conductivity, T is the absolute temperature, and c is (5.02×10^{-9}) a constant, which may be considered as the true Lorenz ratio for the metallic part of the conductivity. The American Brass Corporation's research laboratory passed a large number of experiments [95]. In this study, some alloys were as-cast, while others were precipitation hardened heat treated. The samples were homogenized by annealing before measuring their electrical conductivity.

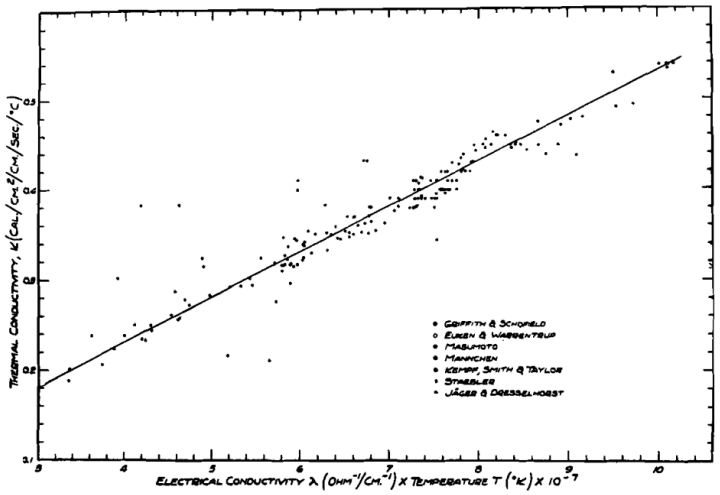

Figure 2-16 Relation of thermal conductivity and product of electrical conductivity and absolute temperature of Al alloy [94].

As shown in Figure 2-17, when the thermal conductivity of a material was plotted against its electrical conductivity at the same temperature, the results were similar between alloys. The curves drawn are based on the theory that thermal conductivity consists of metallic and non-metallic parts [95].

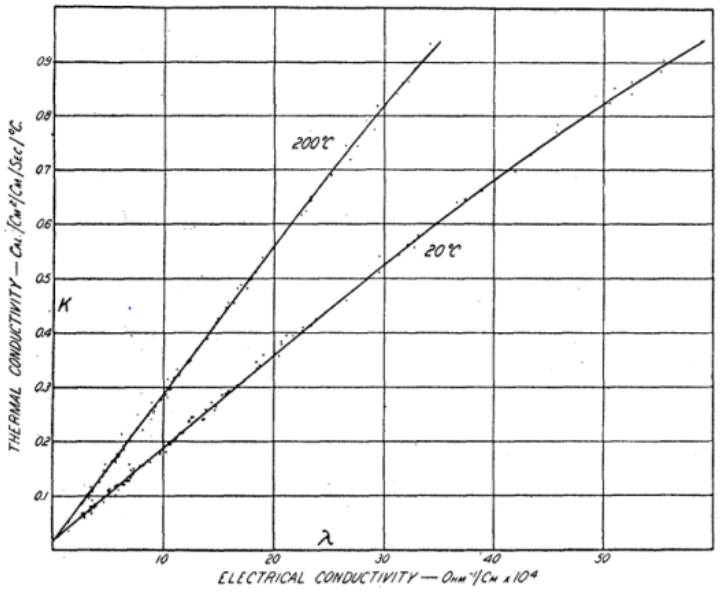

Figure 2-17 Thermal conductivity plotted against the electrical conductivity copper [95].

According to the reference [94], the relationship between electrical conductivity and thermal conductivity in aluminum matrix composites is likely to comply with the above law. Meanwhile, Aydın. [96] found that in Al/SiC composites electrical conductivity and thermal conductivity were observed to be decreased with increasing volume fraction of SiC ceramic particles.

According to the above, it can be known that the influencing factors of the electrical conductivity and thermal conductivity of aluminum matrix composites are very similar, and both are affected by the physical structure and properties of the matrix and particles. According to the heat propagation mechanism, the difference between thermal conductivity and electrical conductivity is that phonons can transmit heat but not electrons. Moreover, it is known from the literature that the thermal conductivity and electrical conductivity of metals and alloys are affected by temperature and are dependent on temperature. Although there are many models of thermal conductivity and electrical conductivity of composite materials, but there are few

studies on the relationship between electrical conductivity and thermal conductivity. To conclude, few reports were found to describe quantitatively described the relationship between electrical conductivity and thermal conductivity in aluminum matrix composites, especially for the Al-B_4C MMCs.

References

[1] L. Huang, L. Geng, and H. Peng, "Microstructurally inhomogeneous composites: is a homogeneous reinforcement distribution optimal?," *Progress in Materials Science*, vol. 71, pp. 93-168, 2015, doi: https://doi.org/10.1016/j.pmatsci.2015.01.002.

[2] V. K. Grigorovič, *The Metallic Bond and the Structure of Metals*, Commack, N.Y., USA: Nova Science.1989..

[3] M. A. Z. Sohag, P. Gupta, N. Kondal, D. Kumar, N. Singh, and A. Jamwal, "Effect of ceramic reinforcement on the microstructural, mechanical and tribological behavior of Al-Cu alloy metal matrix composite," *Materials Today: Proceedings*, vol. 21, pp. 1407-1411, 2020, doi: https://doi.org/10.1016/j.matpr.2019.08.179.

[4] M. Alizadeh, M. Alizadeh, and R. Amini, "Structural and mechanical properties of Al/B_4C composites fabricated by wet attrition milling and hot extrusion," *Journal of Materials Science & Technology*, vol. 29, no. 8, pp. 725-730, 2013, doi: https://doi.org/10.1016/j.jmst.2013.04.015.

[5] Y. Kumar, G. A. Kumar, and T. Madhusudhan, "A review on properties of Al-B_4C composite of different routes," *International Research Journal of Engineering and Technology*, vol. 3, pp. 860-865, 2016. [Online]. Available: https://d1wqtxts1xzle7.cloudfront.net/54560147/IRJET-V3I5179-with-cover-page-v2.pdf?Expires=1652243490&Signature=IYOh3AlsrSSRjR72qivB-NlMD7VChHwTCKUR~FjXJ9Nk2jusDyrGPr8kkrVLfAH7g0kL3A1pwJ3fzT75dQQm5WZzSstfsxaroMeyb-AdWEF9-5eWqNSH8wNFpb1zlYFyS0U86z8whqsocG176Xem2OhCcGUYD0s-ke8FDdqIc3bgGHky1PqJhn4SMYQ2oWkUQM2JBjv-6IyVmtWagF2j3J6FaYeg2-EBRdZ9o6AgAUZDjJHgw8KNq87EX6R6NY~Xe~dO-99Dtir7ijAGlQ-n828xr1i3eMnv2SfVTdd5s22RjQJLgG0AWh-WSrQmVfCCX6TIEkWXZIDyrUMaxz6gIw__&Key-Pair-Id=APKAJLOHF5GGSLRBV4ZA.

[6] H. Lee and R. F. Speyer, "Hardness and fracture toughness of pressureless-sintered boron carbide (B_4C)," *Journal of the American Ceramic Society*, vol. 85, no. 5, pp. 1291-1293, 2002, doi: https://doi.org/10.1111/j.1151-2916.2002.tb00260.x.

[7] Y. Taki, M. Kitiwan, H. Katsui, and T. Goto, "Electrical and thermal properties of off-stoichiometric SiC prepared by spark plasma sintering," *Journal of Asian Ceramic Societies*, vol. 6, no. 1, pp. 95-101, 2018, doi: https://doi.org/10.1080/21870764.2018.1446490.

[8] F. Thevenot, "A review on boron carbide," *Key Engineering Materials*, vol. 56, pp. 59-88, 1991, doi: https://doi.org/10.4028/www.scientific.net/KEM.56-57.59.

[9] K. Yamada and M. Mohri, "Properties and applications of silicon carbide ceramics," *Silicon carbide ceramics—1*: *Fundamental and Solid Reaction*, S. Sömiya and Y. Inomata, Eds., Dordrecht, Netherlands: Springer, Dordrecht, 1991, pp. 13-44. [Online].Available: https://doi.org/10.1007/978-94-011-3842-0_2.

[10] I. Altinsoy, F. G. C. Efe, D. Aytaş, M. Kılıç, I. Ozbek, and C. Bindal, "Some properties of Cu-B_4C composites manufactured by powder metallurgy," *Periodicals of Engineering and Natural Sciences*, vol. 1, no. 1, 2013, doi: http://dx.doi.org/10.21533/pen.v1i1.14.

[11] D. Ni, L. Geng, J. Zhang, and Z. Zheng, "Effect of B_4C particle size on microstructure of in situ titanium matrix composites prepared by reactive processing of Ti–B_4C system," *Scripta materialia*, vol. 55, no. 5, pp. 429-432, 2006, doi: https://doi.org/10.1016/j.scriptamat.2006.05.024.

[12] K. Wang, D. Du, G. Liu, B. Chang, J. Ju, S. Sun, and H. Fu, "Microstructure and property of laser clad Fe-based composite layer containing Nb and B_4C powders," *Journal of Alloys and Compounds*, vol. 802, pp. 373-384, 2019, doi: https://doi.org/10.1016/j.jallcom.2019.06.183.

[13] Y.-t. Yao, L. Jiang, G.-f. Fu, and L.-q. Chen, "Wear behavior and mechanism of B_4C reinforced Mg-matrix composites fabricated by metal-assisted pressureless infiltratio n technique," *Transactions of Nonferrous Metals Society of China*, vol. 25, no. 8, pp. 2543-2548, 2015, doi: https://doi.org/10.1016/S1003-6326(15)63873-0.

[14] U. Gopal Krishna, K. Sreenivas Rao, and B. Vasudeva, "Effect of boron carbide reinf orcement on aluminium matrix composites," *Int J Metall Mater Sci Eng*, vol. 3, no. 1, pp. 41-48, 2013. [Online]. Available: https://www.researchgate.net/publication/235957384_Effect_of_Boron_Carbide_Reinforcement_on_Aluminium_Matrix_Composites.

[15] J. G. Kaufman, *Introduction to aluminum alloys and tempers*. Materials Park, Ohio, U SA: ASM international, 2000.

[16] N. Panwar and A. Chauhan, "Fabrication methods of particulate reinforced Aluminiu m metal matrix composite-A review," *Materials Today: Proceedings*, vol. 5, no. 2, p p. 5933-5939, 2018, doi: https://doi.org/10.1016/j.matpr.2017.12.194.

[17] X. Chen, "Application of Al-B_4C metal matrix composites in the nuclear industry for neutron absorber materials," in *TMS Annual Meeting & Exhibition*, San Antonio, Tex as, USA, 2006, pp. 343-350. [Online]. Available: https://www.researchgate.net/publication/279766054_Application_of_AL-B4C_metal_matrix_composites_in_the_nuclear_industry_for_neutron_absorber_materials.

[18] D. Lloyd, "Particle reinforced aluminium and magnesium matrix composites," *Intern ational materials reviews*, vol. 39, no. 1, pp. 1-23, 1994, doi: https://doi.org/10.1179/imr.1994.39.1.1.

[19] X. G. Chen, Hark, R., "Development of Al-30% B_4C metal matrix composites for neu tron absorber material," in *137th TMS Annual Meeting & Exhibition*, New Orleans, L A, USA, 2008, pp. 3-9. [Online]. Available: https://uqac.on.worldcat.org/search/detail/282762174?queryString=Development%20of%20Al-30%25%20B4C%20metal%20matrix%20composites%20for%20neutron%20absorber%20material&clusterResults=true&stickyFacetsChecked=true&groupVariantRecords=false&scope=&changedFacet=scope.

[20] P. Sharma, D. Khanduja, and S. Sharma, "Tribological and mechanical behavior of pa rticulate aluminum matrix composites," *Journal of Reinforced Plastics and Composit es*, vol. 33, no. 23, pp. 2192-2202, 2014, doi: https://doi.org/10.1177/0731684414556012.

[21] Z. Xu, L. Jiang, Q. Zhang, J. Qiao, D. Gong, and G. Wu, "The design of a novel neutr on shielding B_4C/Al composite containing Gd," *Materials & Design*, vol. 111, pp. 37 5-381, 2016, doi: https://doi.org/10.1016/j.matdes.2016.07.140.

[22] P. Zhang, Y. Li, W. Wang, Z. Gao, and B. Wang, "The design, fabrication and proper ties of B_4C/Al neutron absorbers," *Journal of Nuclear materials*, vol. 437, no. 1-3, pp. 350-358, 2013, doi: https://doi.org/10.1016/j.jnucmat.2013.02.050.

[23] R. Mohanty, K. Balasubramanian, and S. Seshadri, "Boron carbide-reinforced alumni um 1100 matrix composites: Fabrication and properties," *Materials Science and Engi neering: A*, vol. 498, no. 1-2, pp. 42-52, 2008, doi: https://doi.org/10.1016/j.msea.2007.11.154.

[24] D. K. Sharma, M. Sharma, and G. Upadhyay, "Boron carbide (B4C) reinforced alumi num matrix composites (AMCs)," *Int. J. Innovative Technol. Exploring Eng.*, vol. 9, no. 1, pp. 2194-2203, 2019, doi: https://doi.org/10.35940/ijitee.A4766.119119.

[25] K. Butcher, L. Crown, and E. J. Gentry, S. National Institute of, W. Technology, and D. Measures, *The International System of Units (SI) : conversion factors for general use*, Gaithersburg, Md, USA: U.S. Dept. of Commerce, Technology Administration, National Institute of Standards and Technology, 2006. [Online]. Available: https://nvlpubs.nist.gov/nistpubs/Legacy/SP/nistspecialpublication1038.pdf.

[26] M. B. Heaney, "Electrical conductivity and resistivity," in *Electrical measurement, signal processing, and displays*, vol. 7, J. G. Webster Ed., no. (1). Boca Raton, Florida, USA: CRC Press, 2003.

[27] C. Moosbrugger, Ed. *ASM ready reference: electrical and magnetic properties of metals*. Materials Park, Ohio, USA: ASM International, 2000.

[28] L. Solymar, D. Walsh, and R. R. Syms, *Electrical properties of materials*, Ninth edition ed. Oxford, England, UK: Oxford university press, 2014.

[29] J. Janesch, "Two-wire vs. four-wire resistance measurements: Which configuration makes sense for your application," Keithley Instruments. Inc, Cleveland, Ohio, USA, 2013. [Online]. Available: https://xdevs.com/doc/Keithley/Appnotes/2Wire_4Wire%20Resistance%20Article.pdf.

[30] M. P. Meeder, "Modeling the thermal and electrical properties of different density sintered binder jetted copper for verification and revision of the Wiedemann-Franz law," Master thesis, Science in Mechanical Engineering, Virginia Polytechnic Institute and State University, Blacksburg, Virginia, USA, 2016. [Online]. Available: http://hdl.handle.net/10919/72977.

[31] V. Cecco, F. Sharp, and G. Van Drunen, "Eddy current testing; v 1, manual on Eddy current method," CM-P00067661, 1981. [Online]. Available: https://cds.cern.ch/record/135718/files/CM-P00067661.pdf.

[32] H. F. GmbH, "SIGMASCOPE® SMP10 Electrical conductivity measurement of non-ferrous metals enters a new dimension," Germany. [Online]. Available: http://www.mckkorea.com/catalog/fischer/sigmascope/DE_Sigmascope_EN.pdf.

[33] "*Standard Test Method for Determining Electrical Conductivity Using the Electromagnetic (Eddy-Current) Method*,"ASTM E1004-09 (2009), A. International, 2009. [Online]. Available: https://tajhizkala.ir/doc/ASTM/E1004-09.pdf.

[34] M. J. N. Isfahani, F. Payami, M. A. Asadabad, and A. A. Shokri, "Investigation of the effect of boron carbide nanoparticles on the structural, electrical and mechanical properties of Al-B_4C nanocomposites," *Journal of Alloys and Compounds*, vol. 797, pp. 1348-1358, 2019, doi: https://doi.org/10.1016/j.jallcom.2019.05.188.

[35] S. M. Zebarjad and S. A. Sajjadi, "Dependency of physical and mechanical properties of mechanical alloyed Al-Al_2O_3 composite on milling time," *Materials & design*, vol. 28, no. 7, pp. 2113-2120, 2007, doi: https://doi.org/10.1016/j.matdes.2006.05.020.

[36] T. Gomi, Fukushima, and J. Matsushita, "High temperature electrical conductivity of B_4C, SiC and SiB_6 sintered bodies," *Journal of Advanced Science*, vol. 13, no. 1-2, pp. 15-16, 2001, doi: https://doi.org/10.2978/jsas.13.15.

[37] A. H. Committee, "Properties of wrought aluminum and aluminum alloys," *vol. 2, ASM Handbook, Volume 2: Properties and selection: nonferrous alloys and special-purpose materials*, Materials Park, Ohio, USA: ASM International, 1990, pp. 62-122.

[38] R. Morrell, *Handbook of Properties of Technical and Engineering Ceramics. Part 2: Data Reviews. Section I: High-Alumina Ceramics*, Richmond, London, UK: Her Majesty's Stationery Office, 1987, p. 255.

[39] F. Fickett, "Aluminum—1. A review of resistive mechanisms in aluminum," *Cryogenics*, vol. 11, no. 5, pp. 349-367, 1971, doi: https://doi.org/10.1016/0011-2275(71)90036-1.

[40] S. Hussain, I. Barbariol, S. Roitti, and O. Sbaizero, "Electrical conductivity of an insulator matrix (alumina) and conductor particle (molybdenum) composites," *Journal of the European Ceramic Society*, vol. 23, no. 2, pp. 315-321, 2003, doi: https://doi.org/10.1016/S0955-2219(02)00185-1.

[41] S. Sasaki, M. Takeda, K. Yokoyama, T. Miura, T. Suzuki, H. Suematsu, W. Jiang, and K. Yatsui, "Thermoelectric properties of boron-carbide thin film and thin film based thermoelectric device fabricated by intense-pulsed ion beam evaporation," *Science*

and Technology of Advanced Materials, vol. 6, no. 2, p. 181, 2005, doi: https://doi.org/10.1016/j.stam.2004.11.010.

[42] C. Kittel, *Introduction to solid state physics*, Eighth edition ed. Hoboken, New Jersey, USA: John Wiley & Sons, Inc, 2004.

[43] T. M. Tritt, *Thermal conductivity: theory, properties, and applications*. New York, N. Y., USA: Kluwer Academic/Plenum Publishers, 2004.

[44] J. Kovacik, "Electrical conductivity of two-phase composite material," *Scripta materialia*, vol. 39, no. 2, pp. 153-157, 1998, doi: https://doi.org/10.1016/S1359-6462(98)00147-X.

[45] L. Weber, J. Dorn, and A. Mortensen, "On the electrical conductivity of metal matrix composites containing high volume fractions of non-conducting inclusions," *Acta Materialia*, vol. 51, no. 11, pp. 3199-3211, 2003, doi: https://doi.org/10.1016/S1359-6454(03)00141-1.

[46] Y. Xiao, Y. Li, Y. Liang, K. Lu, and B. Zhou, "Nanometre sized SiC particulates reinforced Al base composite material," *Acta Metall Sin*, vol. 6, pp. 658-62, 1996. [Online]. Available: https://www.researchgate.net/publication/295443266_Nanometre_sized_SiC_particlates_reinforced_al_base_composite_material.

[47] N. A. M. Radzuan, A. B. Sulong, and J. Sahari, "A review of electrical conductivity models for conductive polymer composite," *international journal of hydrogen energy*, vol. 42, no. 14, pp. 9262-9273, 2017, doi: https://doi.org/10.1016/j.ijhydene.2016.03.045.

[48] J. C. Maxwell, *A treatise on electricity and magnetism*, 3rd ed. Oxford, England, UK: Oxford University Press, 1955.

[49] K. W. Wagner, "Erklärung der dielektrischen Nachwirkungsvorgänge auf Grund Maxwellscher Vorstellungen," *Archiv für Elektrotechnik*, vol. 2, no. 9, pp. 371-387, 1914/09/01 1914, doi: https://doi.org/10.1007/BF01657322.

[50] V. D. Bruggeman, "Berechnung verschiedener physikalischer Konstanten von heterogenen Substanzen," *Annalen der physik*, vol. 416, no. 7, pp. 636-664, 1935, doi: https://doi.org/10.1002/andp.19354160705.

[51] V. K. Shante and S. Kirkpatrick, "An introduction to percolation theory," *Advances in Physics*, vol. 20, no. 85, pp. 325-357, 1971, doi: https://doi.org/10.1080/00018737100101261.

[52] R. Pal, "On the electrical conductivity of particulate composites," *Journal of Composite materials*, vol. 41, no. 20, pp. 2499-2511, 2007, doi: https://doi.org/10.1177/0021998307076489.

[53] H. Czichos, T. Saito, and L. Smith, *Springer handbook of materials measurement methods*, , Heidelberg, Baden-Württemberg, Germany: Springer Berlin, Heidelberg, 2006.

[54] N. Yüksel, "The review of some commonly used methods and techniques to measure the thermal conductivity of insulation materials," *Insulation materials in context of sustainability*, A. a. A. A. Almusaed, Ed., London, England, UK: IntechOpen, 2016. [Online]. Available: https://www.intechopen.com/chapters/51497!.

[55] W. Parker, R. Jenkins, C. Butler, and G. Abbott, "Flash method of determining thermal diffusivity, heat capacity, and thermal conductivity," *Journal of applied physics*, vol. 32, no. 9, pp. 1679-1684, 1961, doi: https://doi.org/10.1063/1.1728417.

[56] T. I. W. Corporation, "THERMAL CONDUCTIVITY AND THERMAL DIFFUSIVITY," USA, 2021. [Online]. Available: https://www.tainstruments.com/wp-content/uploads/BROCH-ThermalConductivityDiffusivity-EN.pdf.

[57] P. Gaal, M.-A. Thermitus, and D. Stroe, "Thermal conductivity measurements using the flash method," *Journal of Thermal Analysis and Calorimetry*, vol. 78, no. 1, pp. 185-189, 2004, doi: https://doi.org/10.1023/b:jtan.0000042166.64587.33.

[58] C.-W. Nan, R. Birringer, D. R. Clarke, and H. Gleiter, "Effective thermal conductivity of particulate composites with interfacial thermal resistance," *Journal of Applied Physics*, vol. 81, no. 10, pp. 6692-6699, 1997, doi: https://doi.org/10.1063/1.365209.

[59] R. N. Lumley, N. Deeva, R. Larsen, J. Gembarovic, and J. Freeman, "The role of alloy composition and T7 heat treatment in enhancing thermal conductivity of aluminum high pressure diecastings," *Metallurgical and Materials Transactions A*, vol. 44, no. 2, pp. 1074-1086, 2013, doi: https://doi.org/10.1007/s11661-012-1443-7.

[60] A. Rudajevova, M. Staněk, and P. Lukáč, "Determination of thermal diffusivity and thermal conductivity of Mg-Al alloys," *Materials Science and Engineering: A*, vol. 341, no. 1-2, pp. 152-157, 2003, doi: https://doi.org/10.1016/S0921-5093(02)00233-2.

[61] Y. Zhang, S. Feng, C. Ding, H. R. J. Nodooshan, S. Ye, F. Jiang, Z. Li, M. Gu, and P. Yu, "Investigation of the influences of heat treatment on the microstructures and thermal properties of Al-20Si alloy fabricated by powder extrusion," *Materials Characterization*, vol. 168, p. 110522, 2020, doi: https://doi.org/10.1016/j.matchar.2020.110522.

[62] C. Ding and P. Yu, "Effect of extrusion temperatures on the microstructures, mechanical properties and thermal properties of PM Al-20Si alloy," *Journal of Alloys and Compounds*, p. 163979, 2022, doi: https://doi.org/10.1016/j.jallcom.2022.163979.

[63] J. Goela, N. Brese, L. Burns, and M. Pickering, "High-thermal-conductivity SiC and applications," in *High thermal conductivity materials*. New York, N. Y., USA: Springer, New York, NY, 2006, pp. 167-198.

[64] C. Wood, D. Emin, and P. E. Gray, "Thermal conductivity behavior of boron carbides," *Physical Review B*, vol. 31, no. 10, p. 6811, 1985, doi: https://doi.org/10.1103/PhysRevB.31.6811.

[65] K. Huang and R. Han, *Solid state physics*. People's Education Press, 1979. [黄昆, 韩汝琦, 固体物理学. 人民教育出版社, 1979.]

[66] Y. Wang, "Research on thermal conductivity of particle reinforced aluminum matrix composites " Master Dissertation, Material Science and Engineering Nanchang Hangkong University, Nanchang, China 2010. [Online]. Available: https://cdmd.cnki.com.cn/Article/CDMD-10406-1010120394.htm. [王寅, "颗粒增强铝基复合材料导热性能分析," 南昌航空大学, 南昌, 中国 2010.]

[67] Ş. Karabulut, H. Karakoç, and R. Çıtak, "Influence of B_4C particle reinforcement on mechanical and machining properties of Al6061/B_4C composites," *Composites Part B: Engineering*, vol. 101, pp. 87-98, 2016, doi: https://doi.org/10.1016/j.compositesb.2016.07.006.

[68] Z. Tan, Z. Chen, G. Fan, G. Ji, J. Zhang, R. Xu, A. Shan, Z. Li, and D. Zhang, "Effect of particle size on the thermal and mechanical properties of aluminum composites reinforced with SiC and diamond," *Materials & Design*, vol. 90, pp. 845-851, 2016, doi: https://doi.org/10.1016/j.matdes.2015.11.028.

[69] H. S. Lee, K. Y. Jeon, H. Y. Kim, and S. H. Hong, "Fabrication process and thermal properties of SiCp/Al metal matrix composites for electronic packaging applications," *Journal of Materials Science*, vol. 35, no. 24, pp. 6231-6236, 2000/12/01 2000, doi: https://doi.org/10.1023/A:1026749831726.

[70] G. Yang, Y. G. Du, S. X. Bai, Y. Long, J. S. Hu, and J. C. Zhang, "Effect of Thermal Boundary Resistance on the Thermal Conductivity of Diamond/Ag Metal Matrix Composites," *Journal of National University of Defense Technology*, 1998. [Online]. Available: http://journal.nudt.edu.cn/publish_article/1998/6/199806025.pdf. [杨广,堵永国,白书欣,龙雁,胡君遂,张家春, “界面热阻对金刚石/ 银复合材料导热率的影响,” 国防科技大学学报]

[71] W. B. Johnson and B. Sonuparlak, "Diamond/Al metal matrix composites formed by the pressureless metal infiltration process," *Journal of materials research*, vol. 8, no. 5, pp. 1169-1173, 1993, doi: https://doi.org/10.1557/JMR.1993.1169.

[72] R. Progelhof, J. Throne, and R. Ruetsch, "Methods for predicting the thermal conductivity of composite systems: a review," *Polymer Engineering & Science*, vol. 16, no. 9, pp. 615-625, 1976, doi: https://doi.org/10.1002/pen.760160905.

[73] R. Stoner and H. Maris, "Kapitza conductance and heat flow between solids at temperatures from 50 to 300 K," *Physical Review B*, vol. 48, no. 22, p. 16373, 1993, doi: https://doi.org/10.1103/PhysRevB.48.16373.

[74] D. A. Weston, "Quantitative evaluation of rubber/silica particle interphase through measurement of heat capacity," Doctor of Philosophy Dissertation, Physics, Clemson University, Clemson, South Carolina, USA, 2004. [Online]. Available: https://tigerprints.clemson.edu/arv_dissertations/1406/

[75] M. Qiang, H. Xinbo, R. Shubin, and Q. Xuanhui, "Effect of Si on the microstructure and thermal conductivity of pressureless infiltrated SiCp/Al composites," *Chinese Journal of Engineering* vol. 30, no. 1, pp. 45-48, 62, 2008, doi: https://doi.org/10.13374/j.issn1001-053x.2008.01.002.

[76] Y. Sun, C. Zhang, L. He, Q. Meng, B.-C. Liu, K. Gao, and J. Wu, "Enhanced bending strength and thermal conductivity in diamond/Al composites with B_4C coating," *Scientific Reports*, vol. 8, no. 1, pp. 1-12, 2018, doi: https://doi.org/10.1038/s41598-018-29510-7.

[77] C. Kawai, "Effect of interfacial reaction on the thermal conductivity of Al–SiC composites with SiC dispersions," *Journal of the American Ceramic Society*, vol. 84, no. 4, pp. 896-898, 2001, doi: https://doi.org/10.1111/j.1151-2916.2001.tb00764.x.

[78] K. Chu, C. Jia, X. Liang, H. Chen, H. Guo, F. Yin, and X. Qu, "Experimental and modeling study of the thermal conductivity of SiCp/Al composites with bimodal size distribution," *Journal of materials science*, vol. 44, no. 16, pp. 4370-4378, 2009, doi: https://doi.org/10.1007/s10853-009-3655-9.

[79] Z. Che, J. Li, Q. Wang, L. Wang, H. Zhang, Y. Zhang, X. Wang, J. Wang, and M. J. Kim, "The formation of atomic-level interfacial layer and its effect on thermal conductivity of W-coated diamond particles reinforced Al matrix composites," *Composites Part A: Applied Science and Manufacturing*, vol. 107, pp. 164-170, 2018, doi: https://doi.org/10.1016/j.compositesa.2018.01.002.

[80] Z. Che, Q. Wang, L. Wang, J. Li, H. Zhang, Y. Zhang, X. Wang, J. Wang, and M. J. Kim, "Interfacial structure evolution of Ti-coated diamond particle reinforced Al matrix composite produced by gas pressure infiltration," *Composites Part B: Engineering*, vol. 113, pp. 285-290, 2017, doi: https://doi.org/10.1016/j.compositesb.2017.01.047.

[81] Q. Liu, Z. He, J. Cheng, Y. Chen, F. Wang, Z. Lv, and J. Qi, "Theoretical and predictive modeling of interfacial thermal conductance and thermal conductivity in graphite flake/Al composites," *Composite Interfaces*, vol. 28, no. 1, pp. 101-114, 2021, doi: https://doi.org/10.1080/09276440.2020.1726135.

[82] O. Beffort, S. Vaucher, and F. Khalid, "On the thermal and chemical stability of diamond during processing of Al/diamond composites by liquid metal infiltration (squeeze casting)," *Diamond and related materials*, vol. 13, no. 10, pp. 1834-1843, 2004, doi: https://doi.org/10.1016/j.diamond.2004.04.014.

[83] F. Khalid, O. Beffort, U. Klotz, B. Keller, and P. Gasser, "Microstructure and interfacial characteristics of aluminium–diamond composite materials," *Diamond and related materials*, vol. 13, no. 3, pp. 393-400, 2004, doi: https://doi.org/10.1016/j.diamond.2003.11.095.

[84] Z. Tan, Z. Li, G. Fan, Q. Guo, X. Kai, G. Ji, L. Zhang, and D. Zhang, "Enhanced thermal conductivity in diamond/aluminum composites with a tungsten interface nanolayer," *Materials & Design*, vol. 47, pp. 160-166, 2013, doi: https://doi.org/10.1016/j.matdes.2012.11.061.

[85] Z. Tan, Z. Li, D.-B. Xiong, G. Fan, G. Ji, and D. Zhang, "A predictive model for interfacial thermal conductance in surface metallized diamond aluminum matrix composites," *Materials & Design*, vol. 55, pp. 257-262, 2014, doi: https://doi.org/10.1016/j.matdes.2013.09.060.

[86] D. Hasselman, K. Y. Donaldson, and A. L. Geiger, "Effect of reinforcement particle size on the thermal conductivity of a particulate-silicon carbide-reinforced aluminum matrix composite," *Journal of the American Ceramic Society*, vol. 75, no. 11, pp. 3137-3140, 1992, doi: https://doi.org/10.1111/j.1151-2916.1992.tb04400.x.

[87] A. Every, Y. Tzou, D. Hasselman, and R. Raj, "The effect of particle size on the thermal conductivity of ZnS/diamond composites," *Acta metallurgica et materialia*, vol. 40, no. 1, pp. 123-129, 1992, doi: https://doi.org/10.1016/0956-7151(92)90205-S.

[88] H. S. Tekce, D. Kumlutas, and I. H. Tavman, "Effect of particle shape on thermal conductivity of copper reinforced polymer composites," *Journal of reinforced plastics and composites*, vol. 26, no. 1, pp. 113-121, 2007, doi: https://doi.org/10.1177/0731684407072522.

[89] S. V. Gladkovsky, I. S. Kamantsev, S. V. Kuteneva, V. E. Veselova, and M. A. Ryzhkov, "The Thermal Expansion and Thermophysical Properties of an Aluminum and Al/B_4C composite," *AIP Conference Proceedings*, vol. 1915, no. 1, 2017. [Online]. Available: https://uqac.on.worldcat.org/search/detail/7256517937?queryString=The%20thermal%20expansion%20and%20thermophysical%20properties%20of%20an%20aluminum%20and%20Al%2FB4C%20composite&clusterResults=true&stickyFacetsChecked=true&groupVariantRecords=false&scope=&changedFacet=scope.

[90] W. Kingery, "Thermal conductivity: XIV, conductivity of multicomponent systems," *Journal of the American Ceramic Society*, vol. 42, no. 12, pp. 617-627, 1959, doi: https://doi.org/10.1111/j.1151-2916.1959.tb13583.x.

[91] A. Eucken, *Die Wärmeleitfähigkeit keramischer feuerfester Stoffe: ihre Berechng aus d. Wärmeleitfähigkeit d. Bestandteile*. Berlin, Germany: VDI-Verlag, 1932.

[92] M. Kida, L. Weber, C. Monachon, and A. Mortensen, "Thermal conductivity and interfacial conductance of AlN particle reinforced metal matrix composites," *Journal of applied physics*, vol. 109, no. 6, p. 064907, 2011, doi: https://doi.org/10.1063/1.3553870.

[93] R. Franz and G. Wiedemann, "Ueber die Wärme-Leitungsfähigkeit der Metalle," *Annalen der Physik*, vol. 165, no. 8, pp. 497-531, 1853. [Online]. Available: https://ia600708.us.archive.org/view_archive.php?archive=/22/items/crossref-pre-1909-scholarly-works/10.1002%252Fandp.18521620610.zip&file=10.1002%252Fandp.18531650802.pdf.

[94] L. Kempf, C. Smith, and C. Taylor, "Thermal and Electrical Conductivities of Aluminum Alloys," *Trans. Amer. Inst. Min. Metall. Engrs*, vol. 124, pp. 287-298, 1937. [Online]. Available: https://aimehq.org/resources/digital-library.

[95] C. S. Smith, "The relation between the thermal and electrical conductivities of copper alloys," *Physical Review*, vol. 48, no. 2, p. 166, 1935, doi: https://doi.org/10.1103/PhysRev.48.166.

[96] M. Aydin, "An Experimental Study of The Effects of Ceramic Composition on The Electrical and Thermal Properties of Al/SiC Composites," *European Journal of Science and Technology*, 2021, doi: https://doi.org/10.31590/ejosat.943506.

CHAPTER 3 EXPERIMENTAL PROCEDURES

3.1 Materials

3.1.1 1100-B_4C composites

The 1100-B_4C MMCs were supplied in the form of 3mm and 6 mm plates after rolling from Rio Tinto. The Conditions of the studied 1100-B_4C MMCs are listed in the Table 3-1.

Table 3-1 Conditions (Vol.%) of 1100-B_4C MMCs.

Composites code	Matrix	B_4C (Vol. %)	Condition
6-4R		6	Rolled plate (4 mm)
11-3R		11	Rolled plate (3 mm)
11-6R		11	Rolled plate (6 mm)
16-4R		16	Rolled plate (4 mm)
19-3R	1100	19	Rolled plate (3 mm)
19-6R		19	Rolled plate (6 mm)
21-3R		21	Rolled plate (3 mm)
21-6R		21	Rolled plate (6 mm)
30-2R		30	Rolled plate (2 mm)

Note: 6-4R: 6 is the volume fraction of B_4C; 4 is the thickness of the plate; R is the condition for rolling.

3.1.2 6xxx-B_4C composites

The 6xxx-B_4C MMCs were supplied in the form of 3 mm to 7 mm plates after extrusion and rolling process from Rio Tinto. For the 6351-B_4C MMCs the billet was preheated at 480℃ for 12h prior to rolling. During rolling, the material was re-heated 2 times at 480℃ for 1h. The condition of 6063-B_4C MMCs is as-received and the specific heat treatment status unknown. The conditions of the studied 6xxx-B_4C MMCs are listed in the Table 3-2.

Table 3-2 Conditions (Vol.%) of 6xxx-B_4C MMCs.

Composites code	Matrix	B_4C (Vol. %)	Condition
A-6-4E	6063	6	Extrusion plate (4 mm)
A-15-4E		15	Extrusion plate (4 mm)
B-4-7E	6351	4	Extrusion plate (7 mm)
B-17.5-3R		17.5	Rolled plate (3 mm)

Note: A-6-4E: A is the 6063 Al alloy; 6 is the volume fraction of B_4C; 4 is the thickness of plate; E is the condition for extrusion and R is the condition for rolling. B-4-7E: B is the 6351 Al alloy, 4 is the volume fraction of B_4C, 7 is the thickness of plate, E is the condition for extrusion.

3.1.3 Other Al-composites

The 3004-B_4C MMCs and 6061-Al_2O_3 MMCs were supplied in the form of 6 mm plate after the rolling process from Rio Tinto. The condition of 3004-B_4C MMCs and 6061-Al_2O_3 MMCs were as-received and the specific heat treatment status unknown. The conditions of the studied 3004-B_4C MMCs and 6061-Al_2O_3 MMCs are listed in the Table 3-3.

Table 3-3 Conditions (Vol.%) of 3004-B_4C and 6061-Al_2O_3 composites.

Composites code	Matrix	Particle (Vol. %)	Condition
C-10.5-6R	3004	10.5	Rolled plate (6 mm)
D-15-6R	6061	15	Rolled plate (6 mm)

Note: C-10.5-6R:C is the 3004 Al alloy; 10.5 is the volume fraction of B_4C, 15 is the volume fraction of Al2O3; 6 is the thickness of plate, R is the condition for rolling. D-15-6R: D is the 6061 Al alloy, 15 is the volume fraction of Al_2O_3, 6 is the thickness of plate, R is the condition for rolling.

3.2 Heat treatment

To study the influence of heat treatment on the evolution of EC and TC, selected heat treatments were performed on 1100-B_4C MMCs at different annealing temperature and time, which are listed in Table 3-4. All the heat treatments were processed in a forced-air electric furnace with a heating rate of 8.5℃/min.

Table 3-4 Heat treatment parameters for 1100-B_4C MMCs.

Composites code	Temperature (℃)	Time (h)	Cooling
19-3R 21-3R	380	~ 23	Cooling in air
19-3R 21-3R	340, 380, 430,490	4	

3.3 Microstructure Characterization

3.3.1 Metallography preparation

All metallographic samples used for microstructure observation are mechanically cut from the original materials. To characterize the microstructure of B_4C, the volume fraction of reaction products and particles, the composite materials were first mechanically ground with #45 and #80 emery paper followed by the polishing process with 15, 9, 6, 3 and1μm diamond composite paste and diamond extender lubricant, each step was about 15 minutes. The final polishing step is to use 0.5μm colloidal silica suspension and water to polish on the silk polishing pad for 30 minutes.

3.3.2 Electro-etching

To observe the evolution of grain structure during the heat treatment, electro-etching was used in the present work. For as-rolled sample, electrolytic etching is carried out in Barker's reagent at a voltage of 25V for 2 minutes while it is with a voltage of 30V and a duration of 2 minutes for samples after heat treatment.

3.3.3 Microstructure analysis

Nikon Eclipse ME600 computerized optical microscope (OM) equipped with CLEMEX VISION PE 4.0 image analysis system was used to observe the microstructure of

the sample, including the volume fraction of B_4C, reaction products and different intermetallic compounds. The specific morphology of the reaction layer of these composite materials was analyzed with a scanning electron microscope (SEM) equipped with an energy dispersive spectrometer (EDS) and (EBSD) detector.

3.4 Property Evaluations

3.4.1 Thermal conductivity tests

The thermal conductivity (TC) tests were performed on the computerized Flash Line™ 3000 testing machine on the surface of a cylindrical sample with a diameter of 12mm and a thickness of 3mm. According to the ASTM: E1461 Standard [1], all tests are processed on the samples at the same temperature 150℃ and 250℃. After 8 points tested on each sample, the maximum and the minimum value would be eliminated, and after that, the rest 6 values would be calculated for the average TC results. The detailed working principle was introduced in the section 2.3.1.

3.4.2 Electrical conductivity tests

The electrical conductivity (EC) tests were performed using the SIGMASCOPE® SMP10 Electric conductivity measuring instrument. According to the ASTM: E1004 Standard [2], all tests are processed on the surface of samples at the same temperature (room temperature) to ensure no induced error caused by different temperature, which can significantly influence on the results of electric conductivity tests. For the testing process, each sample would be tested for 5 times, and the maximum and the minimum value would be eliminated. After that, the rest 3 values would be calculated to the average as the final electrical conductivity results.

3.4.3 Models to predict the Thermal conductivity and Electrical conductivity

Three thermal conductivity and three electrical conductivity prediction models were used during the experiments. For the TC prediction model, Parallel model, Maxwell model, Every and Tzou verified Bruggeman model (Bruggeman-ET model) have been adopted, as shown in Table 3-5.

Table 3-5 Description of thermal conductivity model for Al-B_4C materials [3-5].

Modelling	Model equation
Parallel model	$k_{eff} = k_p\phi + k_m(1-\phi)$
Maxwell model	$\frac{k_{eff}}{k_m} = \left(\frac{k_p + 2k_m + 2\phi(k_p - k_m)}{k_p + 2k_m - \phi(k_p - k_m)} \right)$
Bruggeman-ET model	$\left(\frac{k_{eff} - k_p(1-\alpha)}{k_m - k_p(1-\alpha)} \right)^{3/(1-\alpha)} \left(\frac{k_m}{k_{eff}} \right)^{(1+2\alpha)/(1-\alpha)} = (1-\phi)^3$

k_m: Matrix thermal conductivity ([W/(m·K)]), k_p: Particle thermal conductivity ([W/(m·K)]), ϕ: Particle volume faction, h_c: Interface thermal conductance ([W/(m^2·K)]), α: Dimensionless parameter, k_{eff}: Effective thermal conductivity of aluminum metal matrix composite ([W/(m·K)]).

Note: The contents are cited from references 3-5.

The interface thermal conductance, (the capability of heat conduction across an interface between two dissimilar materials) values in all combinations are calculated according to the Acoustic Mismatch Model (AMM) model[6], which is given in following equation [7]:

$$h_c = \frac{1}{2}\rho_m C_m \frac{v_m^3}{v_r^2} \frac{\rho_m v_m \rho_r v_r}{\left(\rho_m v_m + \rho_r v_r\right)^2} \tag{3-1}$$

The parameters used in the interface thermal conductivity prediction models are shown in Table 3-6.

Table 3-6 ITC prediction model application basic parameters [8-10].

Material	ρ_m **(*kg* /m^3)**	C_m **[*J* / (*kg*·*k*)]**	v_m **(*m* / *s*)**	ρ_r **(*kg* /m^3)**	v_r **(*m* /*s*)**
1100-B_4C	2713	904			
6063-B_4C	2690	900	3620	2516	9230
6351-B_4C	2700	900			
3004-B_4C	2720	893			

h_c: Interface thermal conductance, ρ_m: Density of matrix, C_m: Specific heat capacity of matrix, v_m: Phonon velocity of matrix, ρ_r: Density of particle, v_r: Phonon velocity of reinforcement.

Note: The contents are cited from references 8-10.

Similar, the Parallel model, Maxwell-Wagner model, Bruggeman model have been adopted to predict the EC, as shown in Table 3-7.

Table 3-7 Description of electrical conductivity model for Al-B_4C materials [11-13].

Modelling	**Model equation**
Parallel model	$\sigma_{eff} = \sigma_p \phi + \sigma_m (1-\phi)$
Maxwell-Wagner model	$\frac{\sigma_{eff}}{\sigma_m} = 1+3\frac{(\sigma_p - \sigma_m)}{(\sigma_p + 2\sigma_m)}\phi$
Bruggeman model	$\frac{(\sigma_p - \sigma_{eff})}{(\sigma_p - \sigma_m)}(\frac{\sigma_m}{\sigma_{eff}})^{\frac{1}{3}} = (1-\phi)$

σ_m: Matrix thermal conductivity (S/m), σ_p: Particle thermal conductivity(S/m), ϕ: Particle volume faction, σ_{eff}: Effective electrical conductivity of aluminum metal matrix composite (S/m).

Note: The contents are cited from references 11-13.

The parameters used in the thermal conductivity and electrical conductivity prediction models are shown in Table 3-8.

Table 3-8 Thermal conductivity and electrical conductivity of the material [14-17].

Material code	**TC of matrix [W/(m·K)]**	**TC of particle [W/(m·k)]**	**EC of matrix (S/m)**	**EC of particle (S/m)**
1100-B_4C	222		3.4×10^7	
6063-B_4C	193		3.1×10^7	
6351-B_4C	176	30	2.7×10^7	300
3004-B_4C	162		2.43×10^7	
6061-Al_2O_3	180		2.49×10^7	

Note: The contents are cited from references 14-17.

References

[1] *Standard Test Method for Thermal Diffusivity by the Flash Method*, ASTM E1461-13 (2022), A. International, 2022. [Online]. Available: https://www.astm.org/e1461-13r22.html

[2] *Standard Test Method for Determining Electrical Conductivity Using the Electromagnetic (Eddy Current) Method*, ASTM E1004-17 (2017), A. International, 2017. [Online]. Available: https://standards.globalspec.com/std/3864794/ASTM%20E1004-17

[3] A. Every, Y. Tzou, D. Hasselman, and R. Raj, "The effect of particle size on the thermal conductivity of ZnS/diamond composites," *Acta metallurgica et materialia*, vol. 40, no. 1, pp. 123-129, 1992, doi: https://doi.org/10.1016/0956-7151(92)90205-S.

[4] W. Kingery, "Thermal conductivity: XIV, conductivity of multicomponent systems," *Journal of the American Ceramic Society*, vol. 42, no. 12, pp. 617-627, 1959, doi: https://doi.org/10.1111/j.1151-2916.1959.tb13583.x.

[5] J. C. Maxwell, *A treatise on electricity and magnetism. Volume I*, 3rd ed. Oxford, England, UK: Oxford University Press, 1955.

[6] S. Polat, Y. Sun, E. Çevik, and H. Colijn, "Evaluation of thermal conductivity of GNPs-doped B_4C/Al-Si composites in terms of interface interaction and electron mobility," *Diamond & Related Materials*, vol. 98, 2019, doi: https://doi.org/10.1016/j.diamond.2019.107457.

[7] Y. Sun, C. Zhang, L. He, Q. Meng, B.-C. Liu, K. Gao, and J. Wu, "Enhanced bending strength and thermal conductivity in diamond/Al composites with B_4C coating," *Scientific Reports*, vol. 8, no. 1, pp. 1-12, 2018, doi: https://doi.org/10.1038/s41598-018-29510-7.

[8] A. Y. Dolgoborodov and M. Voskoboinikov, "Sound velocities in shock-compressed corundum, boron carbide," *Zh. Tekh. Fiz*, vol. 63, pp. 203-208, 1993. [Online]. Available: https://www.researchgate.net/profile/A-Dolgoborodov/publication/253574301_Sound_velocities_in_shock-compressed_corundum_boron_carbide_and_silicon_carbide/links/56eaba8d08ae95fa33c850d0/Sound-velocities-in-shock-compressed-corundum-boron-carbide-and-silicon-carbide.pdf.

[9] Y.-J. Wu, L. Fang, and Y. Xu, "Predicting interfacial thermal resistance by machine learning," *npj Computational Materials*, vol. 5, no. 1, pp. 1-8, 2019, doi: https://doi.org/10.1038/s41524-019-0193-0.

[10] Y. Zhang, T. Mashimo, Y. Uemura, M. Uchino, M. Kodama, K. Shibata, K. Fukuoka, M. Kikuchi, T. Kobayashi, and T. Sekine, "Shock compression behaviors of boron carbide (B_4C)," *Journal of applied physics*, vol. 100, no. 11, p. 113536, 2006, doi: https://doi.org/10.1063/1.2399334.

[11] V. D. Bruggeman, "Berechnung verschiedener physikalischer Konstanten von heterogenen Substanzen," *Annalen der physik*, vol. 416, no. 7, pp. 636-664, 1935, doi: https://doi.org/10.1002/andp.19354160705.

[12] J. Kovacik, "Electrical conductivity of two-phase composite material," *Scripta materialia*, vol. 39, no. 2, pp. 153-157, 1998, doi: https://doi.org/10.1016/S1359-6462(98)00147-X.

[13] K. W. Wagner, "Erklärung der dielektrischen Nachwirkungsvorgänge auf Grund Maxwellscher Vorstellungen," *Archiv für Elektrotechnik*, vol. 2, no. 9, pp. 371-387, 1914/09/01 1914, doi: https://doi.org/10.1007/BF01657322.

[14] A. H. Committee, "Properties of wrought aluminum and aluminum alloys," *vol. 2, ASM Handbook, Volume 2: Properties and selection: nonferrous alloys and special-purpose materials*Materials Park, Ohio, USA: ASM International, 1990, pp. 62-122.

[15] T. Gomi, N. Fukushima, and J. Matsushita, "High temperature electrical conductivity of B_4C, SiC and SiB_6 sintered bodies," *Journal of Advanced Science*, vol. 13, no. 1-2, pp. 15-16, 2001, doi: https://doi.org/10.2978/jsas.13.15.

[16] T. Maruyama and S. Onose, "Fabrication and thermal conductivity of boron carbide/copper cermet," *Journal of nuclear science and technology*, vol. 36, no. 4, pp. 380-385, 1999, doi: https://doi.org/10.1080/18811248.1999.9726221.

[17] Matweb. "Alumina, alpha Al_2O_3, 99.5%." https://www.matweb.com/search/DataSheet.aspx?MatGUID=0654701067d147e88e8a38c646dda195.

CHAPTER 4 EVOLUTION OF THERMAL CONDUCTIVITY AND ELECTRICAL CONDUCTIVITY IN 1100-B_4C MMCS

This chapter introduces the evolution of thermal conductivity (TC) and electrical conductivity (EC) in 1100-B_4C composites (MMCs) with the B_4C volume fraction of 6, 11, 16, 19, 21 and 30 vol.%, the details of experimental 1100-B_4C MMCs are listed in Table 4-1. The B_4C particles and reaction products were characterized and quantified by optical microscopy (OM) and scanning electron microscopy (SEM). The influence of testing temperature, heat treatment and volume fraction/size of B_4C particles on TC and EC is investigated. Besides, the applicability of models to TC/EC of Al-B_4C MMCs are discussed in conjunction with parallel [1, 2], Maxwell [3], Maxwell-Wagner [4], Bruggeman-ET [5] and Bruggeman [6] models. Finally, the relationship between TC and EC is explored and an empirical equation is established.

Table 4-1 Details of experimental 1100-B_4C MMCs used in this chapter.

Composites code	Matrix	B_4C (Vol. %)	Condition
6-4R	1100	6	Rolled plate (4 mm)
11-3R		11	Rolled plate (3 mm)
11-6R		11	Rolled plate (6 mm)
16-4R		16	Rolled plate (4 mm)
19-3R		19	Rolled plate (3 mm)
19-6R		19	Rolled plate (6 mm)
21-3R		21	Rolled plate (3 mm)
21-6R		21	Rolled plate (6 mm)
30-2R		30	Rolled plate (2 mm)

Note: 6-4R: 6 is the volume fraction of B_4C; 4 is the thickness of the plate; R is the condition for rolling.

4.1 Microstructure characterization of composites

Figure 4-1 shows the morphology of two different B_4C powders used in this work. One is F400 (Figure 4-1(a)) with a finer average particle size of 17.5 ± 1.0μm, which is used in MMCs with relative lower volume fraction of B_4C as 6-16vol.%. The other is F320 (Figure 4-1(b)) with average particle size of 29.2 ± 1.5 μm, which is coarser than F400 and widely used in MMCs with high volume of B_4C, such as 19-30%. Both F400 and F320 is approximately ellipsoidal, as shown in Figure 4-1.

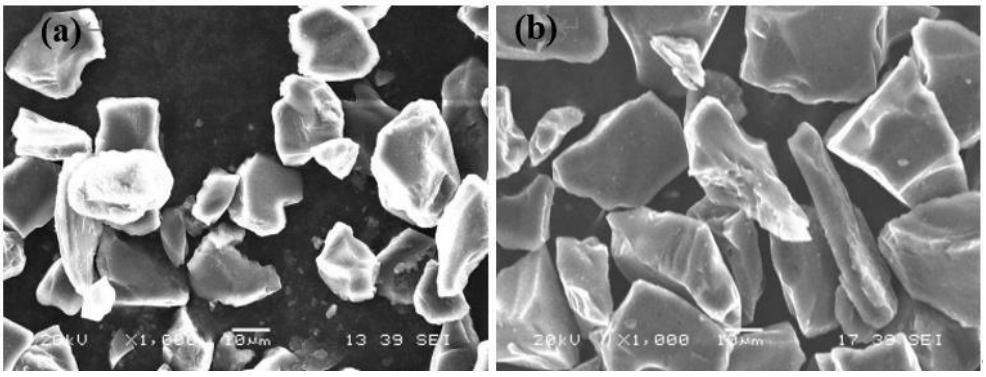

Figure 4-1 SEM image of B_4C powder (a) F400, (b) F320.

Figure 4-2 presents the microstructure of 11-3R and 21-3R as example of composites with F400 and F320, respectively.

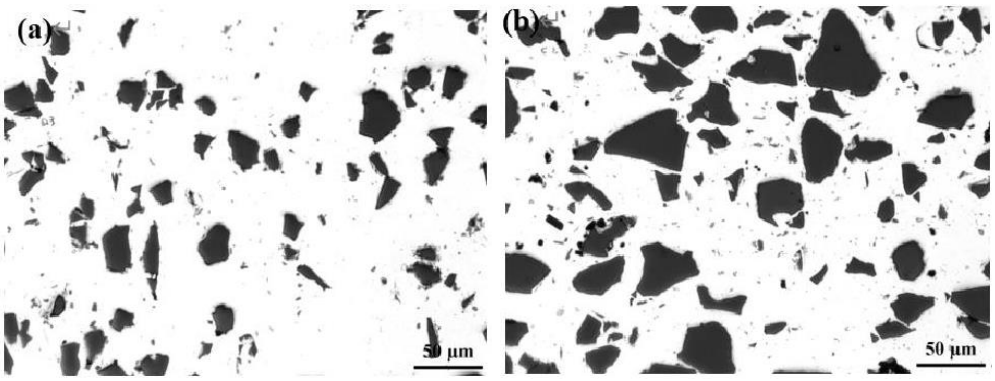

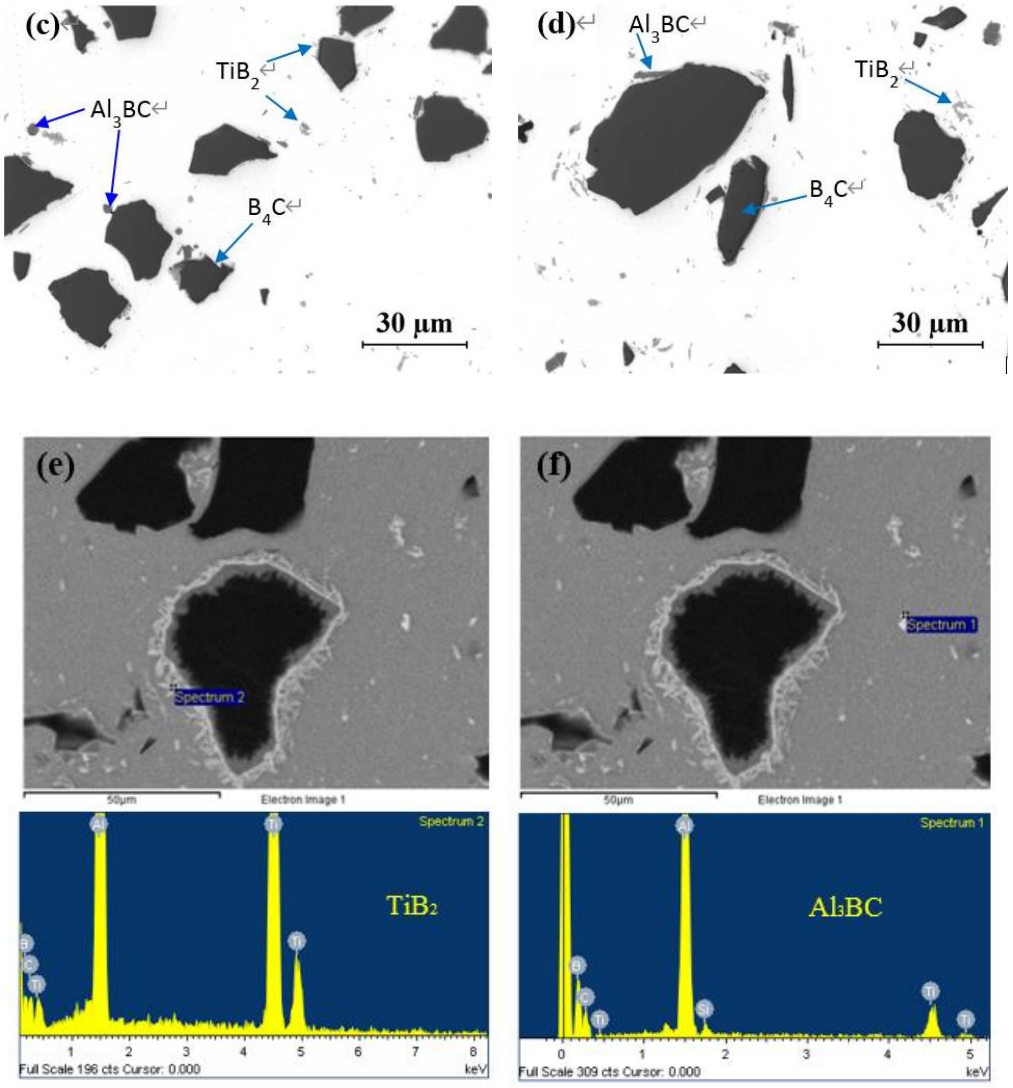

Figure 4-2 Optical microstructure of 1100-B_4C at 200X (a) 11-3R, (b) 21-3R, and 500X (c) 11-3R, (d) 21-3R. And the EDS phase analysis (e) TiB_2, (f) Al_3BC.

It can be observed that the B_4C particles are uniformly distributed without agglomeration in the aluminum matrix with both relative lower (11-3R) and higher volume (21-3R) of B_4C. This indicates that the composite structure is homogeneous and dense. The B_4C particle resembles an ellipsoid as shown in Figure 4-2 and the particle size of 21-3R is larger than that of 11-3R since F320 is used in 21-3R while F400 is for 11-3R. No severe B_4C degradation has occurred during the manufacturing process. Besides, a small amount of

reaction products was observed to attach to or close to the B_4C particles (Figure 4-2 (c) and (d)). The composition analysis of the constituent phases is shown in Figure 4-2 ((e) and (f)) and combined with existing research, the phase can be determined as the dark-gray Al_3BC and light-gray TiB_2 particles (to optimize the interfacial reaction and control the production of reaction products, Ti was added) [7].

Figure 4-3 displays the typical interfacial reaction layer of 21-3R in details. B_4C particles are generally covered with a thin interfacial reactive layer (usually less than 1μm) [8] composed of various reactive particles (Figure 4-3 (a)). According to the Figure 4-2 ((e) and (f)), most of these particles are identified as TiB_2 particles with hexagonal morphology, and a few Al_3BC distributed near B_4C. In the high magnification view (Figure 4-3 (b)), it is evident that two distinct reactive layers are observed at the interface between B_4C and Al. The reaction layer contains TiB_2 and Al_3BC and grows overlapping around the B_4C particles. The layer near the surface of B_4C is a continuous crystalline layer composed of fine grains while a sawtooth layer near the surface of the aluminum matrix is composed of irregularly oriented coarse crystals, which grow randomly from the fine-grained layer to the aluminum substrate and form a discontinuous layer.

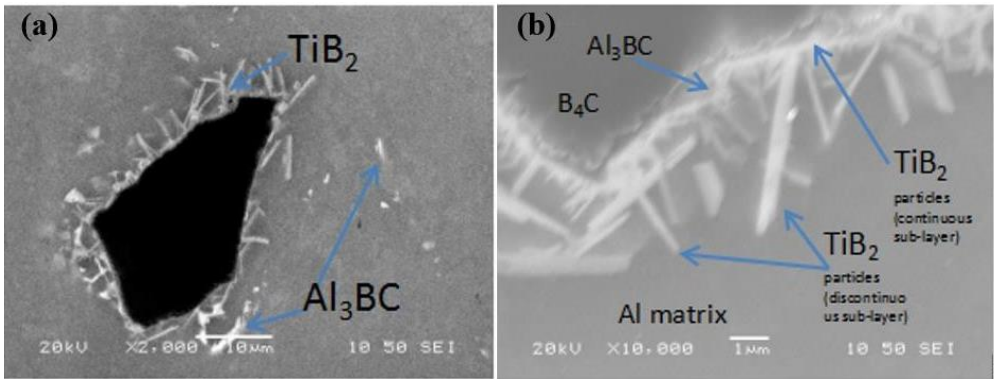

Figure 4-3 SEM image showing the morphology of the interface reaction layer of 21-3R at (a) 2000X, (b) 10000X.

Image analysis is performed to quantify the B_4C particles and the reaction products, which is shown in Figure 4-4. According to the color contrast of various particles, they are highlighted with different colors and then quantified. For instance, blue ones represent B_4C particles and red for Al_3BC while green for TiB_2.

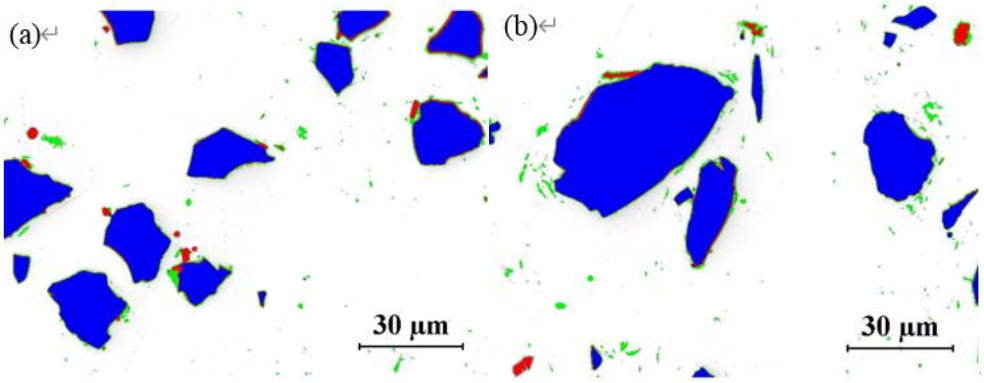

Figure 4-4 CLEMET image analysis on defining the B_4C particles and reaction products at 500X (a) 11-3R, (b) 21-3R.

Table 4-2 shows the area fraction of B_4C particles and reaction products from image analysis. It can be found that the measured volume fraction of B_4C is close to the nominal ones. For instance, the volume fraction of B_4C in 16-4R is 16.3 vol % and 32.2 vol% for 30-2R. Besides, the volume fraction of reaction products increases with increasing B_4C volume fraction, which is rising from 1.43vol % in 6-4R to 4.3 vol % in 19-6R and further to 10.55 vol % in 30-2R. It was also found that the total particle amount (B_4C+reaction product) increased with the volume fraction of B_4C, which is from 8.13 vol% for 6-4R to 25.4 vol% for 19-6R to 42.74 vol% for 30-2R. This is because the chance of interfacial reaction increases with the increase of B_4C volume fraction and thus leads to the increase of reaction products. And the formation of interfacial reaction will consume B_4C, but the consumption of B_4C volume fraction is less than the production of reaction products, so the total particle volume fraction will still increase with the increase of the theoretical B_4C volume fraction [8]. In

addition, it seems there is no obvious difference on the volume of interaction products and total particles in sample with same B_4C volume but with different thickness, Considering the image analysis measurement bias caused by sample preparation quality and equipment errors.

Table 4-2 Volume fraction of B_4C particles and reaction product particles from image analysis.

Material code	$V_{total\ particles}$	V_p	V_r
6-4R	8.13 (1.40)	6.70 (0.79)	1.43 (0.62)
11-3R	15.93 (1.09)	12.80 (0.84)	3.13 (0.25)
11-6R	15.14 (0.81)	12.05 (0.47)	3.09 (0.34)
16-4R	20.04 (1.67)	16.30 (0.99)	3.74 (0.68)
19-3R	25.86 (2.64)	21.26 (2.4)	4.60 (0.64)
19-6R	25.40 (2.51)	21.10 (1.6)	4.30 (0.91)
21-3R	28.83 (1.74)	22.20 (1.12)	5.83 (0.64)
21-6R	26.89 (2.08)	21.63 (1.17)	5.26 (0.91)
30-2R	42.74 (2.09)	32.19 (1.09)	10.55 (1.00)

$V_{total\ particles}$: Particle volume fraction plus reaction product volume fraction, V_p : Volume fraction of B_4C, V_r : Volume fraction of reaction product.

4.2 Evolution of TC/EC in 1100-B_4C MMCs

Figure 4-5 shows the evolution of TC tested at 25℃ [9],150℃ and 250℃ by a laser flash thermal conductivity tester in as-rolled 6-4R (F400) and 30-2R (F320). It can be found that the measured TC are basically the same at all testing temperatures of 25℃ [9], 150℃ and 250℃ for studied MMCs with both F400 and F320 particles, indicating the independence of TC of temperature in the range up to 250-300℃. Meanwhile, due to the higher reliability and thermal conductivity of the laser flash thermal conductivity tester at 250°C. Therefore, the TC data measured at 250℃ is reasonable to be the representative TC at room temperature and used in the follow studied.

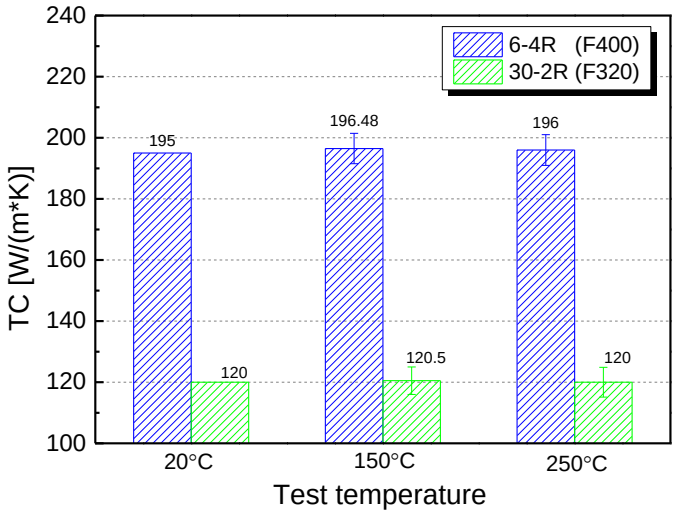

Figure 4-5 Measured TC at various temperatures in as-rolled 6-4R and 30-2R.

4.2.1 Effect of heat treatment on TC/EC in 1100-B_4C MMCs

Figure 4-6 displays the evolution of TC/EC with heat treatment (HT) temperatures (Figure 4-6 (a)) and holding times (Figure 4-6 (b)) of 21-3R. As shown in Figure 4-6 (a), when holding for 4h, TC/EC increases with the increase of HT temperature until to 430℃ and then follows by a plateau at 430℃-490℃. On the other hand, TC/EC is observed to increase with holding time under fixed HT temperature. As shown in Figure 4-6 (b), TC of 21-3R increase from 153.4 [W/(m·K)] at as-rolled condition to 155.2 [W/(m·K)] after 4h and further to 156.6 [W/(m·K)] after 23 h when treated at 380°C. And the EC of 21-3R increased from 2.34831×10^7 in the as-rolled state to 2.34901×10^7 after 4h, and further increased to 2.35011×10^7 after 23h when treated at 380℃.

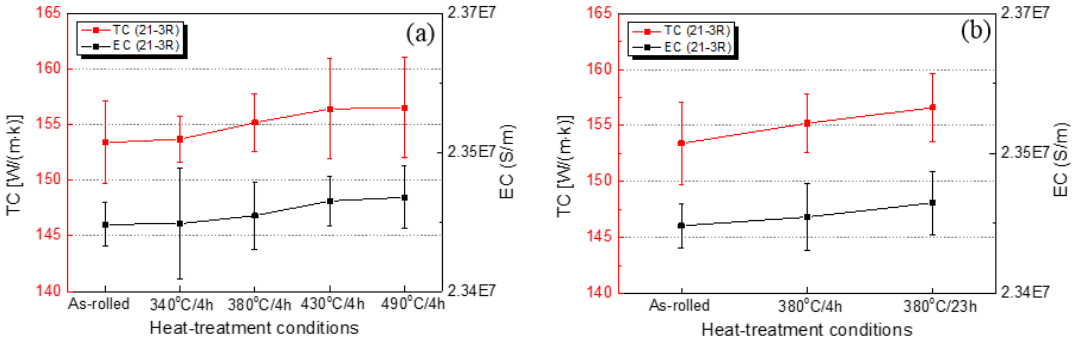

Figure 4-6 Evolution of TC with (a) HT temperature and (b) holding time in 21-3R.

As well known, the TC/EC in the aluminum matrix is achieved by the propagation of electrons and phonons and is mainly affected by lattice vibrations [10, 11]. Therefore, any factors effecting the movement of electrons and phonons can have an influence on TC and EC, which can be B_4C particles, reaction products and matrix, etc. Therefore, when these factors are affected, the corresponding EC and TC will also change. In the present work, due to the materials are hot-rolled, which can lead to the sever deformation during the hot-rolling, introducing a higher volume of dislocations for the matrix [12]. Then the present of high number of dislocations can further act as the barriers for the movement of electrons and phonons, leading to the lower of TC/EC at as-rolled condition [12]. As shown in Figure 4-7 (a), all the grains are all elongated due to the sever deformation in as-rolled condition and the resultant TC of 153.4 [W/(m·K)]. However, during the annealing heat treatment, the dislocations has been partially or fully released due to the recrystallization. Then the barriers from dislocations to electrons/phonons are much lower, resulting in the increase of EC/TC during the annealing heat treatment. As shown in Figure 4-7 (b), the grains are becoming into equiaxed after treated at 380℃/23h and then the TC increases to 156.6 [W/(m·K)].

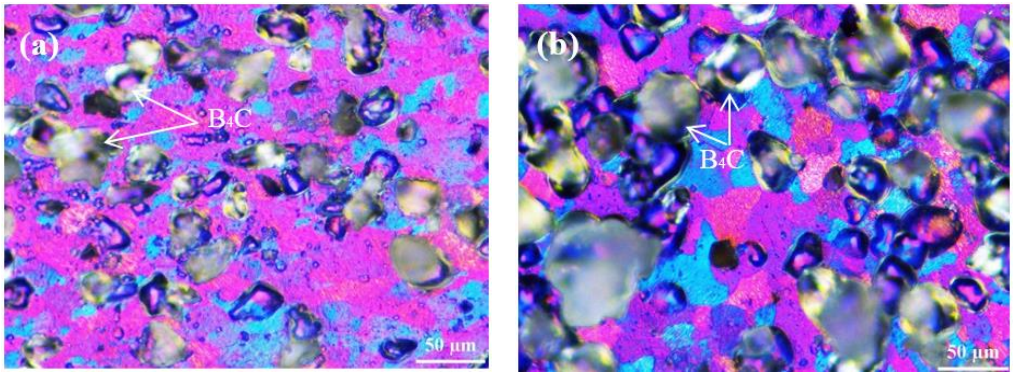

Figure 4-7 Grain shape for 11-3R after electro-etching at the condition (a) As-rolled and (b) HT-380℃/23h.

In addition, the evolution of TC/EC in MMCs with different rolling thicknesses under rolling and 380℃/23h heat treatment conditions are shown in Figure 4-8. It can be observed that the difference of TC/EC between MMCs with 3 and 6 mm thickness is a little bigger in as-rolled than heat-treated condition, especially for TC. Taking 11-6R and 11-3R as example, the difference of TC is ~ 2 (181 vs. 179) [W/(m·K)] at as-rolled condition while this difference decreases to 0.2 [W/(m·K)] (183.9 vs 183.7) at heat-treated condition. This can also be explained by the different grain structures in as-rolled and heat treated conditions. In as-rolled condition, the deformation is slightly higher for 3mm plate than 6mm, which may introduce more dislocations as the barriers for the movement of electrons. Therefore, it is reasonable to have some difference between 3mm and 6mm plates, which is 2 unit for MMCs with 11 vol% B_4C (11-3R vs 11-6R). However, the grains are fully recrystallized after 380℃/23h for both MMCs and the almost all the dislocations are released. Therefore, there is little difference on the grain structure and distribution of dislocations between 3mm and 6mm plates, resulting in the much smaller difference between these two conditions under different thickness (Figure 4-8 (b)).

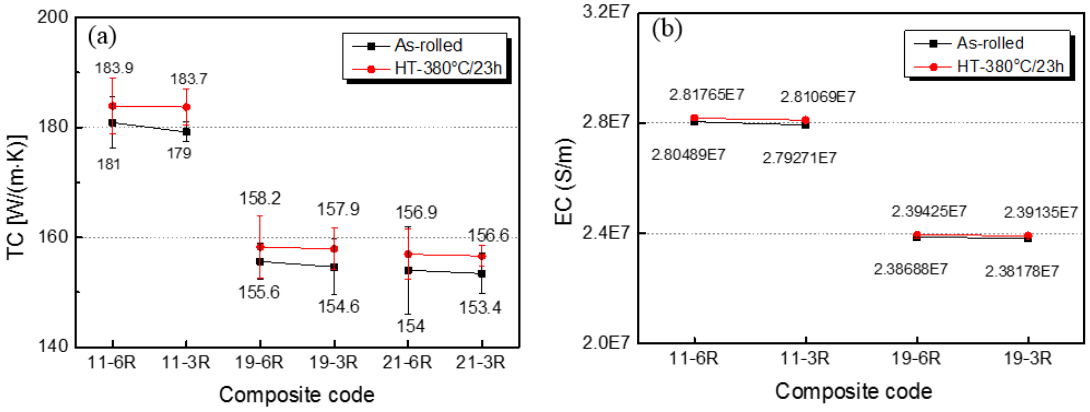

Figure 4-8 Evolution of TC/EC with different thickness at as-rolled and HT-380℃/ 23h (a) TC, (b) EC.

4.2.2 Effect of particle volume fraction on TC/EC

Figure 4-9 displays the relationship between TC/EC and the volume fraction of B_4C in 1100-B_4C MMCs. It can be observed that the TC/EC is linearly decreases with the increase of B_4C volume fraction under the condition of the same particle radius. At lower volume fractions (6-16Vol.%), the TC of 1100-B_4C decreased from 196 [W/(m·K)] to 170 [W/(m·K)], which is ~ 13% reduction (Figure 4-9 (a)). At higher volume fractions (19-30 Vol.%), the TC value of the composite decreases from 155 [W/(m·K)] to 120 [W/(m·K)], which is reduced by 22.5 % (Figure 4-9 (b)). For the evolution of EC, it decreased from 3,210,890 (S/m) to 2,607,690 (S/m) (Figure 4-9 (a)) at lower volume fractions of B_4C (6-16Vol.%), which is ~ 18.8% reduction. At higher volume fractions (19-30 Vol.%), EC decreases from 2,381,780 (S/m) to 11,918,650 (S/m), which is reduced by 19.4 % (Figure 4-9 (b)). Figure 4-9 (c) displays the evolution of TC/EC with volume fraction of B_4C particle without considering the particle size and a linearly relations can also be observed, indicating the minor influence of particle size on the evolution of TC/EC.

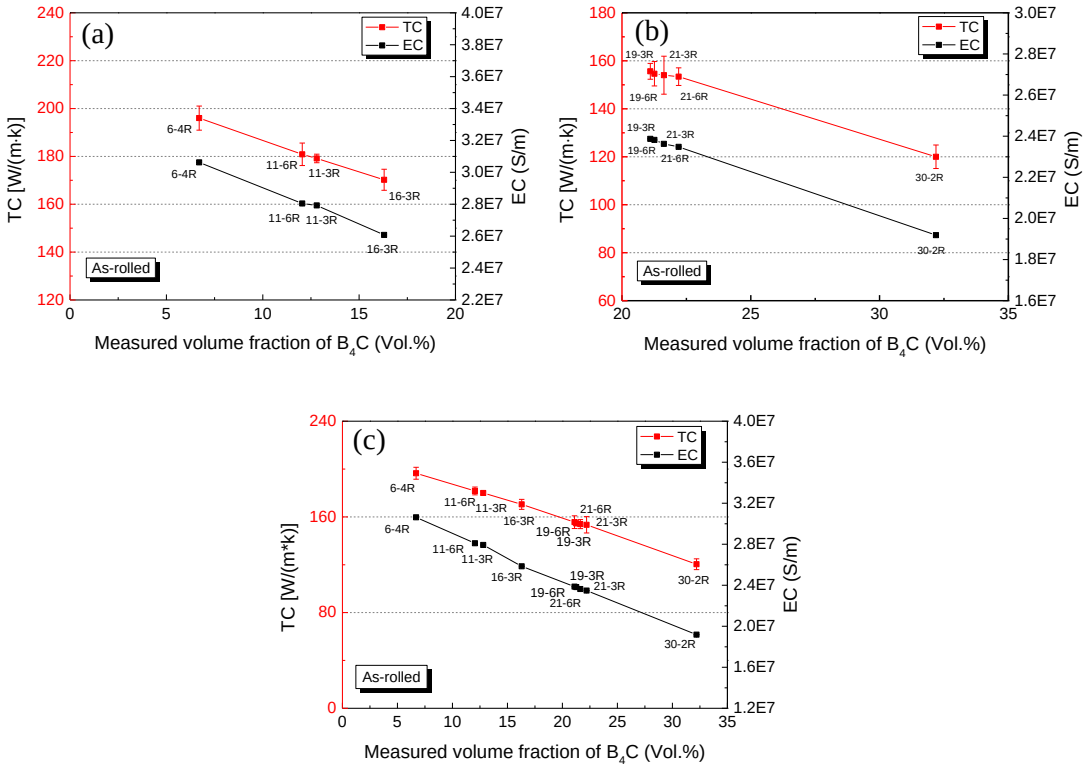

Figure 4-9 Evolution of TC/EC with different volume fraction of B_4C (a) 6-16 Vol.% (F400), (b) 19-30 Vol.% (F320) and (c) 6-30 Vol.%.

In general, both particle size and particle volume fraction can affect the TC/EC of composites. At the same particle size, the TC/EC of the composite will increase (TC/EC of the matrix < TC/EC of the particles) or decrease (TC/EC of the matrix > TC/EC of the particles) with the increase of the filler particles [13]. Since B_4C particles are semiconductors [14] with a poor TC and EC, therefore, the TC/EC of 1100-B_4C decreased as B_4C particles increased at the same particle size. Meanwhile, from Figure 4-9 (c), it can be found that TC/EC generally decreases with two different particle sizes (F400, F320), and the decreasing rate is similar with that in individual particle size, indicating that particle size may have little effect on TC/EC at these two particle sizes. To further verify this conjecture, this study was carried out in conjunction with the TC/EC prediction model in Section 4.3.

4.3 Predictive models for evolution of TC/EC

To explore the applicability of some existing typical TC (Table 4-2)/EC (Table 4-3) prediction models for 1100-B_4C MMCs and the effect of particle size and interfacial thermal resistance/ interfacial resistance on TC/EC, various models are tested in the present work, including the parallel model, Maxwell/Maxwell-Wagner model and Bruggeman-ET/Bruggeman model, which has been listed in Table 4-3 and Table 4-4. The value of parameters for these models are summarized in Table 4-5.

Table 4-3 Description of TC models for 1100-B_4C materials [1, 3, 5].

Modelling	Model equation
Parallel model	$k_{eff} = k_p\phi + k_m(1-\phi)$
Maxwell model	$\frac{k_{eff}}{k_m} = \left(\frac{k_p + 2k_m + 2\phi(k_p - k_m)}{k_p + 2k_m - \phi(k_p - k_m)} \right)$
Bruggeman-ET model	$\left(\frac{k_{eff} - k_p(1-\alpha)}{k_m - k_p(1-\alpha)} \right)^{3/(1-\alpha)} \left(\frac{k_m}{k_{eff}} \right)^{(1+2\alpha)/(1-\alpha)} = (1-\phi)^3$

k_m: Matrix thermal conductivity [W/m·K], k_p: Particle thermal conductivity[W/m·K], ϕ: Particle volume faction, h_c: Thermal boundary conductivity [W/(m^2·K)], α: Dimensionless parameter, k_{eff}: Effective thermal conductivity of aluminum metal matrix composite [W/(m·K)].

Note: The contents are cited from references 1,3,5.

Table 4-4 Description of EC model for 1100-B_4C materials [2, 4, 6].

Modelling	Model equation
Parallel model	$\sigma_{eff} = \sigma_p\phi + \sigma_m(1-\phi)$
Maxwell-Wagner model	$\frac{\sigma_{eff}}{\sigma_m} = 1+3\frac{(\sigma_p - \sigma_m)}{(\sigma_p + 2\sigma_m)}\phi$
Bruggeman model	$\frac{(\sigma_p - \sigma_{eff})}{(\sigma_p - \sigma_m)}\left(\frac{\sigma_m}{\sigma_{eff}}\right)^{\frac{1}{3}} = (1-\phi)$

σ_m: Matrix thermal conductivity (S/m), σ_p: Particle thermal conductivity (S/m), ϕ: Particle volume faction, σ_{eff}: Effective electrical conductivity of aluminum metal matrix composite (S/m).

Note: The contents are cited from references 2,4,6.

Table 4-5 TC/EC and ITC of the material [14-17].

Material code	TC of matrix [W/(m·k)]	TC of particle [W/(m·k)]	EC of matrix (S/m)	EC of particle (S/m)	h_c (ITC) [W/(m^2·k)]
1100-B_4C	222	30	3.4×10^7	300	1.430×10^8

Note: The contents are cited from references 14-17.

Following the various models, Figure 4-10 (a) and (b) show the evolution of k_{eff}/k_m (ratio of effective TC of composite to matrix TC) and σ_{eff}/σ_m (ratio of effective EC of composite to matrix EC) with the volume fraction of B_4C particles, respectively.

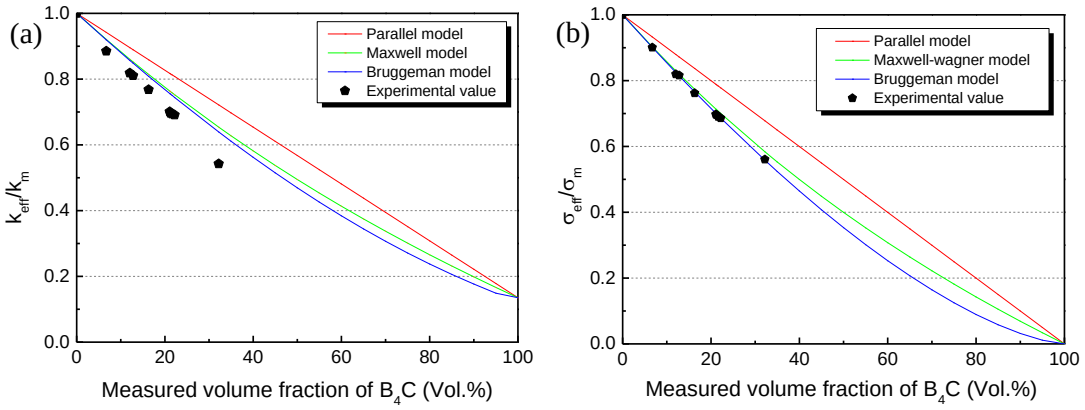

Figure 4-10 Comparison of TC/EC predict value and measured value under different models at (a) k_m/k_p (ratio of matrix TC to particle TC) =7.4, (b) σ_m/σ_p (ratio of matrix EC to particle EC) =1.14×10^5.

Comparing several prediction models of TC/EC, it is found that the parallel model occupies the highest positions of the theoretical predicted values. The Bruggeman-ET/ Bruggeman model approaches the Maxwell/Maxwell-Wagner model when the B_4C volume fraction is low (i.e., kp < 16 Vol.%), and gradually moves away from the Maxwell/Maxwell-Wagner model when the B_4C volume fraction growing high (i.e. 16 Vol.% < kp < 30 Vol.%) but with the largest gap still less than 3%, especially for Maxwell-Wagner and Bruggeman model is only 1.4%. Meanwhile, for low volume fraction B_4C particles, the predicted values

of Bruggeman-ET/Bruggeman and Maxwell/Maxwell-Wagner model are almost the same.

After comparing the predicted values form various models and experiment values, it is found that the predicted values of the Parallel model decreased the least than the matrix TC/EC. In addition, both Maxwell/Maxwell-Wagner model and Bruggeman-ET/Bruggeman model are closest to the experimental TC/EC, when the B_4C volume fraction is lower. Taking 16 Vol.% as examples, the difference between experimental and predict TC/EC is less than 4% TC/EC of AA1100 matrix, especially for EC, which is less than 1%. However, when the B_4C volume fraction is higher, only the Bruggeman-ET/Bruggeman model is closest to the experimental TC/EC. Taking 30 Vol.% as examples, the difference between experimental and predict TC/EC for Maxwell/Maxwell-Wagner model is less than 11% and 3% TC/EC of AA1100 matrix, respectively. But for Bruggeman-ET/Bruggeman model, the difference is less than 10% and 1% TC/EC of AA1100 matrix, respectively. Therefore, it can be concluded that the Bruggeman-ET/Bruggeman model is the most suitable model to predict the TC/EC in experimental 1100-B_4C composites.

Due to in the existing studies [1-6, 8, 14, 18], the predicted TC/EC with parallel model is simply calculated according to the general mixing rule, which is only related to the heat flow direction and the orientation of the continuous phase. And the parallel model represents the maximum value of TC/EC that the composite can theoretically achieve. The Maxwell model gives good results for the TC of composite which with well dispersed non-interacting spherical particles with low particle volume concentrations. However, the model cannot accurately predict the experimental TC at high particle volume fractions since it does not consider influencing factors, such as particle size and interfacial thermal resistance. While the Bruggeman-ET model considers the interfacial thermal resistance and particle size and is more suitable for composites at high volume fractions. Therefore, it is the most suitable prediction

model for the TC of 1100-B_4C MMCs.

Since the Bruggeman-ET model best matched the experimental thermal conductivity values, we simulated the TC of 1100-16 Vol.% B_4C MMCs (use measured B_4C volume fraction) with different particle sizes based on the Bruggeman-ET model. The particle radius is from 5 to 100μm with the thermal conductivity plotted in the Figure 4-11.

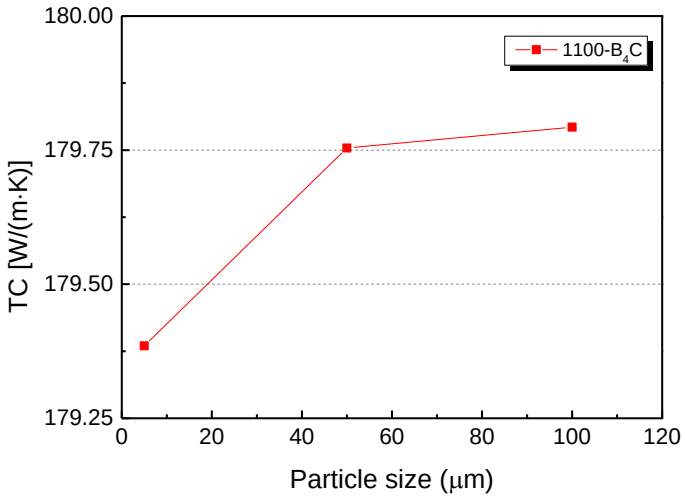

Figure 4-11 TC at different Particle Sizes at k_m/k_p =7.4.

It can be found that the change in TC is less than 0.5 [W/(m·K)] with the increase of particle radius. Since the interfacial thermal resistance is a function of particle size, and both TiB_2 and Al_3BC have good TC [19, 20]. So, it can be inferred that the interfacial thermal resistance has little effect on the TC of these composites [21]. In addition, as the Figures 4-3 and 4-4 shown, most of the reaction products are concentrated in the reaction layer, and there are very few reaction products distributed on the matrix. So, the effects of the reaction products on TC and EC are basically negligible. And the 1% difference between the prediction model and experimental value from Bruggeman-ET model for TC can be principally caused by the volume fraction.

Meanwhile for EC both Maxwell-Wagner and Bruggeman model all suitable for high-volume fraction and do not considering the interfacial electrical resistance and particle size. Moreover, TiB_2 has an EC similar to that of the Al matrix and Al_3BC can increase the stiffness of the lattice near the interface of Al_3BC and Al to a certain extent, so it has no effect on the EC of 1100-B_4C MMCs [22, 23]. Therefore, the EC main affect by B_4C volume fraction of the 1100-B_4C MMCs and not affected by the interfacial electrical resistance and particle size.

However, due to all those models are used for spherical particles, so their predicted value still has a certain gap with the TC/EC of the 1100-B_4C MMCs.

4.4 Relationship between TC and EC

As shown in Figure 4-9 (c), both the EC and TC of 1100-B_4C MMCs tend to decrease with the increase of the volume fraction of B_4C, it is inferred that there is a certain relationship between its EC and TC. It is generally known that the linear relationship between EC and TC in pure metals is verified by the Wiedemann-Franz law proposed by Weidmann and Franz [24], which is expressed as below.

$$K / \sigma = L \times T \tag{4-1}$$

Where K is the TC [W/(m·K)], T is the absolute temperature (K), L is the Lorentz constant (2.45×10^{-8} W·Ω/K^2), and σ is EC (S/m).

From the literature [25], this relationship only applies to a single metal. Hence, L.W. KEMP et al. [26] explored the relationship between TC and EC in Al alloys using data fitting and obtained empirical equations suitable for Al alloys, which is expressed as below:

$$K = L \times T \times \sigma + k \quad (4\text{-}2)$$

Where K is the total TC [W/(m·K)], k is the TC of the non-metallic or atomic part (12.552 [W/(m·K)]), and L is the constant (2.10×10^{-8} W·Ω/K^2) can be regarded as the true Lorentz ratio of the metallic part, σ is the EC (S/m), and T is the absolute temperature (K).

According to the data in Figure 4-9, Figure 4-12 was drawn to explore the relationship between the EC and TC in studied 1100-B_4C MMCs.

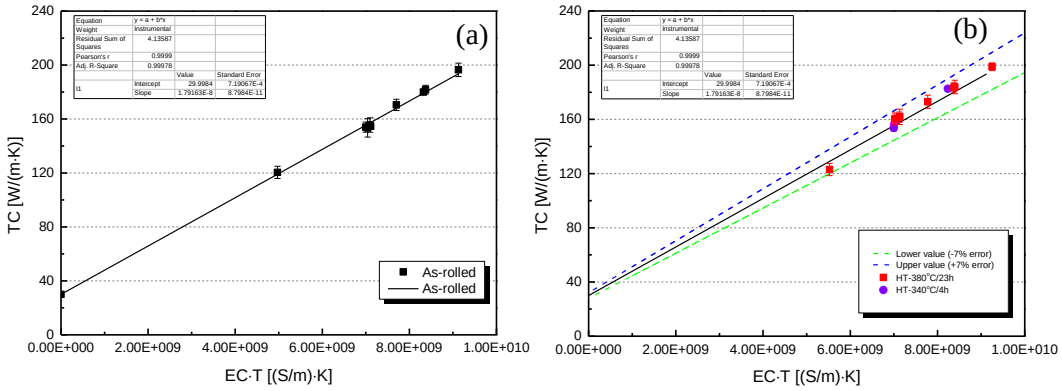

Figure 4-12 Relationship between EC and TC under (a) as-rolled condition (b) verification by 1100-B_4C-HT at 380℃/23h.

As shown in Figure 4-12 (a), the EC and TC data can be fitted as linear with the equation of K=L×T×σ+k, and R^2 as 0.99.

$$K = 1.79163\times10^{-8} \times T \times \sigma + 29.998 \quad (4\text{-}3)$$

Where K is the total TC [W/(m·K)], T is the absolute temperature (K) at room temperature, σ is the EC, and L is a constant (1.79163×10^{-8} W·Ω/K^2), can be regarded as the

true Lorentz ratio of the metallic.

In addition, as shown in Figure 4-12 (b), it is found that the TC values after annealing distributed in the vicinity of the fitted straight line. Therefore, we calculated the ±7% error of this equation and the red line represents the upper value of TC (+7%) while the green line is for the lower value of TC (-7%). As shown in Figure 4-12 (b), the TC values of 1100-B_4C MMCs at HT-380℃/23h and 340℃/4h conditions are 100% included in these two lines. Furthermore, it can be seen that the residual error between the measured TC value after annealing and the TC value after annealing predicted by the equation is about 5% of measured TC value after annealing, which is lower than the laser flash test error of 7% [27]. Therefore, it can be considered that both the EC and TC after annealing also fit equation obtained from as-received condition (K=1.79163×10^{-8}×T×σ+29.998) in Figure 4-12 (a).

4.5 Summary

1. The reaction products increase with the increasing volume fraction of B_4C particles.
2. The thermal conductivity of Al-B_4C composites is not affected by the test temperature in the range of room temperature to 250℃.
3. Annealing treatment can improve the TC/EC of 1100-B_4C composites, and the thermal conductivity reaches the maximum value when it is completely recrystallized at 430℃/4h or 380℃/23h.
4. The TC/EC of 1100-B_4C composites decreased with the increase of B_4C volume fraction. However, particle size and interfacial thermal resistance do not contribute to this decreasing trend.
5. Compared with other TC/EC prediction models, the Bruggeman-ET/Bruggeman model is the most suitable for predicting the TC/EC of 1100-B_4C composites.

6. There is a linear relationship between the electrical and thermal conductivity of 1100-B_4C composites. The fitting equation is $K=1.79163\times10^{-8}\times T\times\sigma+29.998$.

References

[1] W. Kingery, "Thermal conductivity: XIV, conductivity of multicomponent systems," *Journal of the American Ceramic Society*, vol. 42, no. 12, pp. 617-627, 1959, doi: https://doi.org/10.1111/j.1151-2916.1959.tb13583.x.

[2] J. Kovacik, "Electrical conductivity of two-phase composite material," *Scripta materialia*, vol. 39, no. 2, pp. 153-157, 1998, doi: https://doi.org/10.1016/S1359-6462(98)00147-X.

[3] J. C. Maxwell, *A treatise on electricity and magnetism. Volume I*, 3rd ed. Oxford, England, UK: Oxford University Press, 1955.

[4] K. W. Wagner, "Erklärung der dielektrischen Nachwirkungsvorgänge auf Grund Maxwellscher Vorstellungen," *Archiv für Elektrotechnik*, vol. 2, no. 9, pp. 371-387, 1914/09/01 1914, doi: https://doi.org/10.1007/BF01657322.

[5] A. Every, Y. Tzou, D. Hasselman, and R. Raj, "The effect of particle size on the thermal conductivity of ZnS/diamond composites," *Acta metallurgica et materialia*, vol. 40, no. 1, pp. 123-129, 1992, doi: https://doi.org/10.1016/0956-7151(92)90205-S.

[6] V. D. Bruggeman, "Berechnung verschiedener physikalischer Konstanten von heterogenen Substanzen," *Annalen der physik*, vol. 416, no. 7, pp. 636-664, 1935, doi: https://doi.org/10.1002/andp.19354160705.

[7] Z. Zhang, K. Fortin, A. Charette, and X. G. Chen, "Effect of titanium on microstructure and fluidity of Al-B_4C composites," *Journal of Materials Science*, vol. 46, no. 9, pp. 3176-3185, 2011, doi: https://doi.org/10.1007/s10853-010-5201-1.

[8] Z. Zhang, K. Fortin, A. Charette, and X.-G. Chen, "Effect of titanium on microstructure and fluidity of Al–B_4C composites," *Journal of materials science*, vol. 46, no. 9, pp. 3182-3185, 2011, doi: https://doi.org/10.1007/s10853-010-5201-1.

[9] X. G. Chen, Hark, R., and 137th TMS Annual Meeting and Exhibition, 2008 New Orleans, LA, USA 2008 03 09 - 2008 03 13., "Development of Al-30% B_4C metal matrix composites for neutron absorber material," *TMS Annual Meeting*, pp. 3-9, 2008. [Online]. Available: https://uqac.on.worldcat.org/search/detail/282762174?queryString=Development%20of%20Al-30%25%20B4C%20metal%20matrix%20composites%20for%20neutron%20absorber%20material&clusterResults=true&stickyFacetsChecked=true&groupVariantRecords=false&scope=&changedFacet=scope.

[10] C. Uher, "Thermal Conductivity of Metals " in Thermal conductivity: theory, properties, and applications, T. M. Tritt Ed.: Springer Science & Business Media, 2005, pp. 21-88.

[11] G. S. Nolas and H. J. Goldsmid, "Thermal Conductivity of Semiconductors " in Thermal conductivity: theory, properties, and applications, T. M. Tritt Ed.: Springer Science & Business Media, 2005, pp. 105-120.

[12] M. Khademian, A. Alizadeh, and A. Abdollahi, "Fabrication and characterization of hot rolled and hot extruded boron carbide (B_4C) reinforced A356 aluminum alloy matrix composites produced by stir casting method," *Transactions of the Indian Institute of Metals*, vol. 70, no. 6, pp. 1635-1646, 2017, doi: https://doi.org/10.1007/s12666-016-0962-0.

[13] C.-W. Nan, R. Birringer, D. R. Clarke, and H. Gleiter, "Effective thermal conductivity of particulate composites with interfacial thermal resistance," *Journal of Applied Physics*, vol. 81, no. 10, pp. 6692-6699, 1997, doi: https://doi.org/10.1063/1.365209.

[14] T. Gomi, N. Fukushima, and J. Matsuita, "High temperature electrical conductivity of B_4C, SiC and SiB_6 sintered bodies," *Journal of Advanced Science*, vol. 13, no. 1-2, pp. 15-16, 2001, doi: https://doi.org/10.2978/jsas.13.15.

[15] F. Alhama, D. Alcaraz, and S. Gomez-Lopera, "Bounds of the thermal conductivity i n discontinuously reinforced metal-matrix composites," in *Materials Science Forum*, 2005, vol. 475: Trans Tech Publ, pp. 3335-3338.

[16] A. H. Committee, "Properties of wrought aluminum and aluminum alloys," *vol. 2, AS M Handbook, Volume 2: Properties and selection: nonferrous alloys and special-pur pose materials*Materials Park, Ohio, USA: ASM International, 1990, pp. 62-122.

[17] T. Maruyama and S. Onose, "Fabrication and thermal conductivity of boron carbide/c opper cermet," *Journal of nuclear science and technology*, vol. 36, no. 4, pp. 380-385, 1999, doi: https://doi.org/10.1080/18811248.1999.9726221.

[18] Y. Sun, C. Zhang, L. He, Q. Meng, B.-C. Liu, K. Gao, and J. Wu, "Enhanced bending strength and thermal conductivity in diamond/Al composites with B4C coating," *Scie ntific Reports*, vol. 8, no. 1, pp. 1-12, 2018, doi: https://doi.org/10.1038/s41598-018-2 9510-7.

[19] B. Basu, G. B. Raju, and A. K. Suri, "Processing and properties of monolithic TiB_2 ba sed materials," *International Materials Reviews*, vol. 51, no. 6, pp. 352-374, 2006/12/ 01 2006, doi: https://doi.org/ 10.1179/174328006X102529.

[20] A. Huguenot, A. l. Riot, B. t. Boucher, B. Fontaine, S. p. Cordier, R. Al Rahal Al Ora bi, H. Hillebrecht, T. Mori, J.-F. o. Halet, and R. g. Gautier, "Is the alumino-boron ca rbide Al_3BC a promising thermoelectric material? A computational exploration," *Soli d State Sciences*, vol. 104, 2020, doi: https://doi.org/ 10.1016/j.solidstatesciences.202 0.106205.

[21] Y.-S. Jhong, H.-T. Tseng, and S.-J. Lin, "Diamond/Ag-Ti composites with high therm al conductivity and excellent thermal cycling performance fabricated by pressureless sintering," *Journal of Alloys and Compounds*, vol. 801, pp. 589-595, 2019, doi: https: //doi.org/10.1016/j.jallcom.2019.06.167.

[22] M. Rahman, C. Wang, W. Chen, S. A. Akbar, and C. Mroz, "Electrical Resistivity of Titanium Diboride and Zironium Diboride," *Journal of the American Ceramic Societ y*, vol. 78, pp. 1380-1382, 09/28 2005, doi: https://doi.org/10.1111/j.1151-2916.1995. tb08498.x.

[23] Q. Zhao, X. Cui, Z. Qian, and X. Liu, "The synergistic effect of Al-B-C master alloy t o improve conductivity and strength of 1070 alloy," *Journal of Alloys and Compound s*, vol. 639, pp. 478-482, 2015/08/05/ 2015, doi: https://doi.org/10.1016/j.jallcom.201 5.03.091.

[24] R. Franz and G. Wiedemann, "Ueber die Wärme - Leitungsfähigkeit der Metalle," *An nalen der Physik*, vol. 165, no. 8, pp. 497-531, 1853. [Online]. Available: https://ia60 0708.us.archive.org/view_archive.php?archive=/22/items/crossref-pre-1909-scholarl y-works/10.1002%252Fandp.18521620610.zip&file=10.1002%252Fandp.18531650 802.pdf.

[25] L. D. George, C. B. Plummer, D. Ruiz, and X. Wang, "Thermal and Electrical Transp ort Measurements in Wrought and Cast Aluminum Alloys," Bachelor, Science, Worc ester Polytechnic Institute Worcester, Massachusetts, USA, 2015. [Online]. Availabl e: https://scholar.google.com/scholar?hl=zh-CN&as_sdt=0%2C5&q=Thermal+and+ Electrical+Transport+Measurements+in+Wrought+and+Cast+Aluminum+Alloys&bt nG.

[26] L. Kempf, C. Smith, and C. Taylor, "Thermal and Electrical Conductivities of Alumi num Alloys," *Trans. Amer. Inst. Min. Metall. Engrs*, vol. 124, pp. 287-298, 1937. [On line]. Available: https://aimehq.org/resources/digital-library.

[27] A. corporation, "FlashLineTM 3000 THERMAL PROPERTIES TESTER," Pittsburg h, PA, USA, Technical Report 2016. [Online]. Available: http://www.smmmf.pub.ro/ wp-content/uploads/2016/03/FlashLine_3000.pdf.

CHAPTER 5 THERMAL CONDUCTIVITY AND ELECTRICAL CONDUCTIVITY IN OTHER Al-MMCS

This chapter introduces the evolution of TC and EC in some other typical Al-MMCs, including 6063-B_4C MMCs with the volume of B_4C of 6 and 15vol.%, 6351-B_4C MMCs with 4, 15 and 17.5% B_4C, 3004-10.5 Vol% B_4C as well as 6061-15% Al_2O_3. The Al-MMCs used in this chapter is simply summarized in Table 5-1 while detailed information can be found. The distribution of various reinforcement particles and reaction products were characterized and quantified by optical microscopy (OM). Meanwhile, Bruggeman model as most suitable model in 1xxx-B_4C MMCs was also used to simulate the evolution of TC and EC in these Al-MMCs. In addition, the relationship between EC and TC was also investigated and an empirical equation representing this relationship was discussed.

Table 5-1 Details of experimental for other Al-MMCs used in this chapter.

Composites code	Matrix	B_4C (Vol. %)	Condition
A-6-4E	6063	6	Extrusion plate (4 mm)
A-15-4E		15	Extrusion plate (4 mm)
B-4-7E		4	Extrusion plate (7 mm)
B-15-7E	6351	15	Extrusion plate (7 mm)
B-17.5-3R		17.5	Rolled plate (3 mm)
C-10.5-6R	3004	10.5	Rolled plate (6 mm)
D-15-6R	6061	15	Rolled plate (6 mm)

5.1 Microstructure Characterization of composites

Figure 5-1 shows the typical microstructure of experimental Al-MMCs. It can be found that the reaction products are composed of TiB_2 (light gray particles) and Al_3BC (dark gray particles) and AlB_2 (yellow particles) for B_4C-containing MMCs (Figure 5-1(a), (b) and (c)),

while no reactions products in 6061-Al_2O_3 MMCs (Figure 5-1(d)). Most of the reaction product surrounds the B_4C particles, while a small part is dispersed on the matrix away from the B_4C particles. Exceptionally, big titanium-rich intermetallic is observed in the 6063 and 6351 matrixes (Figure 5-1 (a) and (f), while only iron intermetallic exist in the 3004 and 6061 matrixes, especially in the 3004 has lots of iron intermetallic.

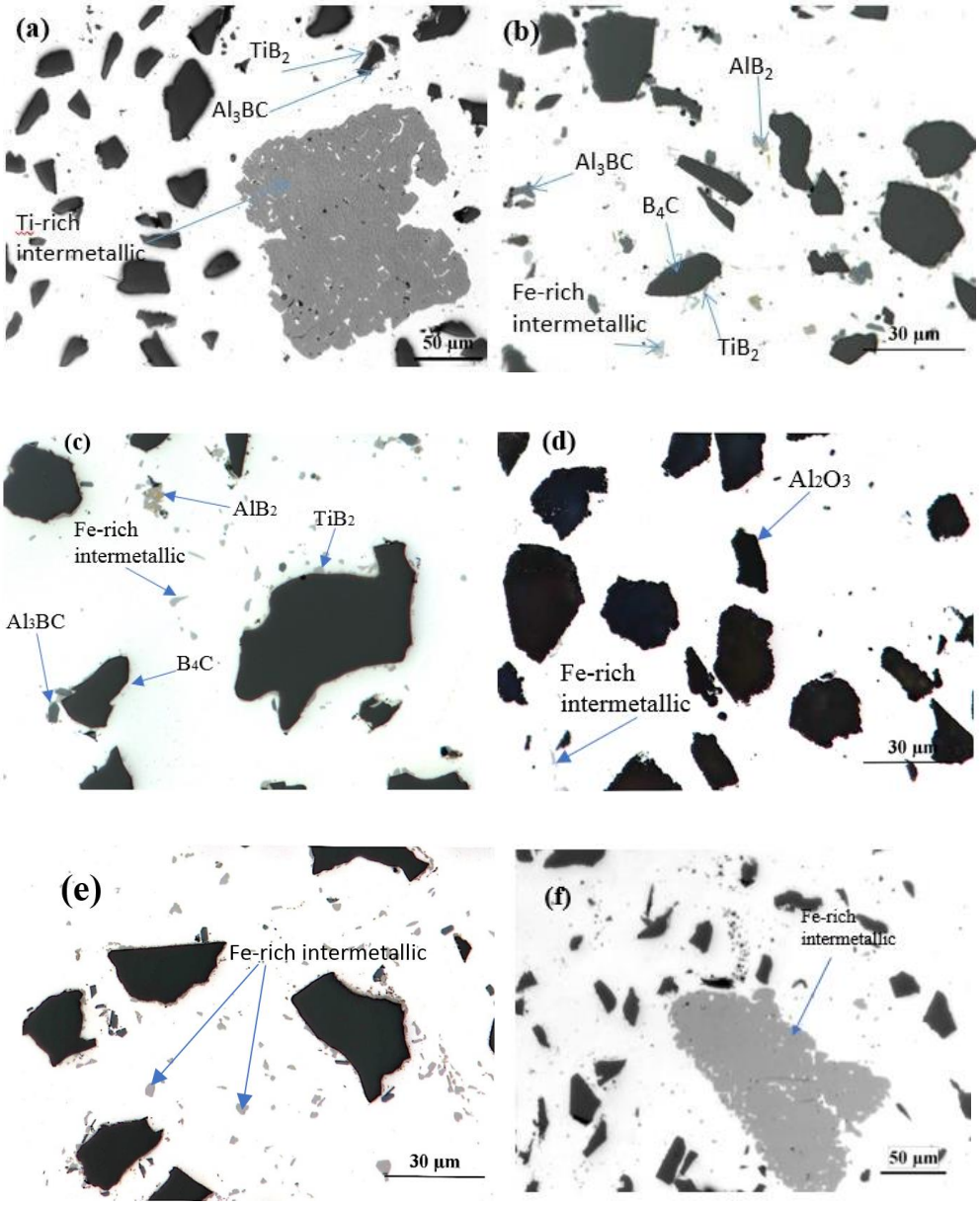

Figure 5-1 Optical microscope pictures of Al-MMCs (a) A-15-4E 200x, (b) B-17.5-3R 500x, (c) C-10.5-6R 500x, (d) D-15- 6R 500x, (e) C-10.5-6R 500x, (f) B-15-7E 200x.

The volume fraction of reinforcement particles and total reaction products are quantified by image analysis and summarized in Table 5-2.

Table 5-2 Volume fraction of reinforcement particles and reaction products particles in experimental Al-MMCs.

Composites code	$V_{total\ particles}$	V_p	V_r
A-6-4E	9.20 (1.23)	7.50 (0.65)	1.70 (0.58)
A-15-4E	19.50 (1.42)	16.60 (0.78)	2.90 (0.64)
B-4-7E	5.80 (0.67)	4.10 (0.25)	1.60 (0.42)
B-15-7E	20.00 (1.43)	16.90 (0.71)	3.10 (0.72)
B-17.5-3R	22.90 (0.99)	18.60 (0.36)	4.30 (0.63)
C-10.5-6R	15.61 (1.07)	12.9 (0.58)	3.00 (0.45)
D-15-6R	15.45 (0.72)	15.45 (0.72)	0

$V_{total\ particles}$: Particle volume fraction plus reaction product volume fraction, V_p: Volume fraction of B_4C/Al_2O_3, V_r : Volume fraction of reaction product.

As shown in Table 5-2, the measured volume fraction of B_4C and Al_2O_3 are close to the nominal ones. For instance, the volume fraction of B_4C in B-4-7E is 4.1 Vol % and 15.45 Vol % in D-15-6R. Besides, the volume fraction of reaction product increases with increasing B_4C volume fraction, which is rising from 1.7 Vol % in A-6-4E to 2.9 Vol % in A-15-4E. Meanwhile, the volume fraction of total particles increases with increasing B_4C volume fraction. The volume fraction of total particle is 9.2Vol% in A-6-4E compared with 19.5% in A-15-4E.

5.2 Evolution of TC/EC in other Al-MMCs

Figure 5-2 (a) and (b) displays the evolution of TC and EC in the experimental Al-MMCs with different reinforcement particles and volume fractions, respectively. Similar tendency is observed for both TC and EC in experimental other Al-MMCs. It can be observed that TC/EC generally decreases with the increase of volume fraction of reinforcement particles. Taking 6xxx-B_4C MMCs as example, the TC of A-6-4E to A-15-4E decreases from

174 [W/(m·K)] to 138 [W/(m·K)], which is ~ 20.7% reduction while TC decreases from 163 [W/(m·K)] in B-4-7E to 121 [W/(m·K)] in B-15-7E, which is reduced by 25.7 %. Similar to TC, EC is decreasing from 26343721.18 (S/m) in A-6-4E to 20880096.05 (S/m) in A-15-4E, which is ~ 20.7% reduction while EC decreases from 2.41×10^7 (S/m) in B-4-7E to 1.68 $\times10^7$ (S/m) in B-15-7E, which is reduced by 26.4 %. All these results are in consistent with the results found in 1xxx-B_4C MMCs.

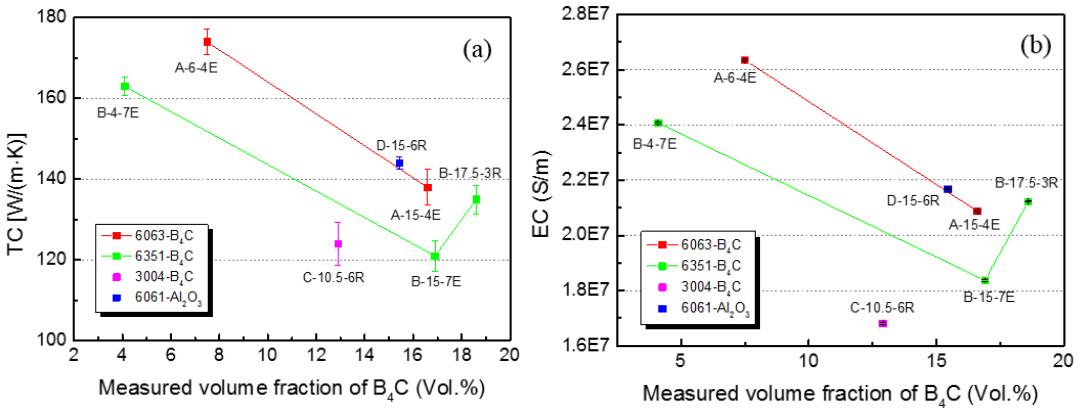

Figure 5-2 Evolution of TC/EC with different measured volume fraction (a) TC, (b) EC.

But for 6351-B_4C MMCs, the TC of B-15-7E to B-17.5-3R increased from 121 [W/(m·K)] to 135 [W/(m·K)]. Similar to TC, EC increased from 1.83 $\times10^7$ (S/m) to 2.12×10^7 (S/m). Those can be attributed to the high volume of Ti-rich particles in B-15-7E which could reduce the TC/EC. Meanwhile, TC of D-15-6R is higher than A-15-4E, the TC of 6061 is lower than 6063 and the TC of B_4C and Al_2O_3 is the same. Similar to TC, EC has the same tendence. Those can also be attributed to the high volume of Ti-rich particles in A-15-4E which could reduce the TC/EC.

On the other hand, with similar B_4C content, TC/EC is higher in 6063-B_4C MMCs than 6351-B_4C MMCs and further higher than 3004-B_4C MMCs. This can be explained by the different TC/EC from the matrix that TC/EC is higher in low-alloyed 6063 alloy but lower in

high-alloyed 3004 alloy.

5.3 Predictive model for evolution of TC/EC

As shown in Chapter 4, the Bruggeman-ET [1] /Bruggeman model [2] is the one of the most suitable models to predict the TC/EC of the 1100-B_4C MMCs. Hence, Bruggeman-ET/Bruggeman model is also selected to predict the evolution of TC/EC in experimental Al-MMCs, which are list in Table 5-3, The value of parameters for these models are summarized in Table 5-4.

Table 5-3 Description of TC/EC models for other Al-B_4C materials [1, 2].

Modelling	Model equation
Bruggeman-ET model (TC)	$\left(\frac{k_{eff}-k_p(1-\alpha)}{k_m-k_p(1-\alpha)}\right)^{3/(1-\alpha)}\left(\frac{k_m}{k_{eff}}\right)^{(1+2\alpha)/(1-\alpha)}=(1-\phi)^3$
Bruggeman model (EC)	$\frac{(\sigma_p-\sigma_{eff})}{(\sigma_p-\sigma_m)}(\frac{\sigma_m}{\sigma_{eff}})^{\frac{1}{3}}=(1-\phi)$

k_m: Matrix thermal conductivity [W/m·K], k_p: Particle thermal conductivity[W/m·K], ϕ: Particle volume faction, h_c: Interface thermal conductance [W/(m^2·K)], α: Dimensionless parameter, k_{eff}: Effective thermal conductivity of aluminum metal matrix composite [W/(m·K)]. σ_m: Matrix thermal conductivity (S/m), σ_p: Particle thermal conductivity (S/m), σ_{eff}: Effective electrical conductivity of aluminum metal matrix composite (S/m).

Note: The contents are cited from references 1 and 2.

Table 5-4 TC/EC and ITC of the material [3-6].

Material code	TC of matrix [W/(m·k)]	TC of particle [W/(m·k)]	EC of matrix (S/m)	EC of particle (S/m)	h_c (ITC) [W/(m^2·k)]
6063-B_4C	193		3.1×10^7		1.403×10^8
6351-B_4C	176	30	2.7×10^7	300	1.424×10^8
3004-B_4C	162		2.44×10^7		1.414×10^8
6061-Al_2O_3	180		2.72×10^7	1×10^{-12}	-

Note: The contents are cited from references 3-6.

Figure 5-3 (a) shows the experimental TC (solid indications) and predicted TC from Bruggeman-ET model (empty indications) in studied Al-MMCs. It can be found that the difference between the experimental TC and predicted TC is small in most studied Al-MMCs, which is less 3% of each matrix TC. For instance, it is only 1% of 6063 aluminum matrix TC for A-6-4E and 2.5% of 6351 aluminum matrix TC for both B-4-7E and B-17.5-3R. However, the difference is bigger in A-15-4E, B-15-7E and C-10.5-6R, which is likely due to the high volume of big Ti-rich intermetallic and Fe-rich intermetallic in Figure 5-1 (a), (e) and (f).

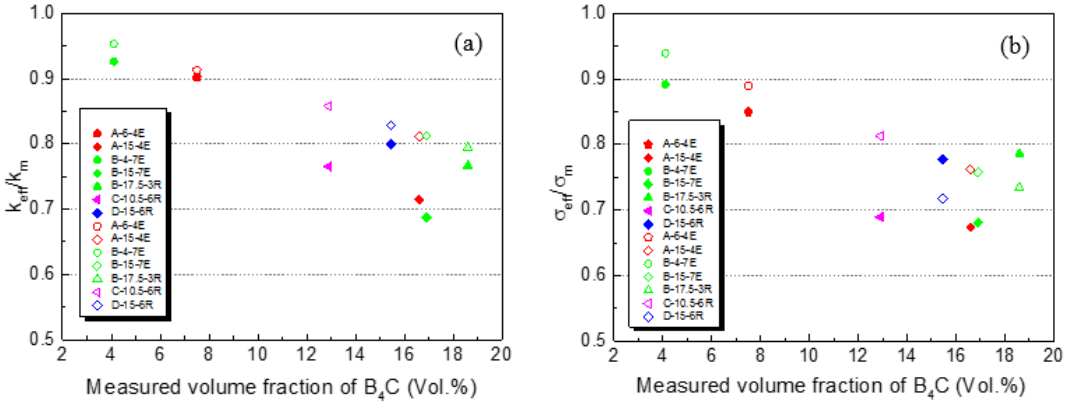

Figure 5-3 Comparison of TC/EC theoretical value and measured value under different models (a) TC, (b) EC.

Note: Solid points are experimental values, and open points are model calculated values.

(a):6063-B_4C at k_m/k_p(ratio of matrix TC to particle TC) = 6.43; 6351-B_4C at k_m/k_p = 5.87; 3004-B_4C at k_m/k_p = 5.4 and 6061-Al_2O_3 at k_m/k_p = 6.

(b): 6063-B_4C at δ_m/δ_p(ratio of matrix EC to particle EC) = 1.14×10^5; 6351-B_4C at δ_m/δ_p =0.9×10^5; 3004-B_4C at δ_m/δ_p = $0.81\times10^5$and 6061-Al_2O_3 at δ_m/δ_p =0.91×10^5.

Similar tendency is also found in the EC between the experimental EC (solid indications) and predicted EC from Bruggeman model (empty indications). As shown in Figure 5-3 (b), most of studied Al-MMCs shows close experimental and predicted EC, which is less 5% of each matrix EC. But for A-15-4E, B-15-7E and C-10.5-6R has big difference with the experimental EC. Those can be also explained by the high volume of big Ti-rich intermetallic and Fe-rich intermetallic in Figure 5-1 (a), (e) and (f).

5.4 Relationship between TC and EC

Since both TC and EC of those composite have the same tendency, as shown in Figure 5-2, it is inferred that there is a certain relationship between its EC and TC. In 1100-B_4C MMCs, we found an equation that matches its TC and EC as

$$K = 1.79163 \times 10^{-8} \times T \times \sigma + 29.998 \quad (5\text{-}1)$$

To explore whether the relationship between TC and EC of 6xxx-B_4C, 3004-B_4C and 6061-Al_2O_3 MMCs conforms to this equation, these points are drawn on Figure 4-12 to form Figure 5-4. It can be found that these points distributed in the vicinity of the fitted straight line. Therefore, we calculated the $\pm 7\%$ error of this equation the red line is represent the upper value of TC (7%) and the green line is representing the lower value of TC (-7%). As shown in Figure 5-4, the TC values of 6xxx-B_4C, 3004-B_4C and 6061-Al_2O_3 MMCs are include in the two lines. And it can be found from the residual error between the measured TC value after annealing and the TC value after annealing calculation by the equation is about 6% of measured TC value, which is lower than the laser flash test error of 7% [7]. Therefore, it can be considered that the electrical and thermal conductivities of 6xxx-B_4C, 3004-B_4C and 6061-Al_2O_3 MMCs fit this equation.

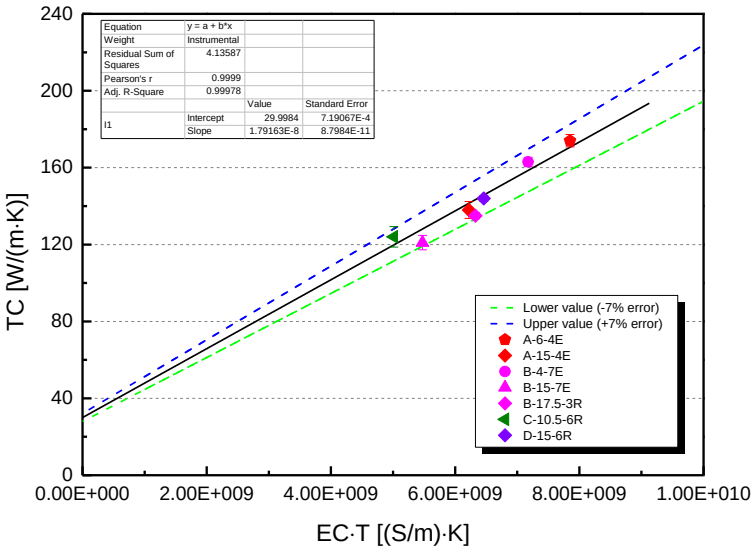

Figure 5-4 Relationship between EC and TC under 1100-B_4C as-rolled condition verification by 6xxx-B_4C, 3004-B_4C and 6061-Al_2O_3 MMCs.

5.5 Summary

1. TC/EC generally decreases with the increase volume of reinforcement particles in the same matrix while they are also varying with the matrix.
2. Bruggeman-ET/ Bruggeman model are suitable for predicting the TC/EC of Al-MMCs.
3. A linear relationship between the EC and TC is found in studied Al-MMCs with different matrix and reinforcement particles, which is also matching the equation obtained from 1100-B_4C MMCs.

References

[1] A. Every, Y. Tzou, D. Hasselman, and R. Raj, "The effect of particle size on the ther mal conductivity of ZnS/diamond composites," *Acta metallurgica et materialia*, vol. 40, no. 1, pp. 123-129, 1992, doi: https://doi.org/10.1016/0956-7151(92)90205-S.

[2] V. D. Bruggeman, "Berechnung verschiedener physikalischer Konstanten von hetero genen Substanzen," *Annalen der physik*, vol. 416, no. 7, pp. 636-664, 1935, doi: https://doi.org/10.1002/andp.19354160705.

[3] A. H. Committee, "Properties of wrought aluminum and aluminum alloys," *vol. 2, AS M Handbook, Volume 2: Properties and selection: nonferrous alloys and special-pur pose materials*Materials Park, Ohio, USA: ASM International, 1990, pp. 62-122.

[4] T. Gomi, N. Fukushima, and J. Matsushita, "High temperature electrical conductivity of B_4C, SiC and SiB_6 sintered bodies," *Journal of Advanced Science*, vol. 13, no. 1-2, pp. 15-16, 2001, doi: https://doi.org/10.2978/jsas.13.15.

[5] T. Maruyama and S. Onose, "Fabrication and thermal conductivity of boron carbide/c opper cermet," *Journal of nuclear science and technology*, vol. 36, no. 4, pp. 380-385, 1999, doi: https://doi.org/10.1080/18811248.1999.9726221.

[6] Matweb. "Alumina, alpha Al_2O_3, 99.5%." https://www.matweb.com/search/DataSheet.aspx?MatGUID=0654701067d147e88e8a38c646dda195.

[7] A. corporation, "FlashLineTM 3000 THERMAL PROPERTIES TESTER," Pittsburg h, PA, USA, Technical Report 2016. [Online]. Available: http://www.smmmf.pub.ro/wp-content/uploads/2016/03/FlashLine_3000.pdf

CHAPTER 6 CONCLUSIONS

In this thesis, the evolution of TC and EC and their relationship in Al-B_4C composites was investigated and following conclusions can be drawn according to the study:

1. The reaction products increase with the increasing volume fraction of B_4C particles.
2. The thermal conductivity of Al-B_4C MMCs is not affected by the test temperature in the range of room temperature to 250℃.
3. Annealing treatment can improve the TC/EC of 1100-B_4C MMCs, and the thermal con ductivity reaches the maximum value when it is completely recrystallized at 430℃/4h or 380℃/23h.
4. The TC/EC of Al-MMCs decreased with the increase of B_4C volume fraction. However, particle size and interfacial thermal resistance do not contribute to this decreasing trend.
5. Compared with other EC/TC prediction models, the Bruggeman-ET model is the most suitable for predicting the EC/TC in studied Al-MMCs.
6. Particle size and interfacial thermal resistance/resistance contribute little to EC/TC when the EC/TC of the particles is much lower than that of the matrix.
7. When the EC/TC of the particles is much lower than the EC/TC of the matrix, the funct ional relationship between EC and TC in the range of 20-250°C for studied Al-MMCs is $K=1.79163\times10^{-6}\times T\times\sigma+29.998$.

CHAPTER 7 RECOMMENDATIONS

According to the present work, the following recommendations can be made:

1. In the present work, the difference of particle size is small and then it has little effect on the TC of Al-B_4C/Al_2O_3 MMCs. Therefore, future work can be extended to explore the influence of particle size in a bigger range on the evolution of EC and TC for Al-MMCs.
2. The empirical equation between EC and TC is found to be valid for studied Al-MMCs with B_4C and Al_2O_3 ceramic particles, which has much lower EC/TC than matrix. Hence, it is suggested to verify if it still be valid for other reinforcement particles which has higher EC/TC, such as carbon fibers.
3. According to the empirical equations in this project, TC is mainly related to the diffusion process and number of electrons and phonons. Therefore, the TC of the composites can be improved in future work by optimizing any factors that may affect the electron and phonon diffusion processes.